Electronic Supplementary Information

Trinuclear (Aminonitrone)Zn^{II} Complexes as Key Intermediates in Zinc(II)-mediated Generation of 1,2,4-Oxadiazoles from Amidoximes and Nitriles

Dmitrii S. Bolotin, Mikhail V. Il'in, Alexander S. Novikov, Nadezhda A. Bokach,

Vitalii V. Suslonov, and Vadim Yu. Kukushkin

Table of Contents

Analytical and Spectroscopy Data……....2

X-ray Structure Determinations, the structures of the O-iminoacylated oximes…….5

Spectra of **2a**–**d**…….5

Spectra of [**3a–d**](OTf)$_4$…….17

Spectra of [**4a–c**(OTf)$_2$]…….29

Spectra of [**5a–d**](OTf)…….38

Crystal data for **2a**–**c** and [**3a**](OTf)$_4$…….50

Crystal data for [**4b**(OTf)(EtOH)](OTf), [**4c**(OTf)$_2$], [**5a**](OTf), and [**5d**](OTf)…….51

Theoretical study of bonding situation in solid state structures of **2** and [**4**(OTf)$_2$]…….52

Calculated Wiberg bond indices for selected bonds in **2a**–**c**……..56

Cartesian atomic coordinates of model structures……..…57

References……..64

Analytical and Spectroscopy Data

Complexes **2a**–**d**, [**3a**–**d**](OTf)$_4$, [**4a**–**c**(OTf)$_2$], and salts [**5a**–**d**](OTf) gave satisfactory C, H, and N elemental analyses for the proposed formulas, and these species were also characterized by high-resolution ESI-MS, IR, ^{1}H NMR, and CP-MAS TOSS ^{13}C{^{1}H} NMR (for poorly soluble **2a**–**d**, [**3a**–**d**](OTf)$_4$, and [**5d**](OTf)) or ^{13}C{^{1}H} NMR spectroscopy (for [**4a**–**c**(OTf)$_2$] and [**5a**–**c**](OTf) exhibiting sufficient solubility) and additionally by single-crystal X-ray diffraction for eight species (**2a**–**c**, [**3a**](OTf)$_4$, [**4b**(OTf)(EtOH)](OTf), [**4c**(OTf)$_2$], [**5a**–**d**](OTf), and [**5d**](OTf)). The positive mode HRESI mass spectra of **2a**–**d** exhibit sets of peaks corresponding to the quasi-ions [Zn(**1**)$_2$ – H]$^+$, [Zn$_2$(**1**)$_2$ – H]$^+$, [Zn$_2$(OAc)(**1**)$_2$]$^+$, [Zn$_2$(OAc)$_2$(**1**)$_3$ – H]$^+$, [Zn$_2$(OAc)$_3$(**1**)$_4$ – 2H]$^+$, and in the negative mode spectra, sets of peaks from [Zn(OAc)$_3$]$^-$, [Zn$_2$(OAc)$_5$]$^-$ were identified. The HRESI$^+$-MS of [**3a**–**d**](OTf)$_4$ display several groups of peaks corresponding to the fragmentation ions [Zn(OAc)]$^+$, [Zn$_2$(**1**)$_2$ – H]$^+$, [Zn$_2$(OAc)$_2$(**1**) – H]$^+$, [Zn$_2$(OAc)(**1**)$_2$ – 2H]$^+$, [Zn$_2$(OAc)$_2$(**1**)$_2$ – H]$^+$, [Zn$_2$(OAc)$_3$(**1**)$_2$]$^+$, and in the negative mode spectra, sets of peaks from [Zn(OTf)$_3$(**1**)]$^-$ and [Zn$_2$(OTf)$_4$(**1**) – H]$^-$. The HRESI$^+$-MS of complexes [**4a**–**c**(OTf)$_2$] exhibit sets of peaks corresponding to the quasi-ions [Zn{RC(NH$_2$)=NOC(N(CH$_3$)$_2$)=NH}(OTf)]$^+$ and [Zn{RC(NH$_2$)=NOC(N(CH$_3$)$_2$)=NH}$_2$(OTf)]$^+$, whereas in the negative mode the only observed peaks are due to [RC(NH$_2$)=NOC(N(CH$_3$)$_2$)=NH$_2$ + 2OTf]$^-$. The positive and negative mode ESI spectra of amidinium salts [**5a**–**d**](OTf) display group of peaks from [M]$^+$, [2M + OTf]$^+$, and [M + 2OTf]$^-$, respectively.

The IR spectra of **2a**–**d**, [**3a**–**d**](OTf)$_4$, [**4a**–**c**(OTf)$_2$], and [**5a**–**d**](OTf) display two to four bands from medium to very strong intensities at 3498–3126 cm^{-1}, which can be attributed to the N−H stretches. Weak to medium bands at 3088–2772 cm^{-1} observed in the spectra were assigned to ν(C–H). The IR spectra of **2a**–**d**, [**3a**–**d**](OTf)$_4$, and [**4a**–**c**(OTf)$_2$] exhibit one ν(C=N) band in the range 1678–1638 cm^{-1}, which is specific to amidoximes,[1] whereas the spectra of [**5a**–**d**](OTf) exhibit two C=N absorption bands in the range 1694–1650 cm^{-1}, which are characteristic for *O*-carbamidinium amidoximes. The spectra of **2a**–**d** and [**3a**–**d**](OTf)$_4$ also feature three strong to very

strong bands in the region 1608–1340 cm^{-1} from ν(C=O) of the ligated acetate group. In addition, the spectra of [**3a**–**d**](OTf)$_4$, [**4a**–**c**(OTf)$_2$], and [**5a**–**d**](OTf) display a two to three very strong bands in the region 1290–1160 cm^{-1}, characteristic to the ν(S=O) of the triflate anion.

The ^{1}H NMR spectra of **2a**–**d** and [**3a**–**d**](OTf)$_4$ recorded in $(CD_3)_2SO$ are equal to the spectra of corresponding **1a**–**d**, which indicates solvolysis of the complexes and therefore their spectra were recorded in $(CD_3)_2CO$, where the dissociation was not observed. Characteristic feature of the spectra is the absence of the N*H* signal due to a fast exchange with water protons. Another feature is the availability of broad singlets attributed to the NH_2 resonances at 6.40–5.29 ppm (for **2a**–**d**) and 8.48–7.93 (for [**3a**–**d**](OTf)$_4$). Low-field shift of the signal in the spectra of [**3a**–**d**](OTf)$_4$ is probably due to the positive charge on the $HNCNH_2$ moiety provided by the stabilization of **1a**–**d** ligand in the aminonitrone form. The ^{1}H NMR spectra of [**4a**–**c**(OTf)$_2$] and [**5a**–**d**](OTf) were recorded in $(CD_3)_2SO$ and no solvolysis was observed for [**4a**–**c**(OTf)$_2$] likely due to bidentate character of the ligands that imparts the substitutional intertness. Characteristic feature of the spectra of [**4a**–**c**(OTf)$_2$] is availability of two or three broad signals at 7.98–7.57 and 7.12–4.78 ppm corresponding to the peaks of the N*H* and NH_2 moieties, respectively. The spectra of [**5a**–**d**](OTf) exhibit two sets of one or two broad singlets at 8.74–7.92 and 7.34–6.63 ppm attributed to the carbamidinium and amidoxime NH_2 resonances, correspondingly.

The ^{13}C{^{1}H} NMR spectra of [**4a**–**c**(OTf)$_2$] and [**5a**–**d**](OTf) were recorded in $(CD_3)_2SO$. The spectra exhibit two signals at 161.89–155.68 ppm, which are characteristic for the R–*C*(=N)–NH_2, and O–*C*(=N)–$N(CH_3)_2$ resonances and the quartet at 122.77–119.54 ppm of the C atom of the triflate anion. In high-field region, the spectra of [**4a**–**c**(OTf)$_2$] display one signal at 37.61–37.32 ppm, whereas in the spectra of [**5a**–**d**](OTf) two signals at 38.35–37.09 ppm, which are characteristic of the N(*C*H_3)$_2$ resonances, were observed.

The solid state CP-MAS TOSS ^{13}C{^{1}H} NMR spectra of **2a**–**d**, [**3a**–**d**](OTf)$_4$, and [**5d**](OTf) were measured due to poor solubility of these species in $(CD_3)_2CO$. The spectra of **2a**–**d** and [**3a**–**d**](OTf)$_4$ display one to two signals in the region 182.47−175.69 ppm, which can be

attributed to CH_3–CO_2 and one to three signals of the CH_3–CO_2 resonances were observed at 27.27–20.12 ppm. In addition, the spectra of **2a**–**d** and [**3a**–**d**](OTf)$_4$ exhibit one signal at 164.47–152.40 ppm corresponding to the C atom of the carbamidoxime group.

X-ray Structure Determinations, the structures of the O-iminoacylated oximes

In the molecular structures of [**5a**](OTf) and [**5d**](OTf), the N(2)−C(1) [1.342(3) and 1.334(3) Å] and the N(4)–C(3/4) [1.463(3)–1.467(3) Å] are normal single bonds (**Figure 6**).[2] The N(1)–C(1), N(4)–C(2), and N(3)–C(2) bond lengths [1.285(6)–1.323(3) Å] indicate intermediate order between typical single and double bonds,[2] which reflects the amide character of these bonds. The O(1)−N(1) distances [1.471(2) and 1.483(2) Å] are longer than usual O−N^{sp2} bonds, which is specific for *O*-imidoylamidoximes.[3] In the carbamidoxime groups of both complexes, the HO- and H_2N-moieties are in the *sin*-configuration. An intramolecular hydrogen bond exists between one of the amidinium H atoms and the oxime N atom ($N_{amidinium}$•••N_{oxime} 2.207 and 2.519 Å; $N_{amidinium}$–H•••N_{oxime} 104.30 and 105.78, respectively). In both crystal structures, hydrogen bonds between the amide H atoms and the triflate O atoms were observed.

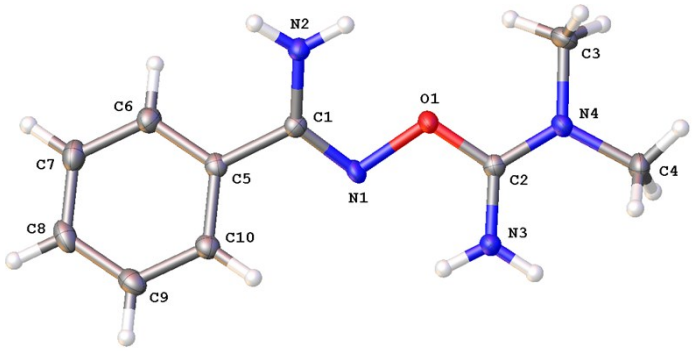

Figure 1S. The structure of [**5a**]$^+$ showing the atomic numbering scheme. Thermal ellipsoids are given at the 50% probability level.

Spectra of 2a–d

2a

Acquisition Parameter

Source Type	ESI	Ion Polarity	Positive	Set Nebulizer	0.4 Bar
Focus	Not active			Set Dry Heater	180 °C
Scan Begin	50 m/z	Set Capillary	4500 V	Set Dry Gas	4.0 l/min
Scan End	3000 m/z	Set End Plate Offset	-500 V	Set Divert Valve	Source

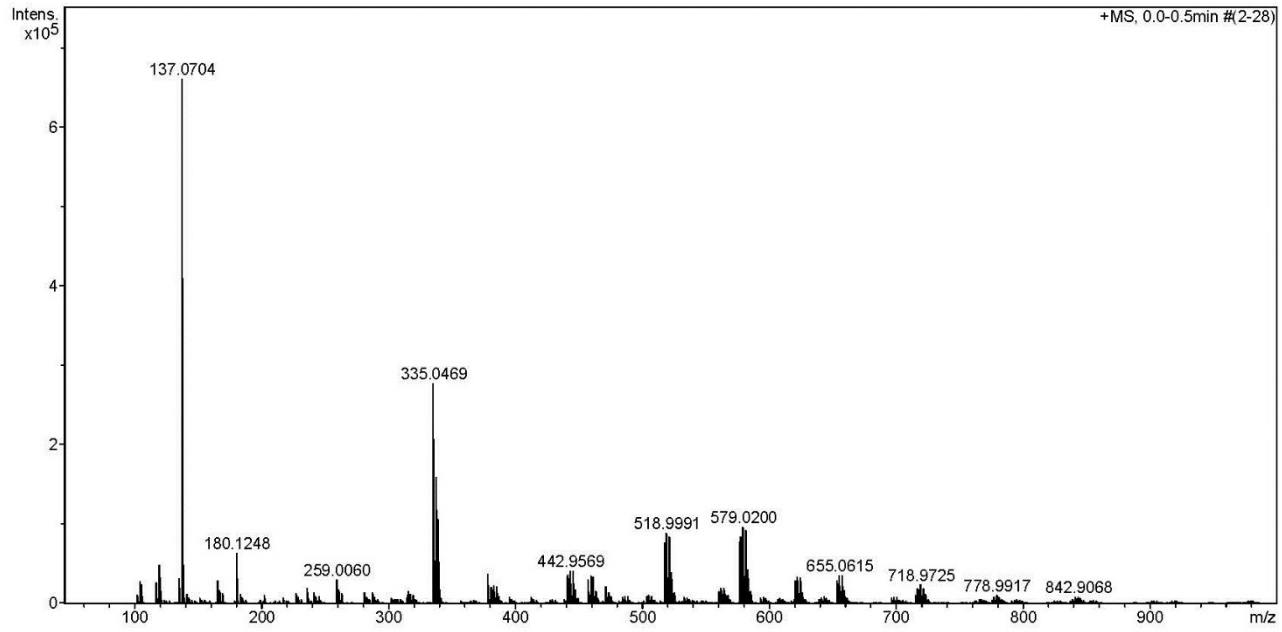

Figure 2S. Positive mass-spectrum of **2a.**

Acquisition Parameter

Source Type	ESI	Ion Polarity	Negative	Set Nebulizer	0.4 Bar
Focus	Not active			Set Dry Heater	180 °C
Scan Begin	50 m/z	Set Capillary	3500 V	Set Dry Gas	4.0 l/min
Scan End	3000 m/z	Set End Plate Offset	-500 V	Set Divert Valve	Source

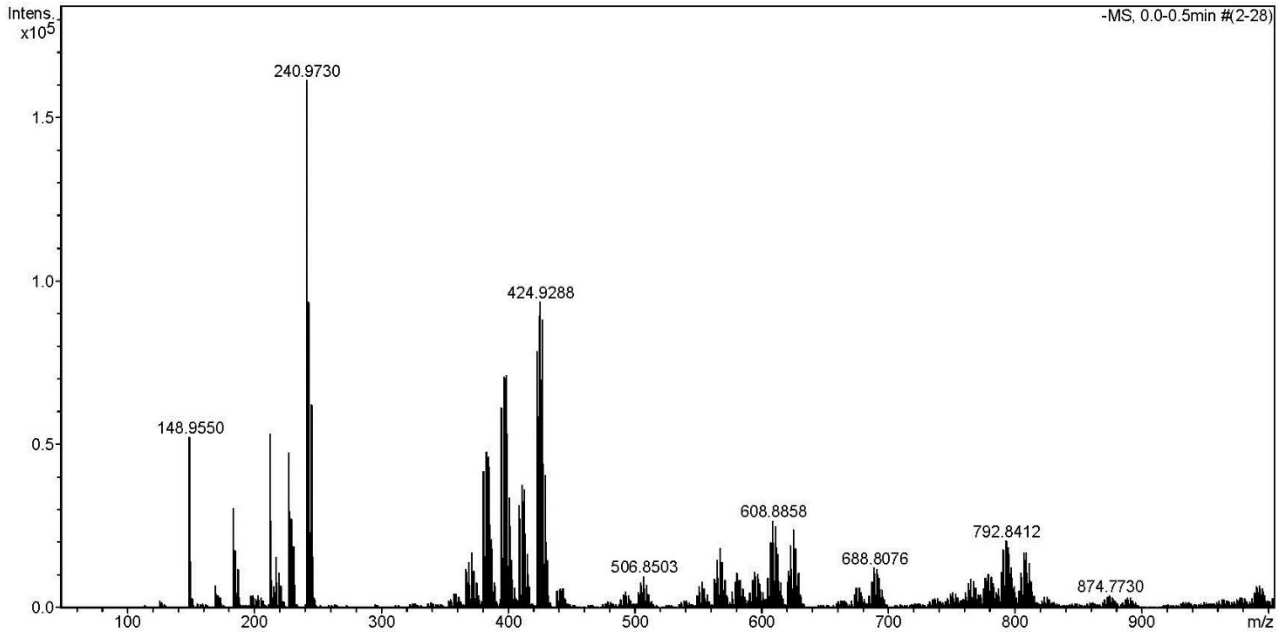

Figure 3S. Negative mass-spectrum of **2a.**

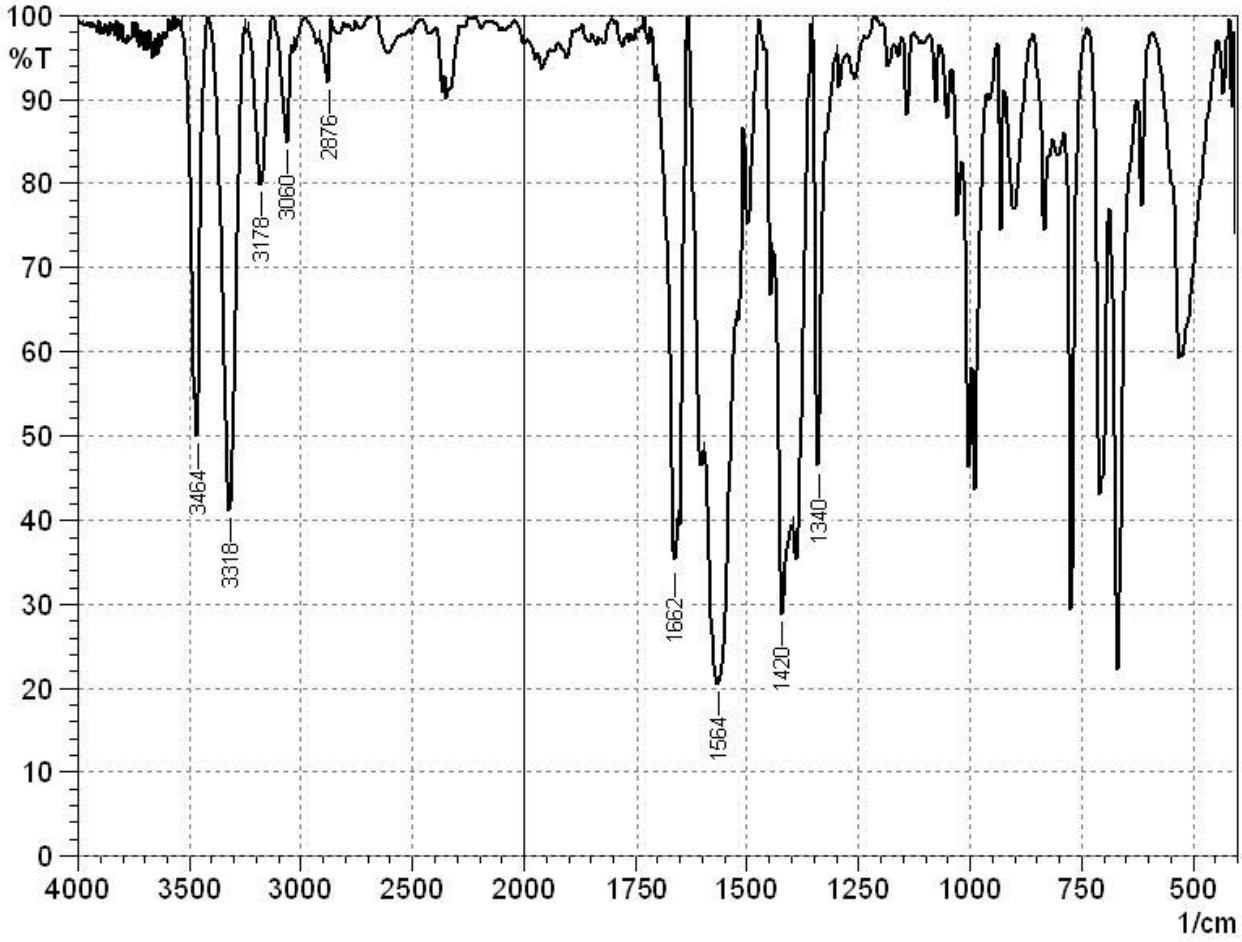

Figure 4S. IR spectrum of **2a.**

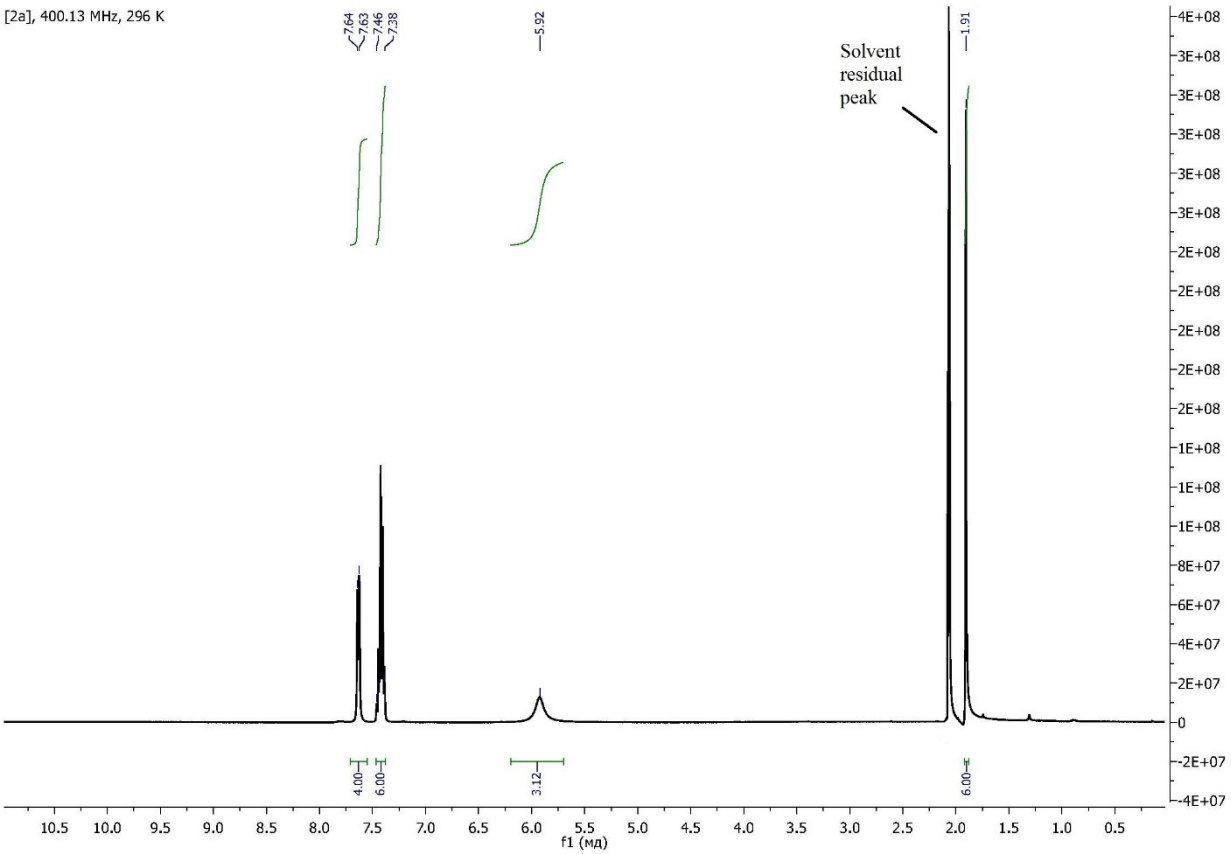

Figure 5S. [1]H NMR spectrum of **2a.**

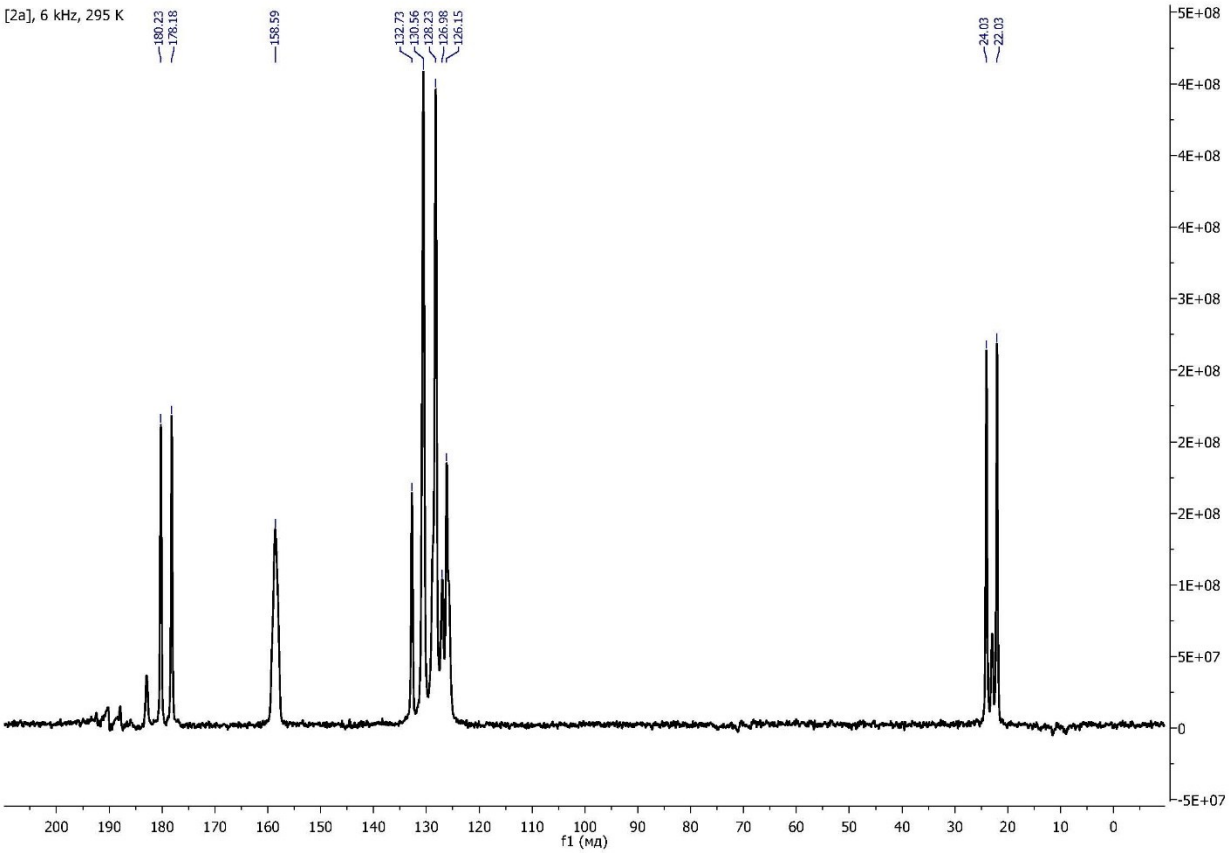

Figure 6S. 13C{1H} CP-MAS TOSS NMR spectrum of **2a.**

2b

Acquisition Parameter

Source Type	ESI	Ion Polarity	Positive	Set Nebulizer	0.4 Bar
Focus	Not active			Set Dry Heater	180 °C
Scan Begin	50 m/z	Set Capillary	4500 V	Set Dry Gas	4.0 l/min
Scan End	3000 m/z	Set End Plate Offset	-500 V	Set Divert Valve	Source

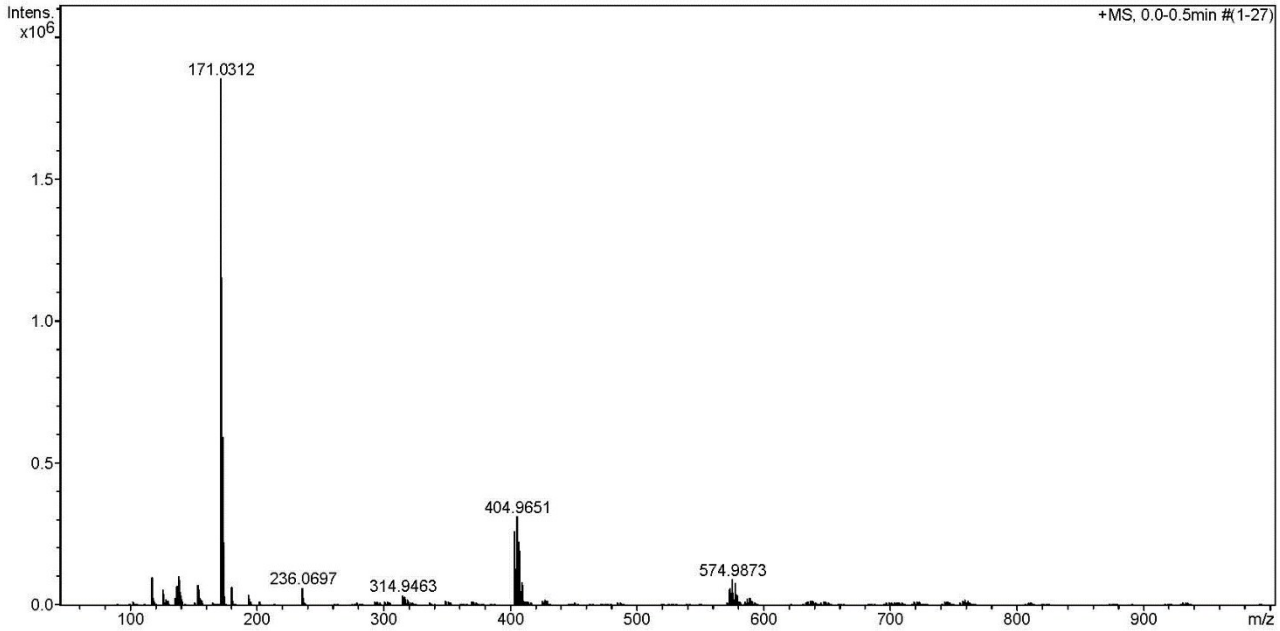

Figure 7S. Positive mass-spectrum of **2a.**

Acquisition Parameter

Source Type	ESI	Ion Polarity	Negative	Set Nebulizer	0.4 Bar
Focus	Not active			Set Dry Heater	180 °C
Scan Begin	50 m/z	Set Capillary	3500 V	Set Dry Gas	4.0 l/min
Scan End	3000 m/z	Set End Plate Offset	-500 V	Set Divert Valve	Source

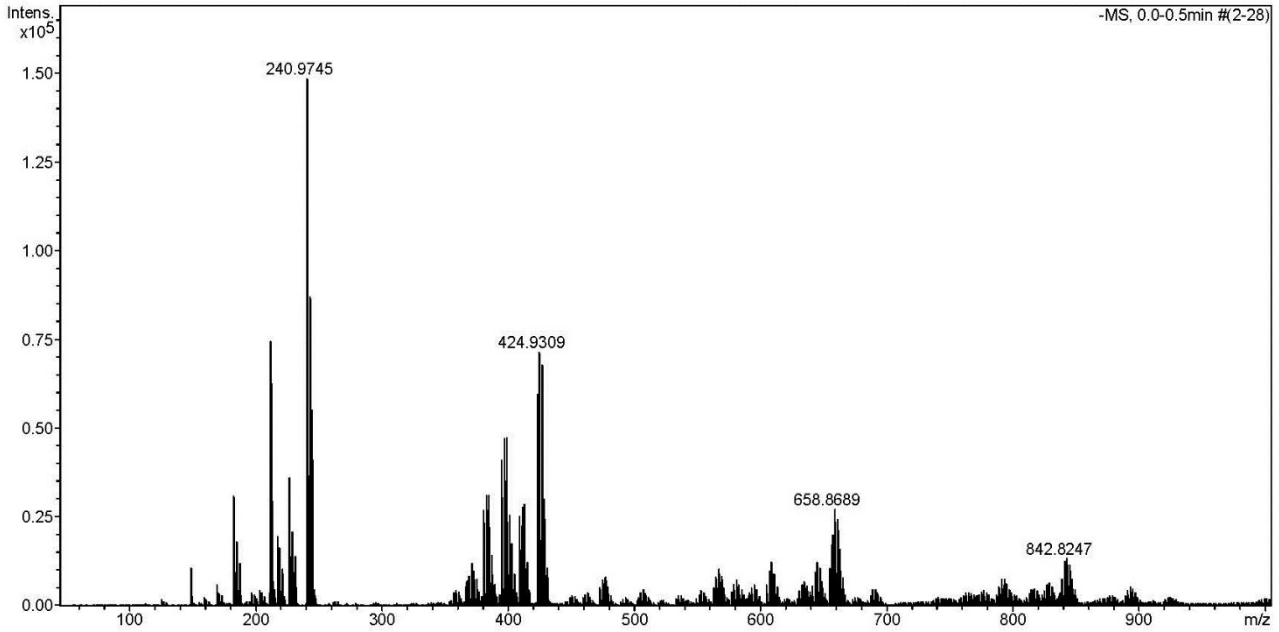

Figure 8S. Negative mass-spectrum of **2b.**

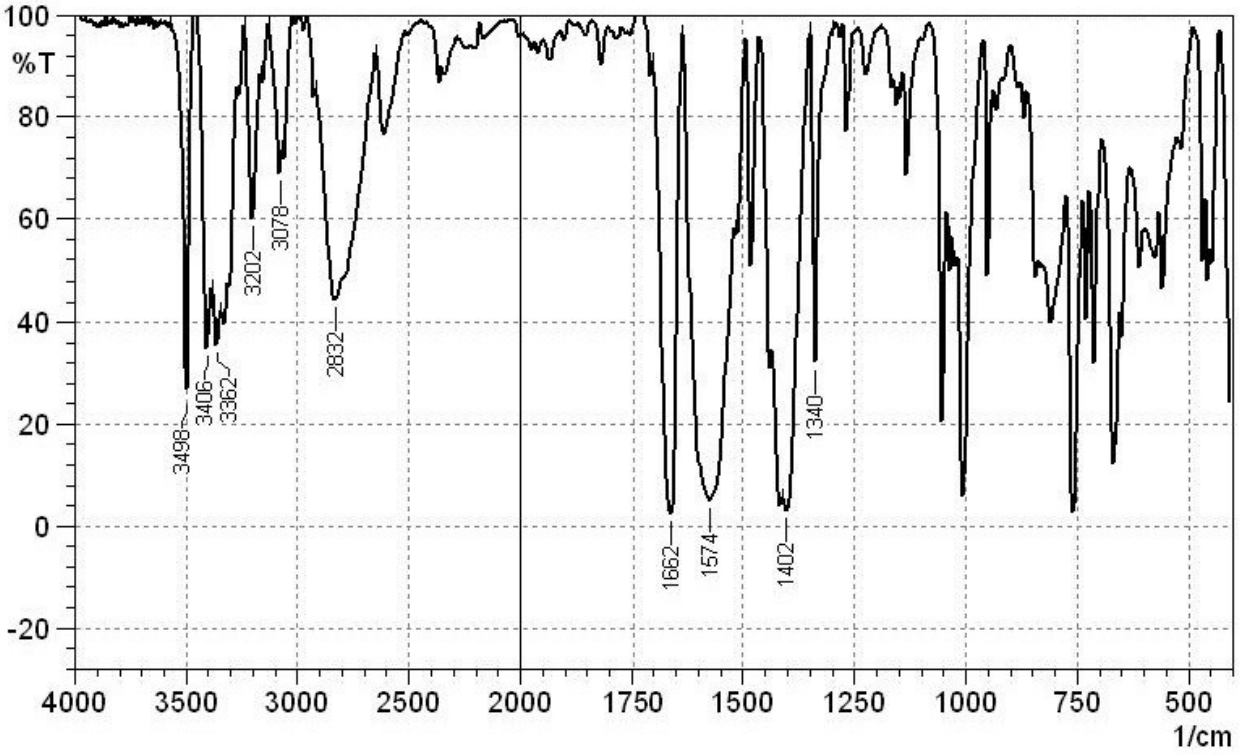

Figure 9S. IR spectrum of **2b.**

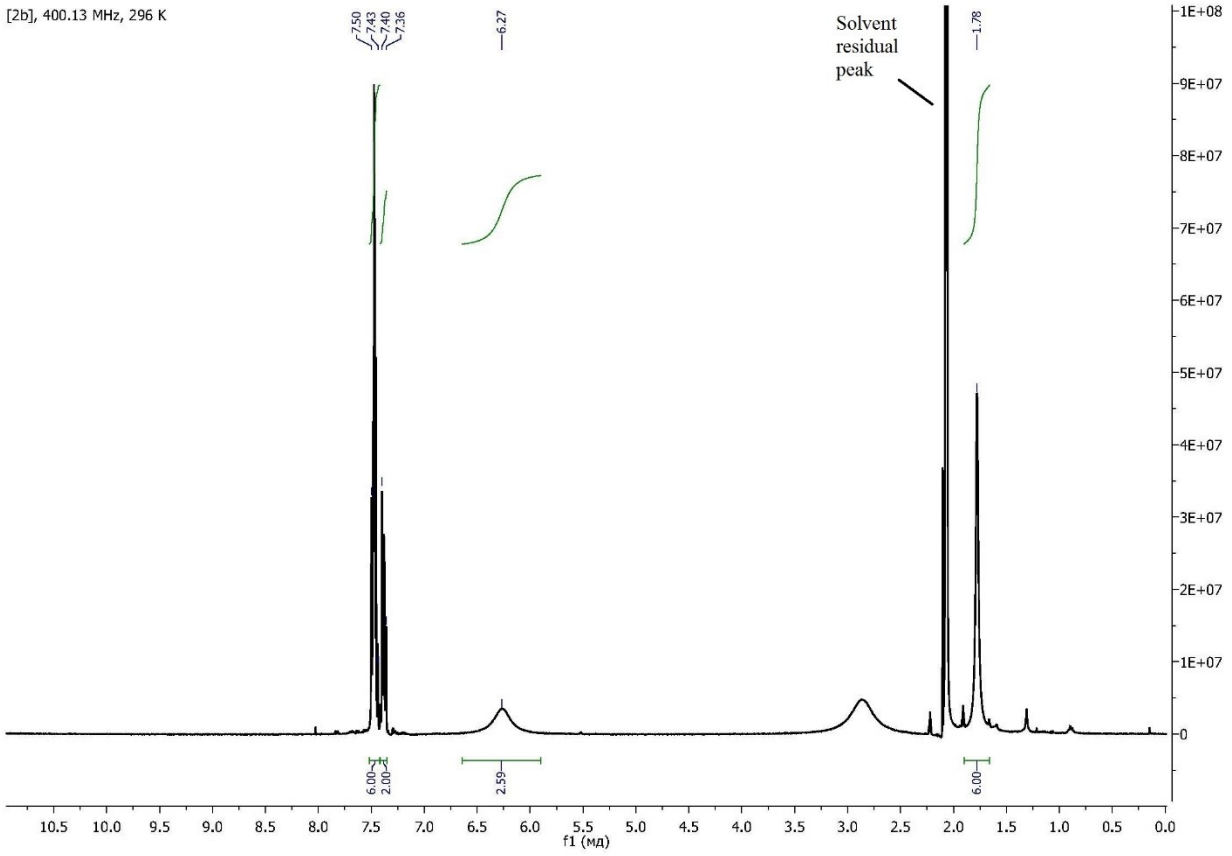

Figure 10S. ^{1}H NMR spectrum of **2b.**

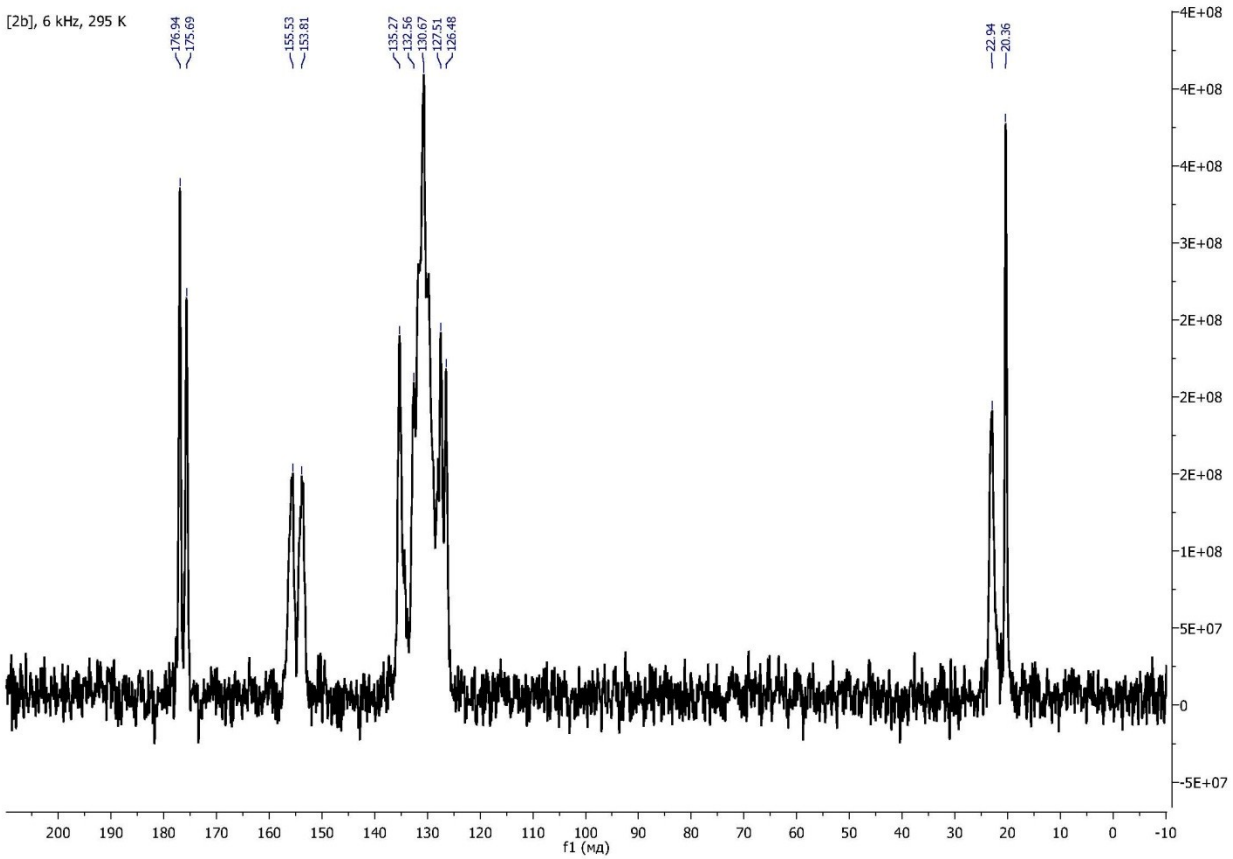

Figure 11S. 13C{1H} CP-MAS TOSS NMR spectrum of **2b.**

2c

Acquisition Parameter

Source Type	ESI	Ion Polarity	Positive	Set Nebulizer	0.4 Bar
Focus	Not active			Set Dry Heater	180 °C
Scan Begin	50 m/z	Set Capillary	4500 V	Set Dry Gas	4.0 l/min
Scan End	3000 m/z	Set End Plate Offset	-500 V	Set Divert Valve	Source

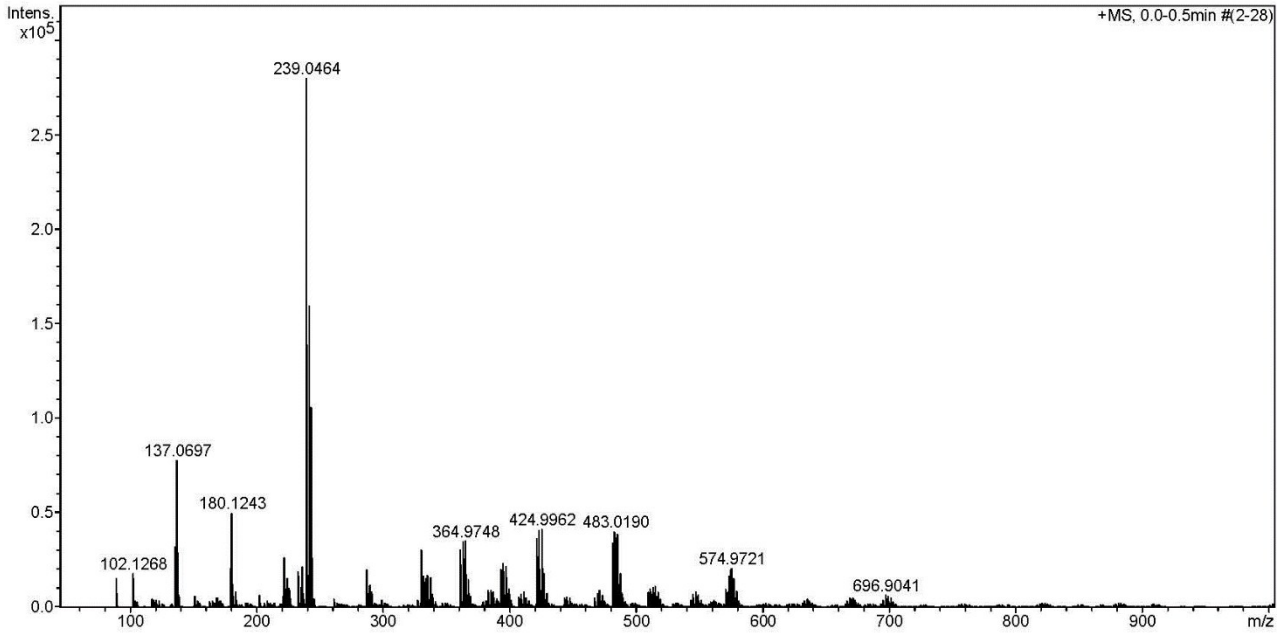

Figure 12S. Positive mass-spectrum of **2c.**

Acquisition Parameter

Source Type	ESI	Ion Polarity	Negative	Set Nebulizer	0.4 Bar
Focus	Not active			Set Dry Heater	180 °C
Scan Begin	50 m/z	Set Capillary	3500 V	Set Dry Gas	4.0 l/min
Scan End	3000 m/z	Set End Plate Offset	-500 V	Set Divert Valve	Source

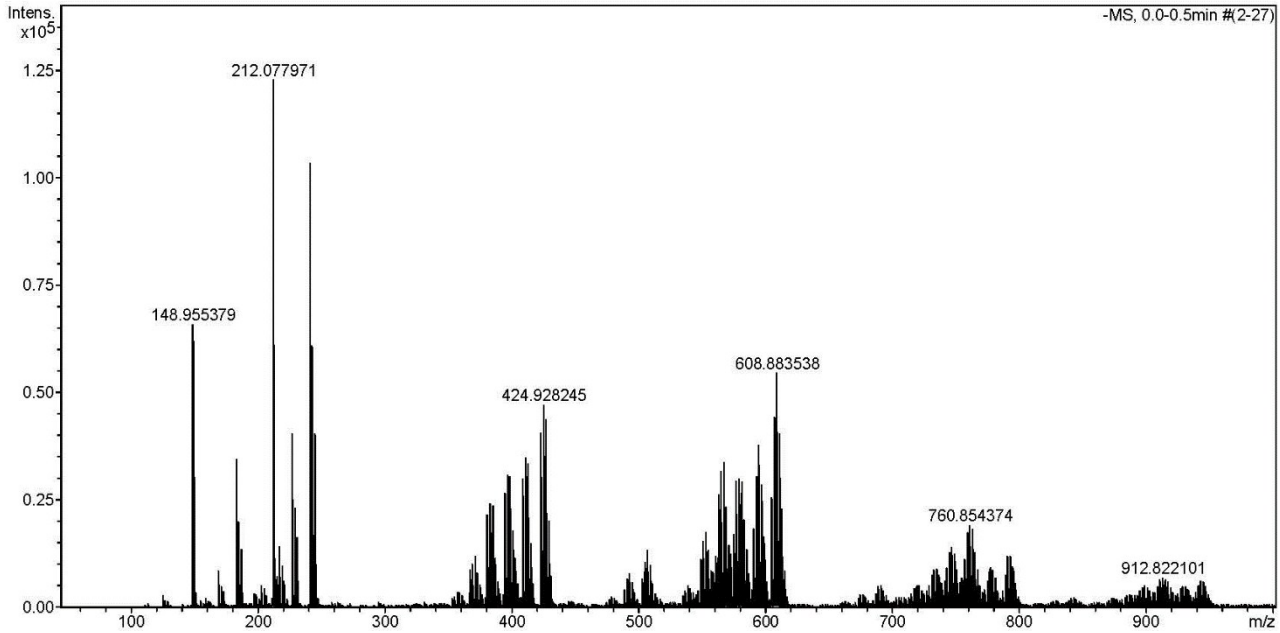

Figure 13S. Negative mass-spectrum of **2c.**

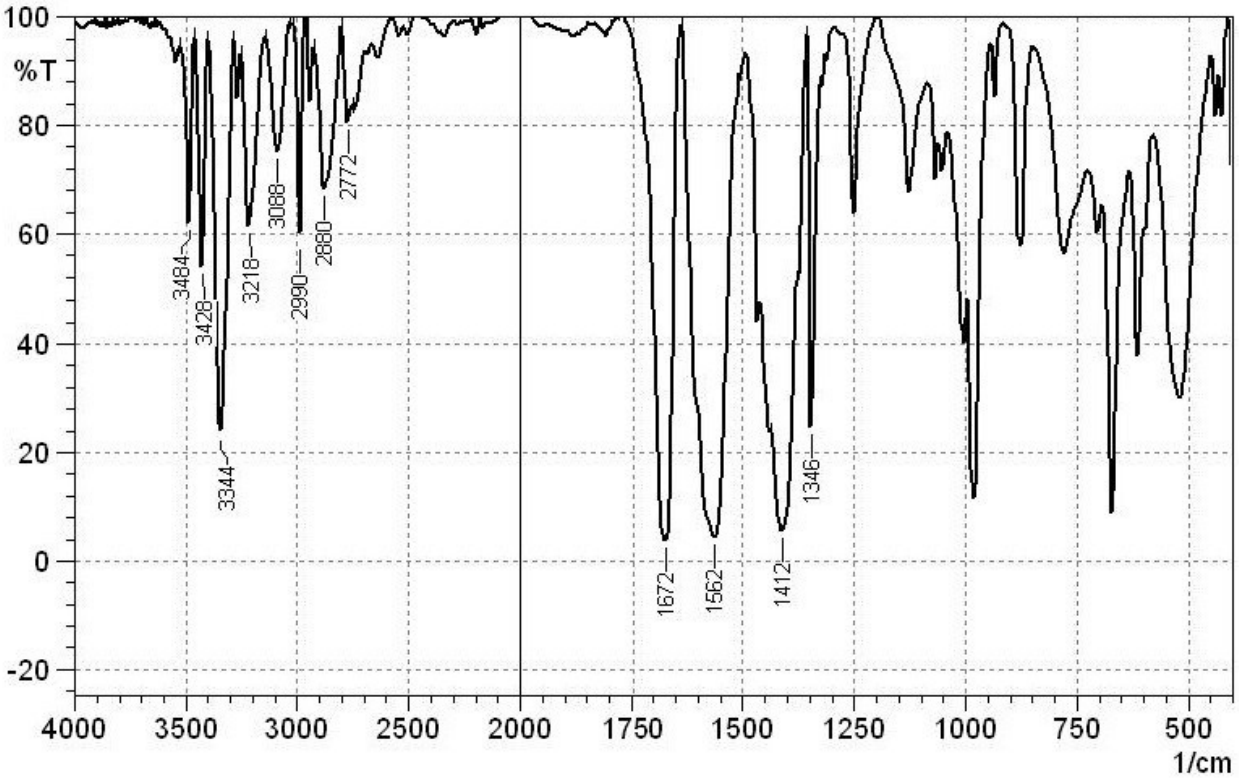

Figure 14S. IR spectrum of **2c.**

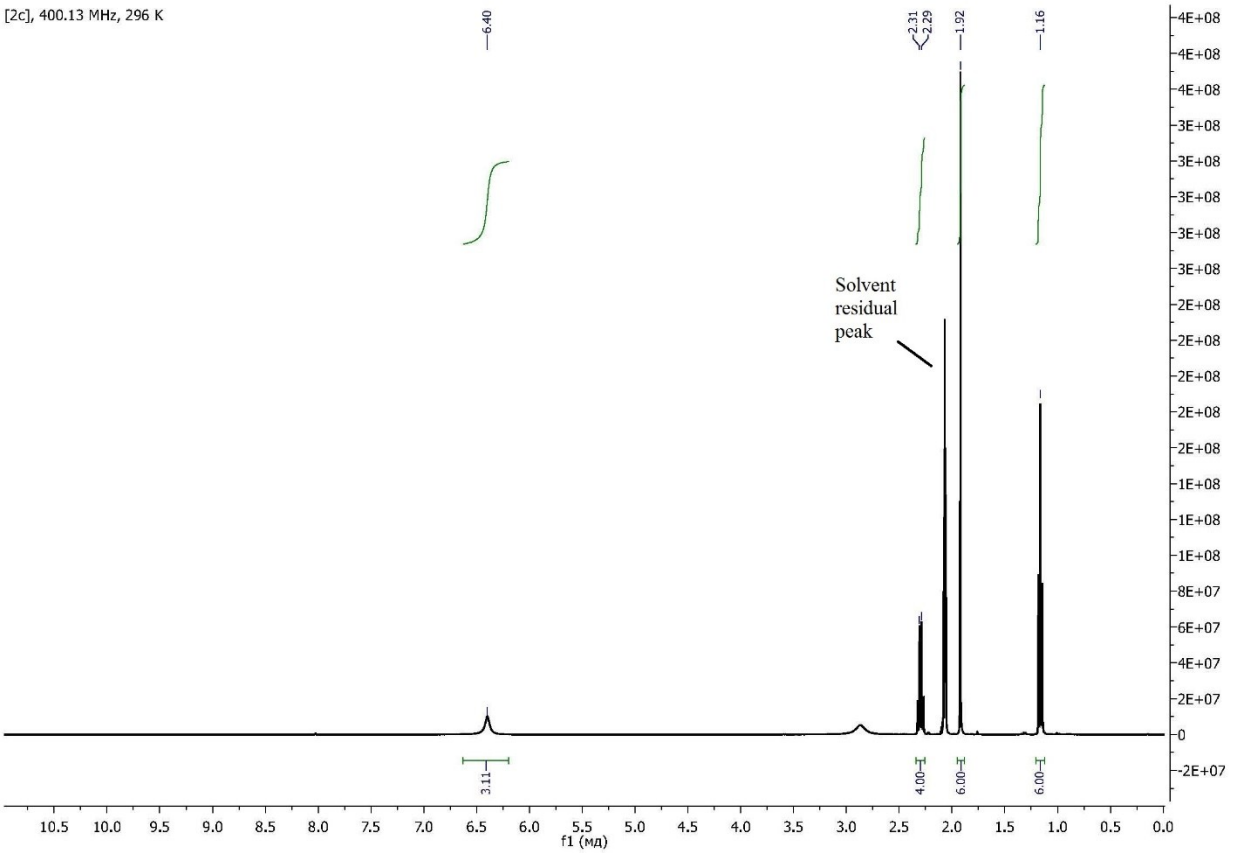

Figure 15S. [1]H NMR spectrum of **2c.**

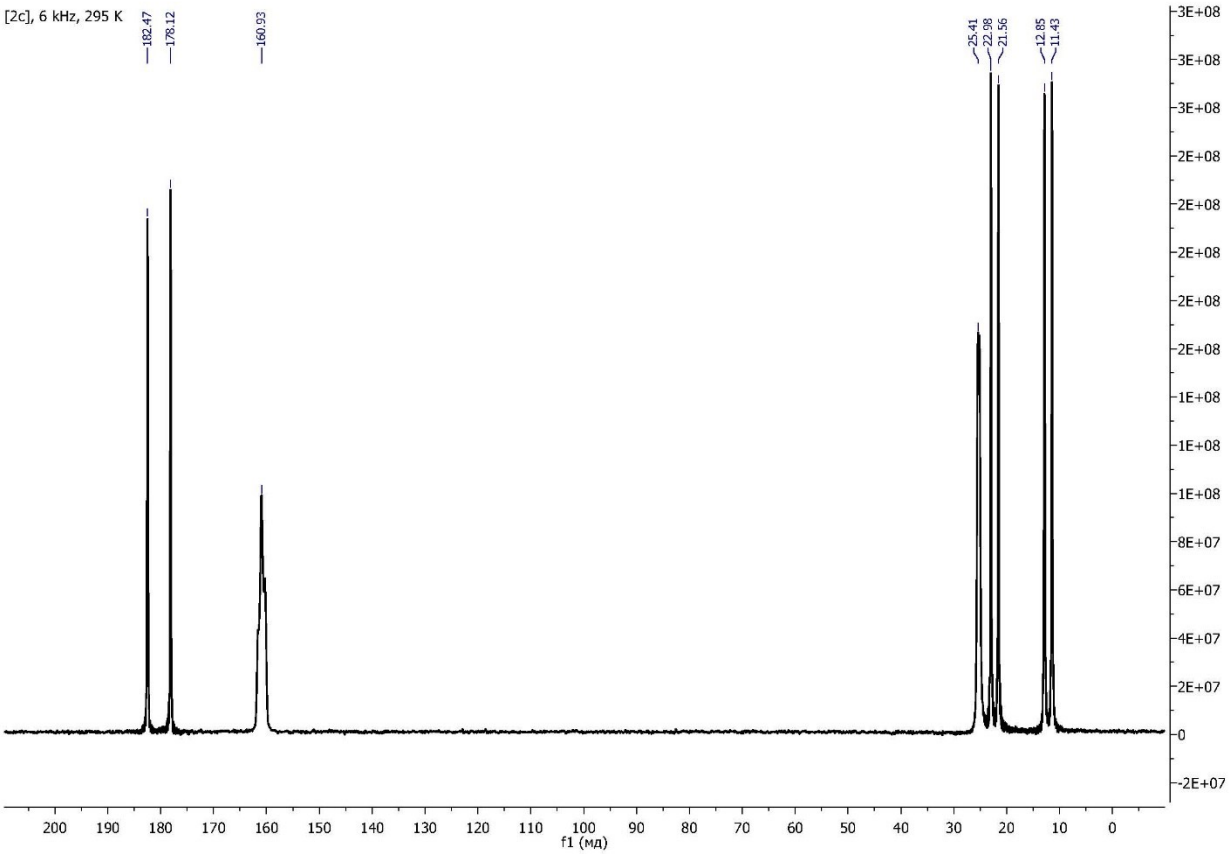

Figure 16S. 13C{1H} CP-MAS TOSS NMR spectrum of **2c.**

2d

Acquisition Parameter					
Source Type	ESI	Ion Polarity	Positive	Set Nebulizer	0.4 Bar
Focus	Not active			Set Dry Heater	180 °C
Scan Begin	50 m/z	Set Capillary	4500 V	Set Dry Gas	4.0 l/min
Scan End	3000 m/z	Set End Plate Offset	-500 V	Set Divert Valve	Source

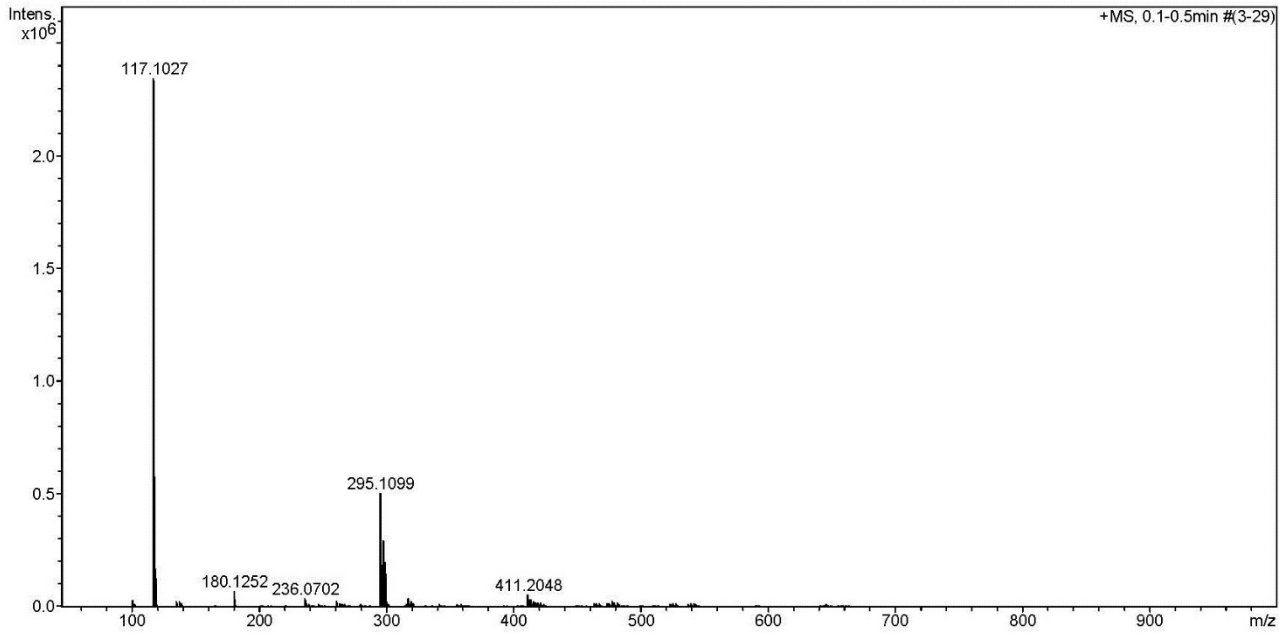

Figure 17S. Positive mass-spectrum of **2d.**

Acquisition Parameter					
Source Type	ESI	Ion Polarity	Negative	Set Nebulizer	0.4 Bar
Focus	Not active			Set Dry Heater	180 °C
Scan Begin	50 m/z	Set Capillary	3500 V	Set Dry Gas	4.0 l/min
Scan End	3000 m/z	Set End Plate Offset	-500 V	Set Divert Valve	Source

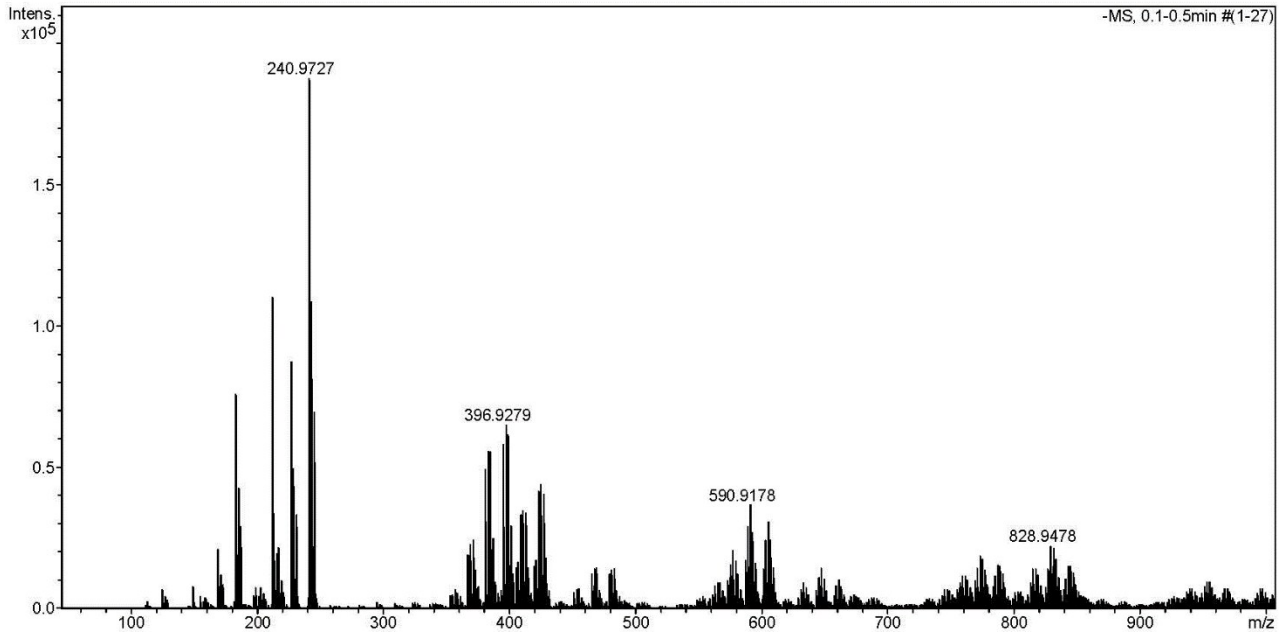

Figure 18S. Negative mass-spectrum of **2d.**

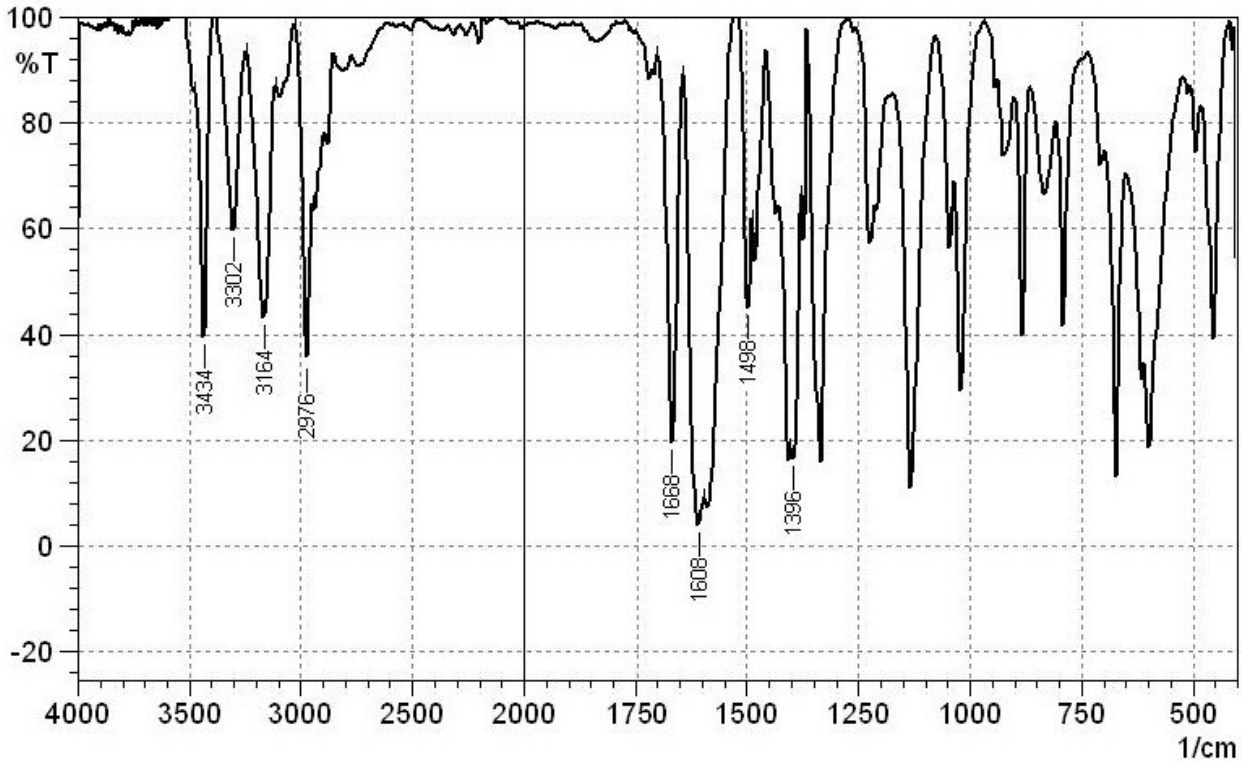

Figure 19S. IR spectrum of **2d.**

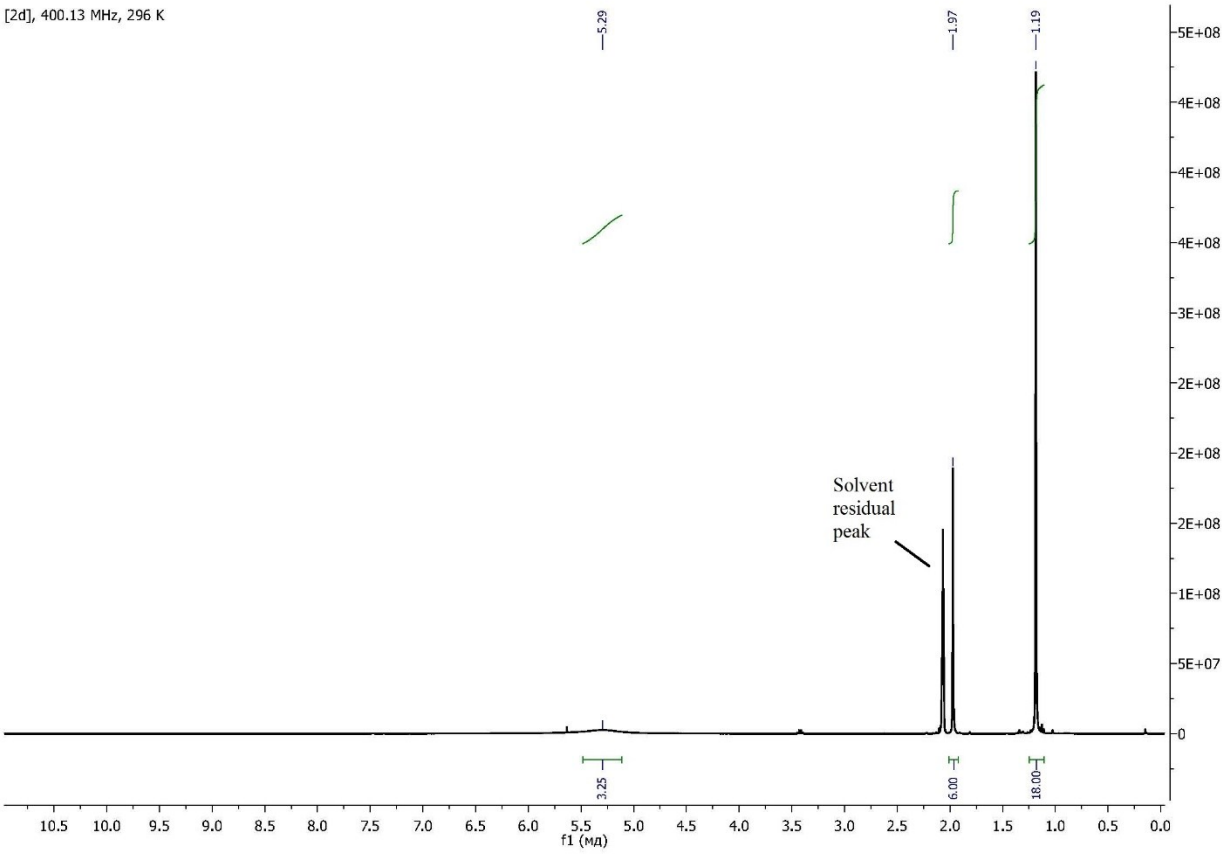

Figure 20S. ^{1}H NMR spectrum of **2d.**

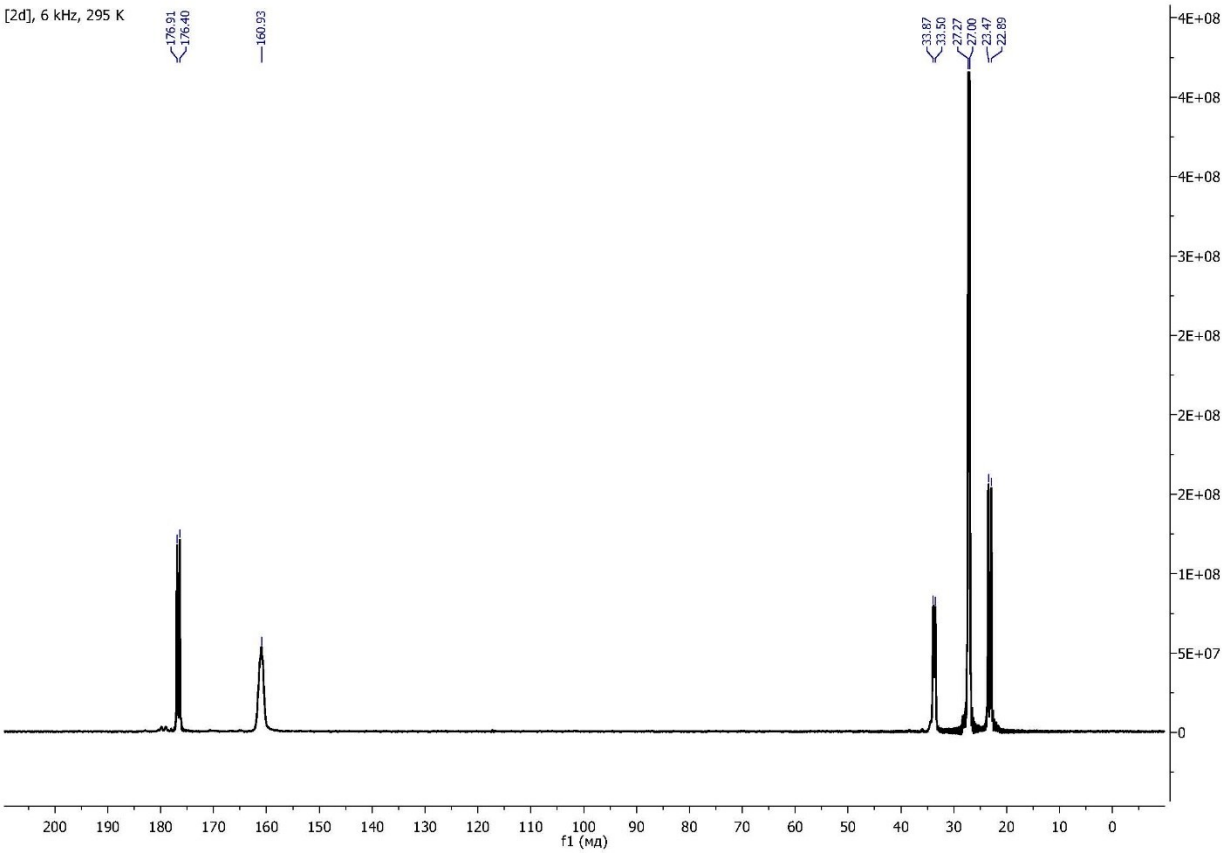

Figure 21S. 13C{1H} CP-MAS TOSS NMR spectrum of **2d.**

Spectra of [3a–d](OTf)$_4$

[**3a**](OTf)$_4$

Acquisition Parameter					
Source Type	ESI	Ion Polarity	Positive	Set Nebulizer	0.4 Bar
Focus	Not active			Set Dry Heater	180 °C
Scan Begin	50 m/z	Set Capillary	4500 V	Set Dry Gas	4.0 l/min
Scan End	3000 m/z	Set End Plate Offset	-500 V	Set Divert Valve	Source

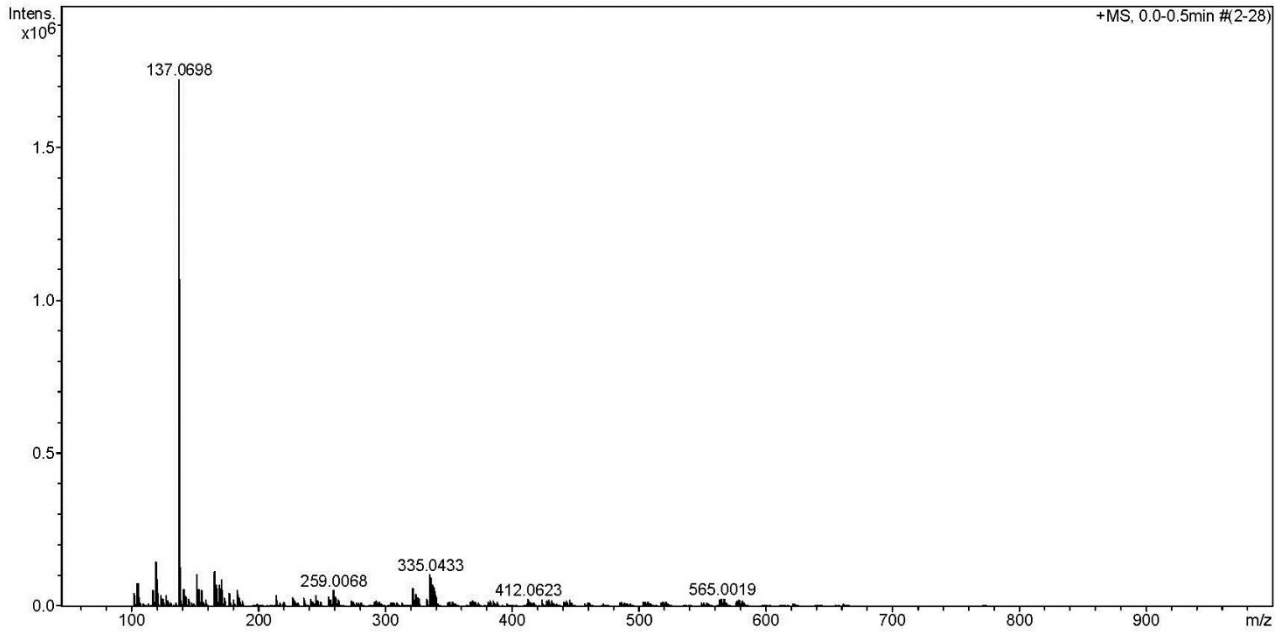

Figure 22S. Positive mass-spectrum of [**3a**](OTf)$_4$.

Acquisition Parameter					
Source Type	ESI	Ion Polarity	Negative	Set Nebulizer	0.4 Bar
Focus	Not active			Set Dry Heater	180 °C
Scan Begin	50 m/z	Set Capillary	3500 V	Set Dry Gas	4.0 l/min
Scan End	3000 m/z	Set End Plate Offset	-500 V	Set Divert Valve	Source

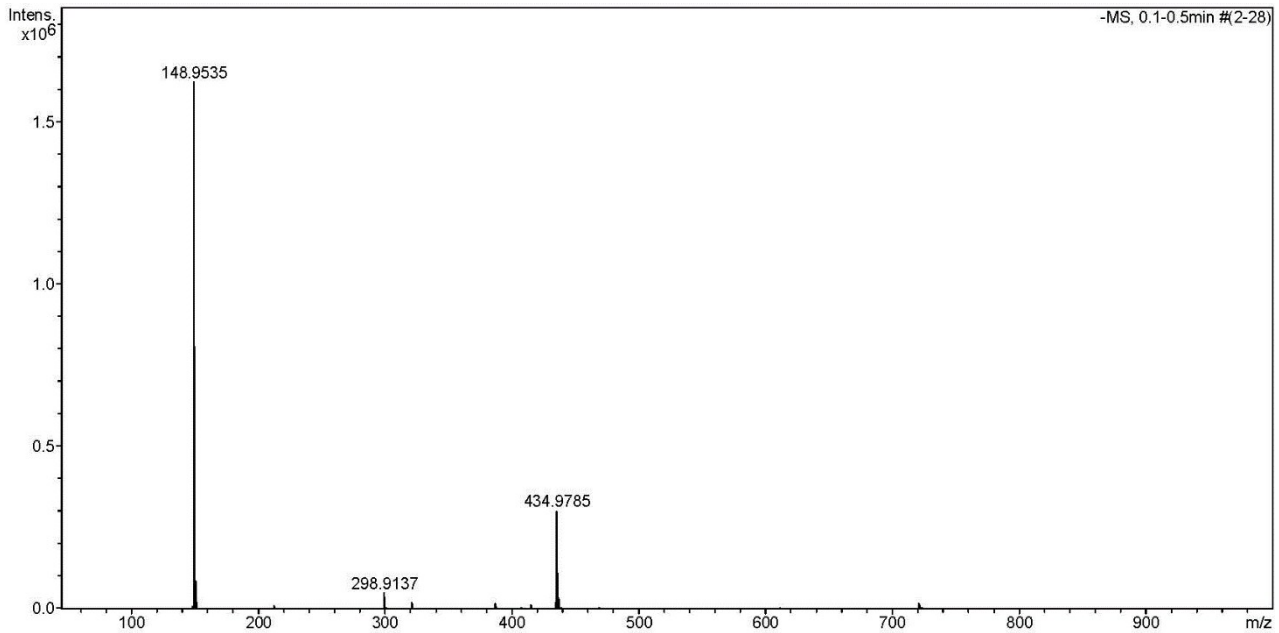

Figure 23S. Negative mass-spectrum of [**3a**](OTf)$_4$.

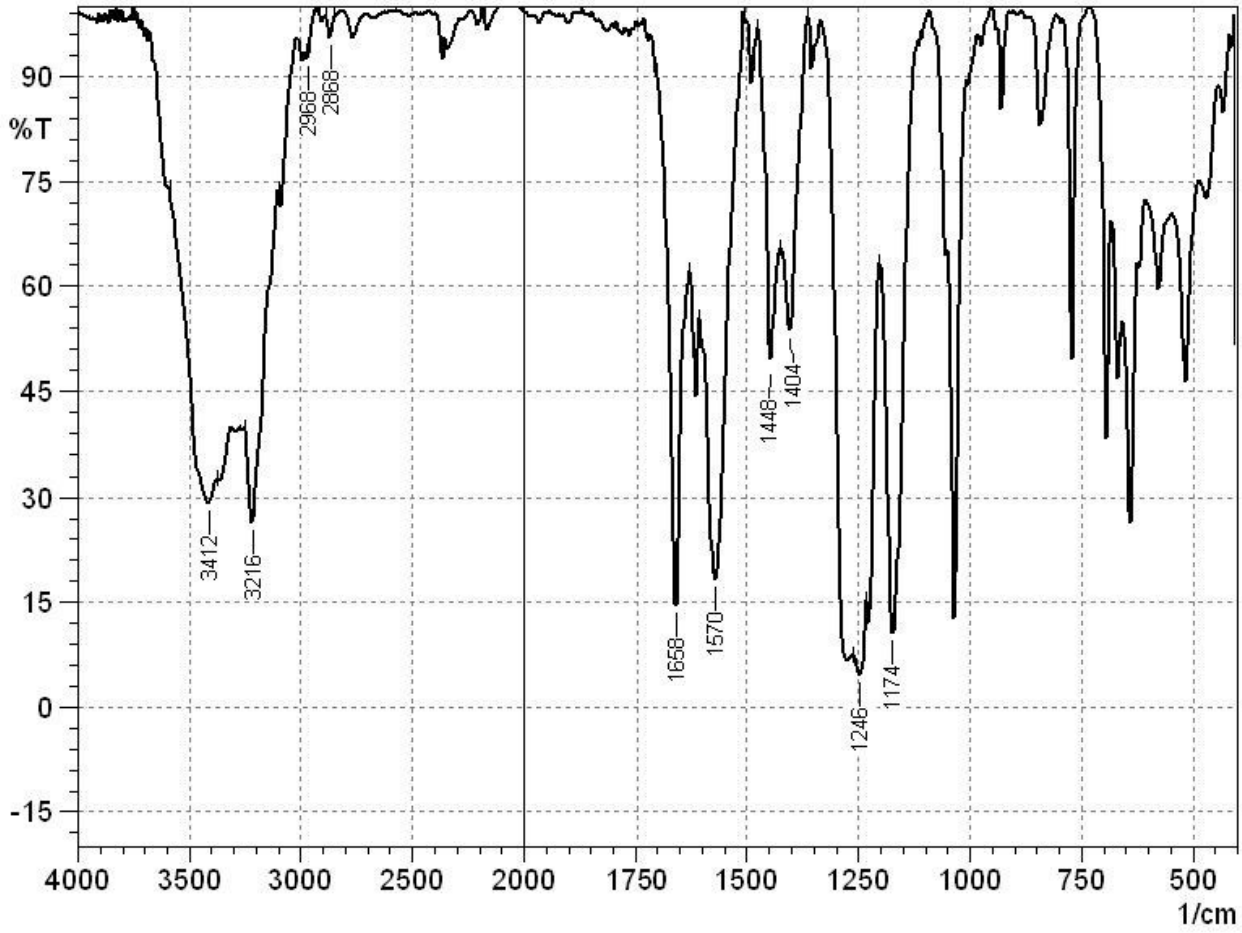

Figure 24S. IR spectrum of [**3a**](OTf)$_4$.

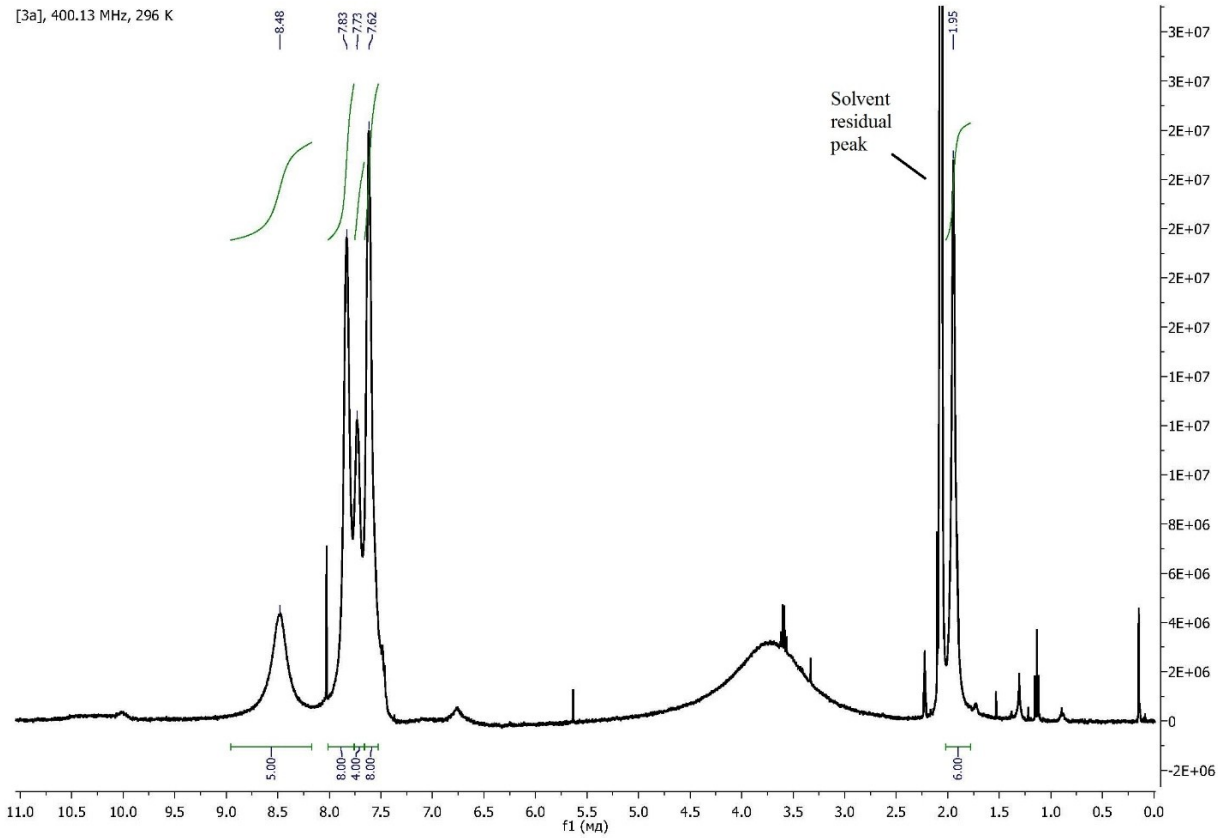

Figure 25S. ^{1}H NMR spectrum of [**3a**](OTf)$_4$.

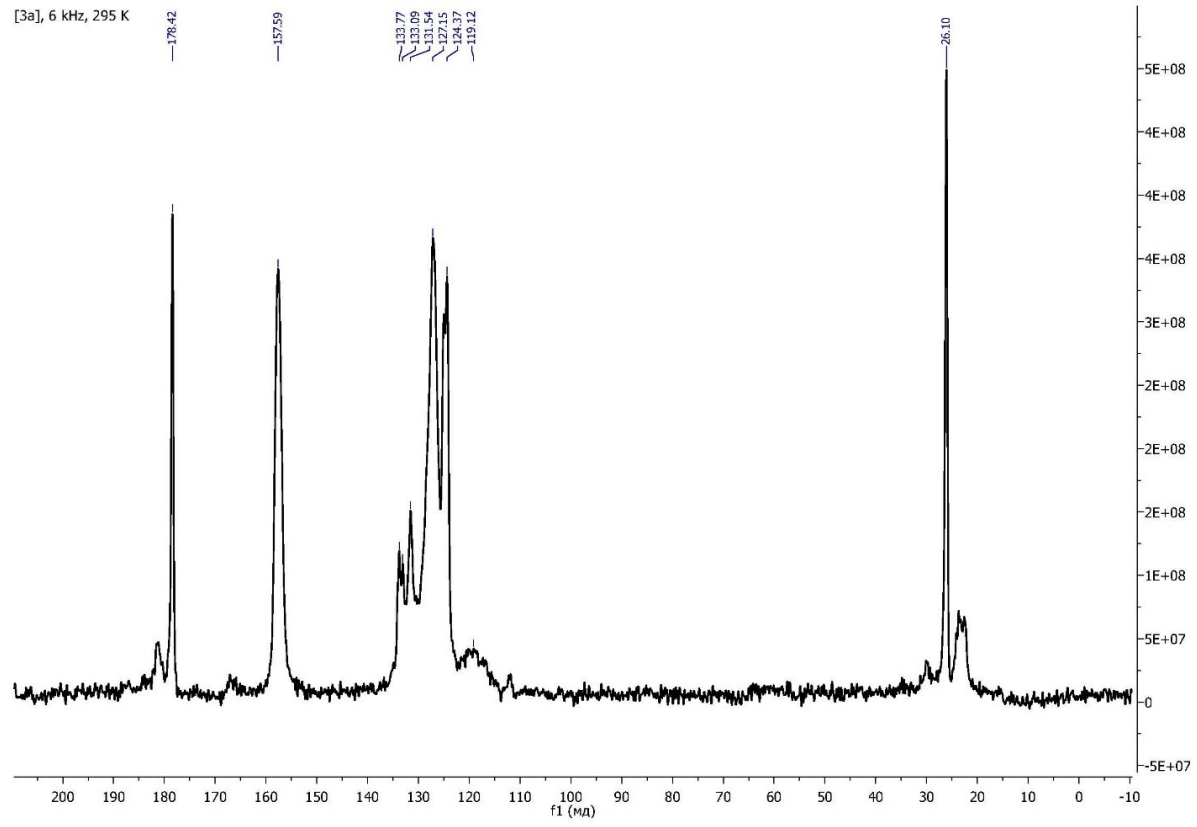

Figure 26S. 13C{1H} CP-MAS TOSS NMR spectrum of [**3a**](OTf)$_4$.

[**3b**](OTf)$_4$

Acquisition Parameter

Source Type	ESI	Ion Polarity	Positive	Set Nebulizer	0.4 Bar
Focus	Not active			Set Dry Heater	180 °C
Scan Begin	50 m/z	Set Capillary	4500 V	Set Dry Gas	4.0 l/min
Scan End	3000 m/z	Set End Plate Offset	-500 V	Set Divert Valve	Source

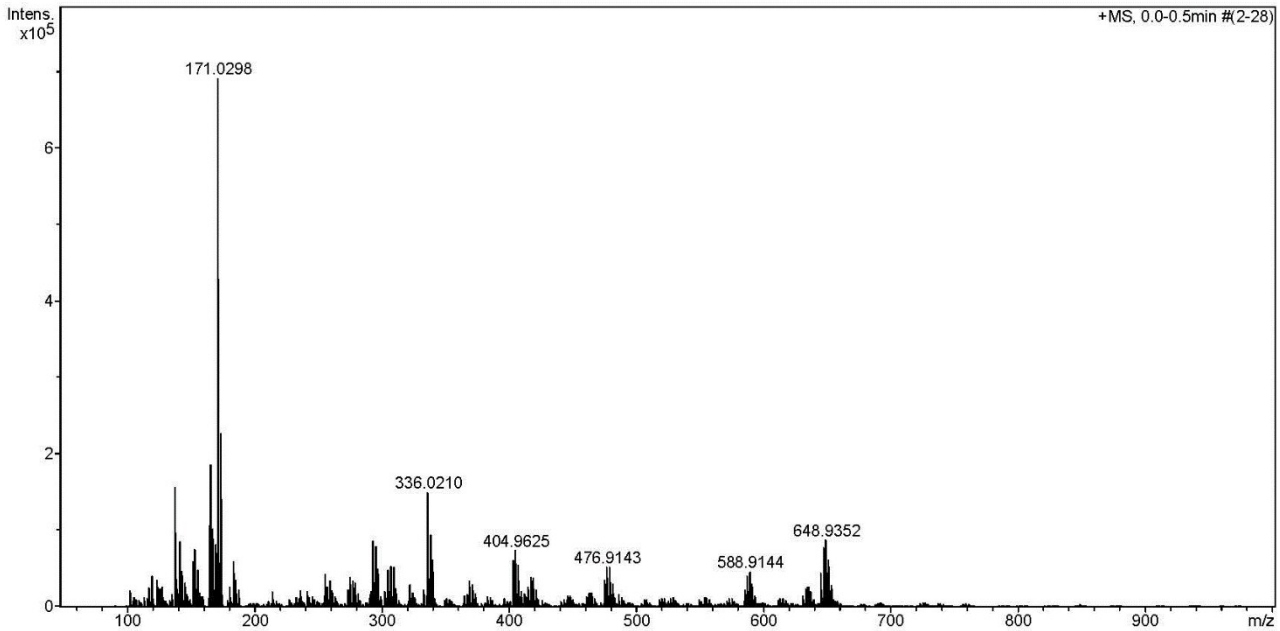

Figure 27S. Positive mass-spectrum of [**3b**](OTf)$_4$.

Acquisition Parameter

Source Type	ESI	Ion Polarity	Negative	Set Nebulizer	0.4 Bar
Focus	Not active			Set Dry Heater	180 °C
Scan Begin	50 m/z	Set Capillary	3500 V	Set Dry Gas	4.0 l/min
Scan End	3000 m/z	Set End Plate Offset	-500 V	Set Divert Valve	Source

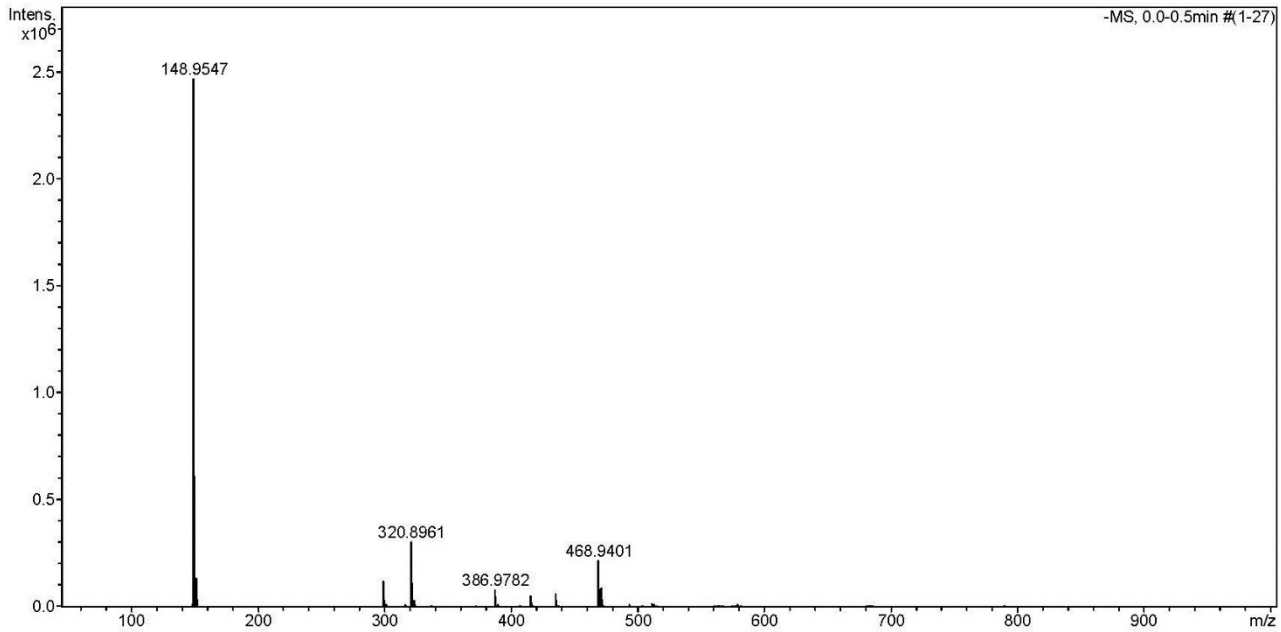

Figure 28S. Negative mass-spectrum of [**3b**](OTf)$_4$.

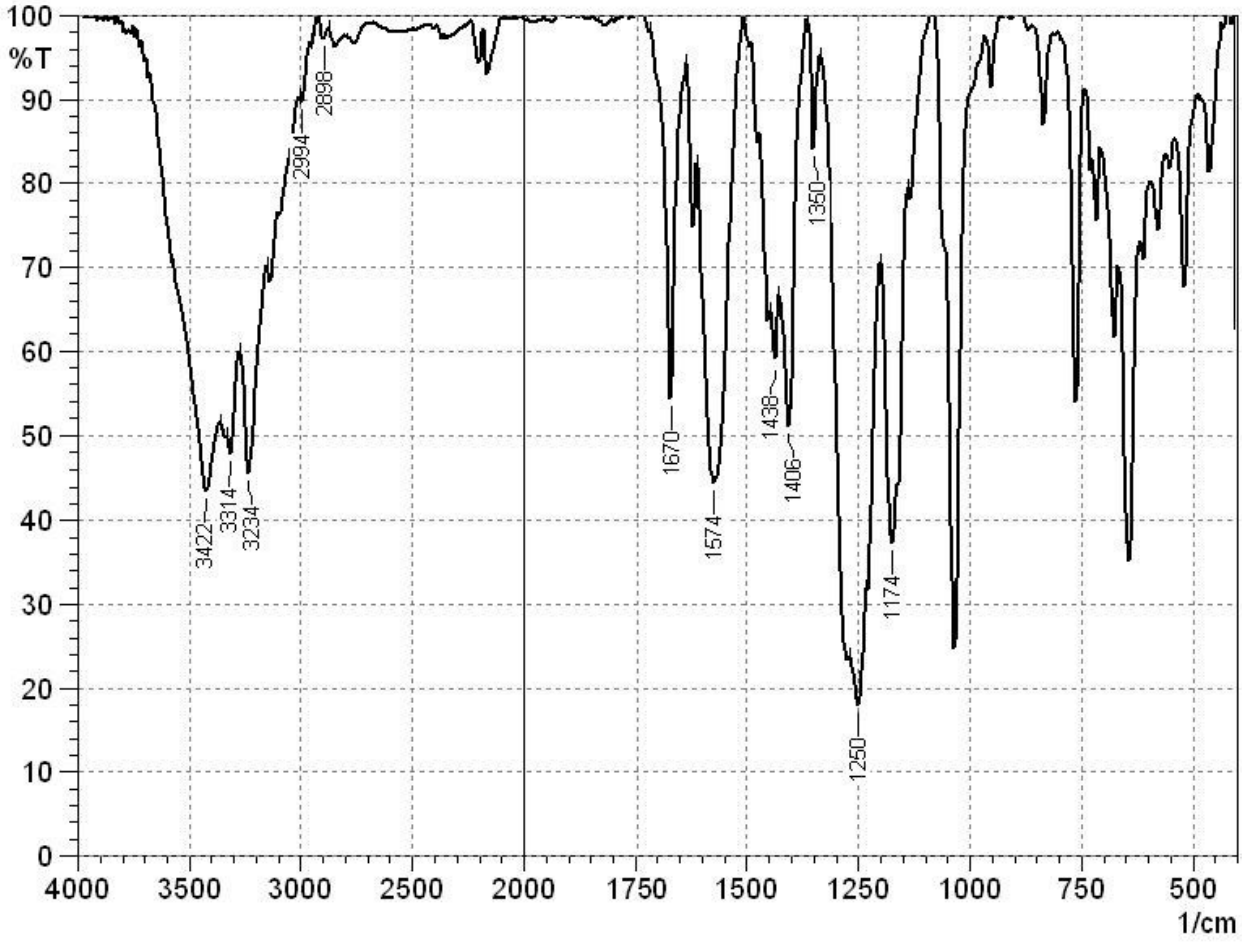

Figure 29S. IR spectrum of [**3b**](OTf)$_4$.

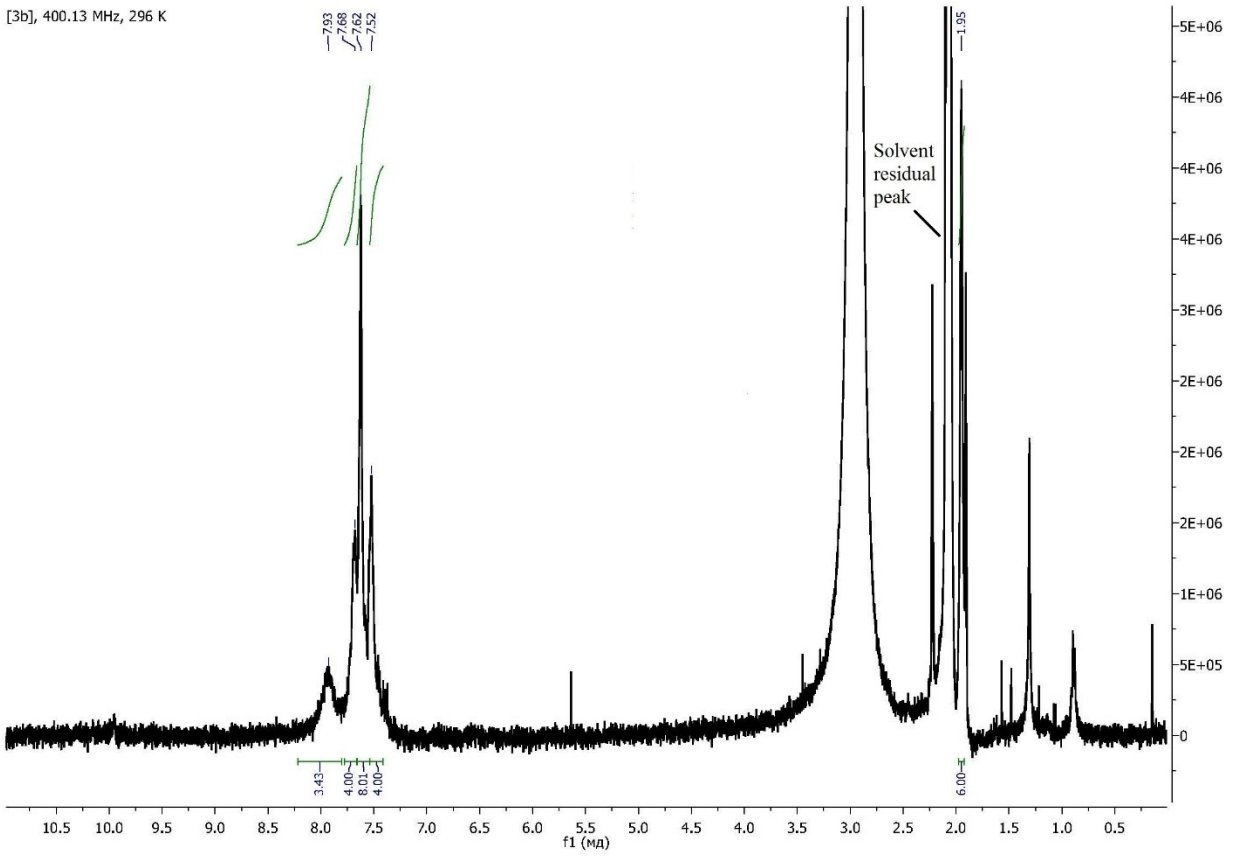

Figure 30S. ^{1}H NMR spectrum of [**3b**](OTf)$_4$.

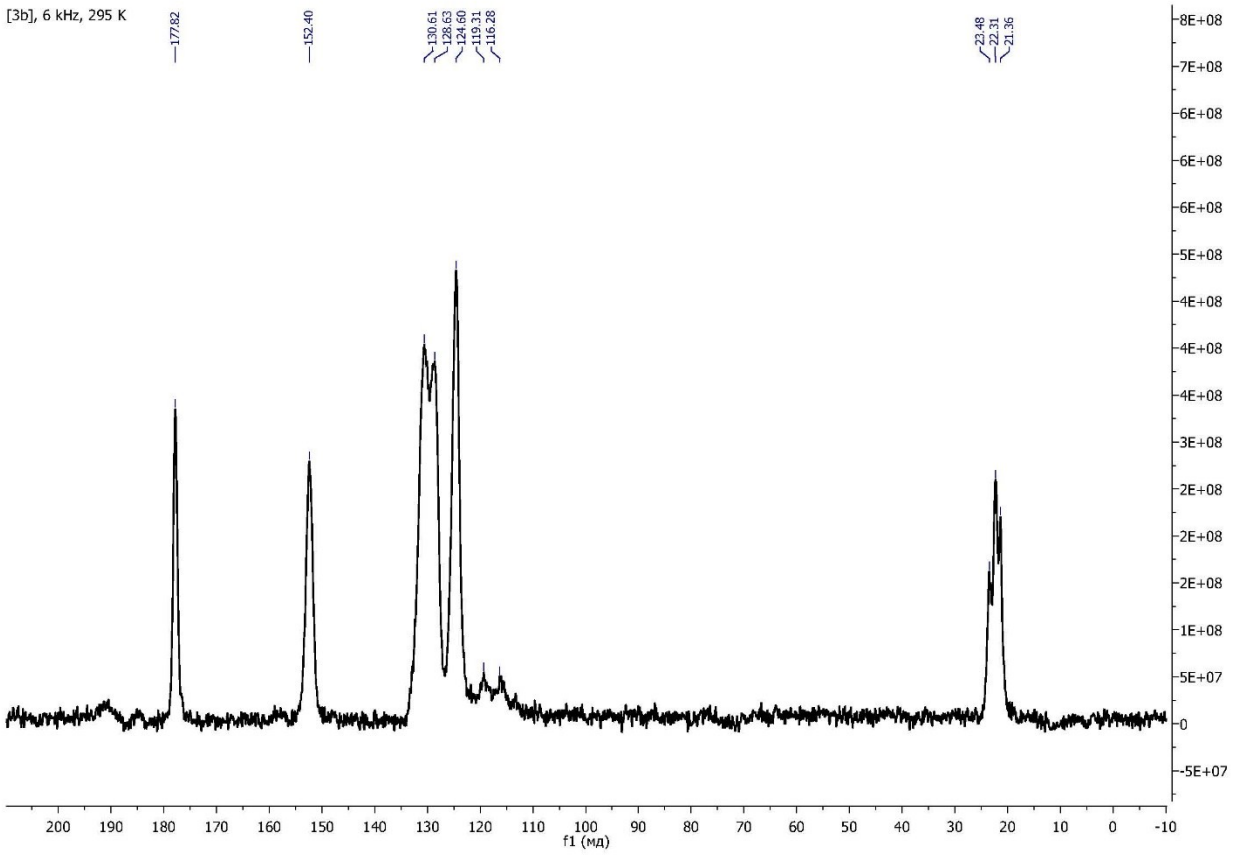

Figure 31S. 13C{1H} CP-MAS TOSS NMR spectrum of [**3b**](OTf)$_4$.

[**3c**](OTf)$_4$

Acquisition Parameter

Source Type	ESI	Ion Polarity	Positive	Set Nebulizer	0.4 Bar
Focus	Not active			Set Dry Heater	180 °C
Scan Begin	50 m/z	Set Capillary	4500 V	Set Dry Gas	4.0 l/min
Scan End	3000 m/z	Set End Plate Offset	-500 V	Set Divert Valve	Source

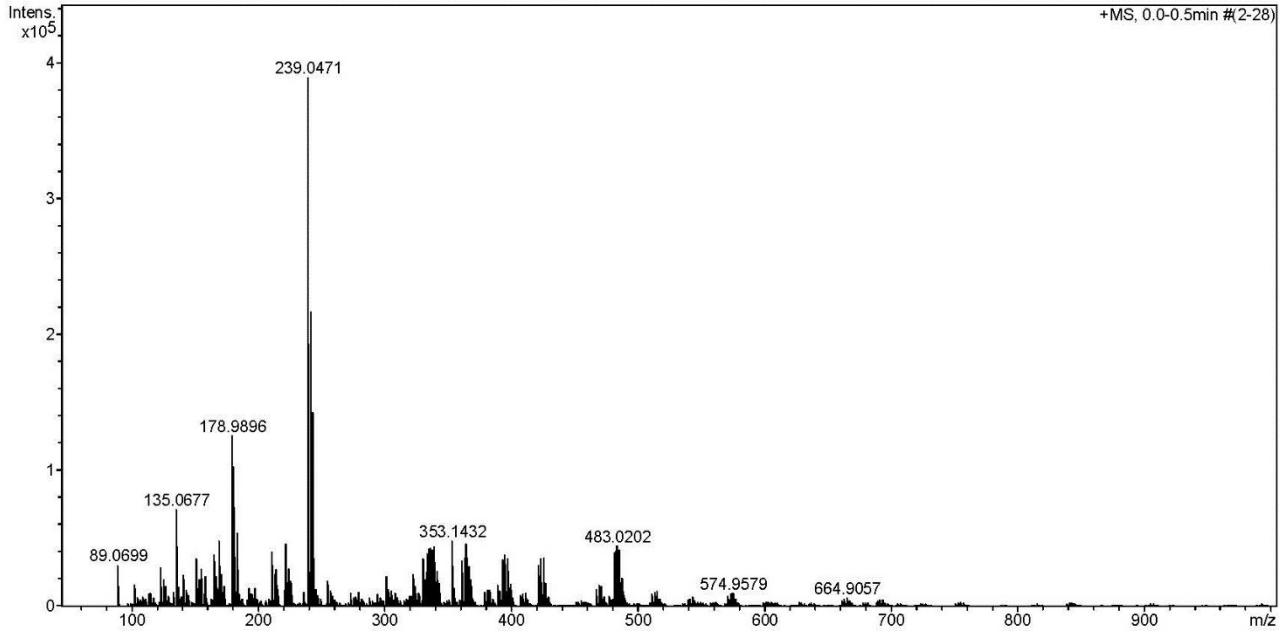

Figure 32S. Positive mass-spectrum of [**3c**](OTf)$_4$.

Acquisition Parameter

Source Type	ESI	Ion Polarity	Negative	Set Nebulizer	0.4 Bar
Focus	Not active			Set Dry Heater	180 °C
Scan Begin	50 m/z	Set Capillary	3500 V	Set Dry Gas	4.0 l/min
Scan End	3000 m/z	Set End Plate Offset	-500 V	Set Divert Valve	Source

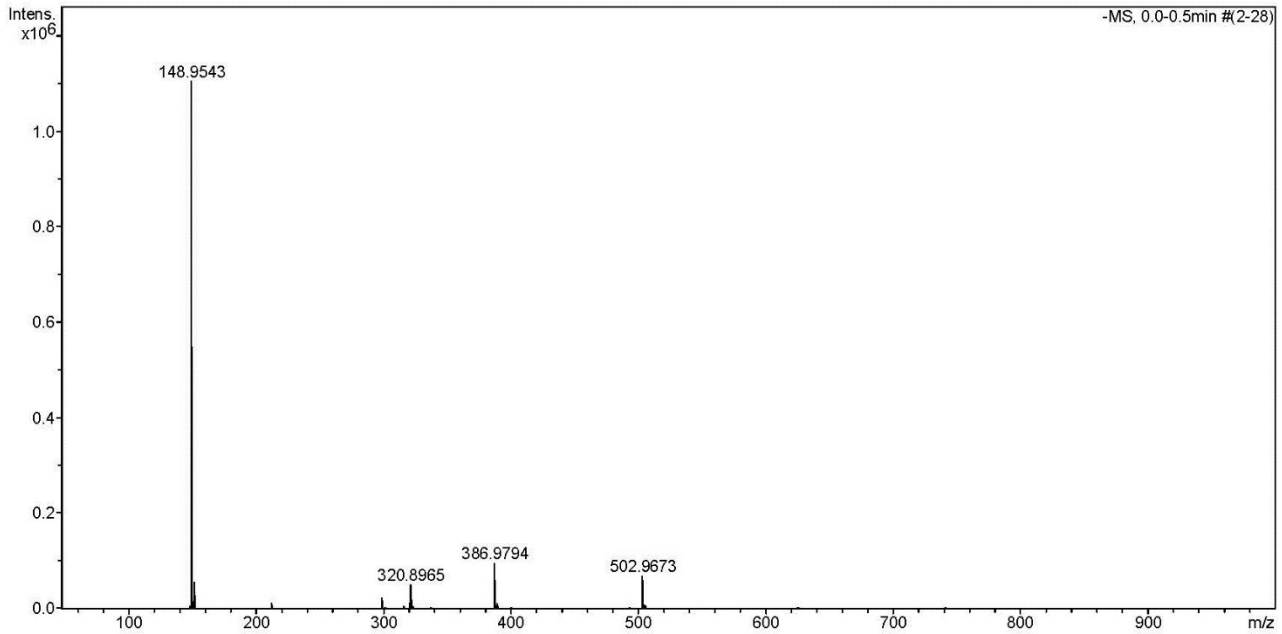

Figure 33S. Negative mass-spectrum of [**3c**](OTf)$_4$.

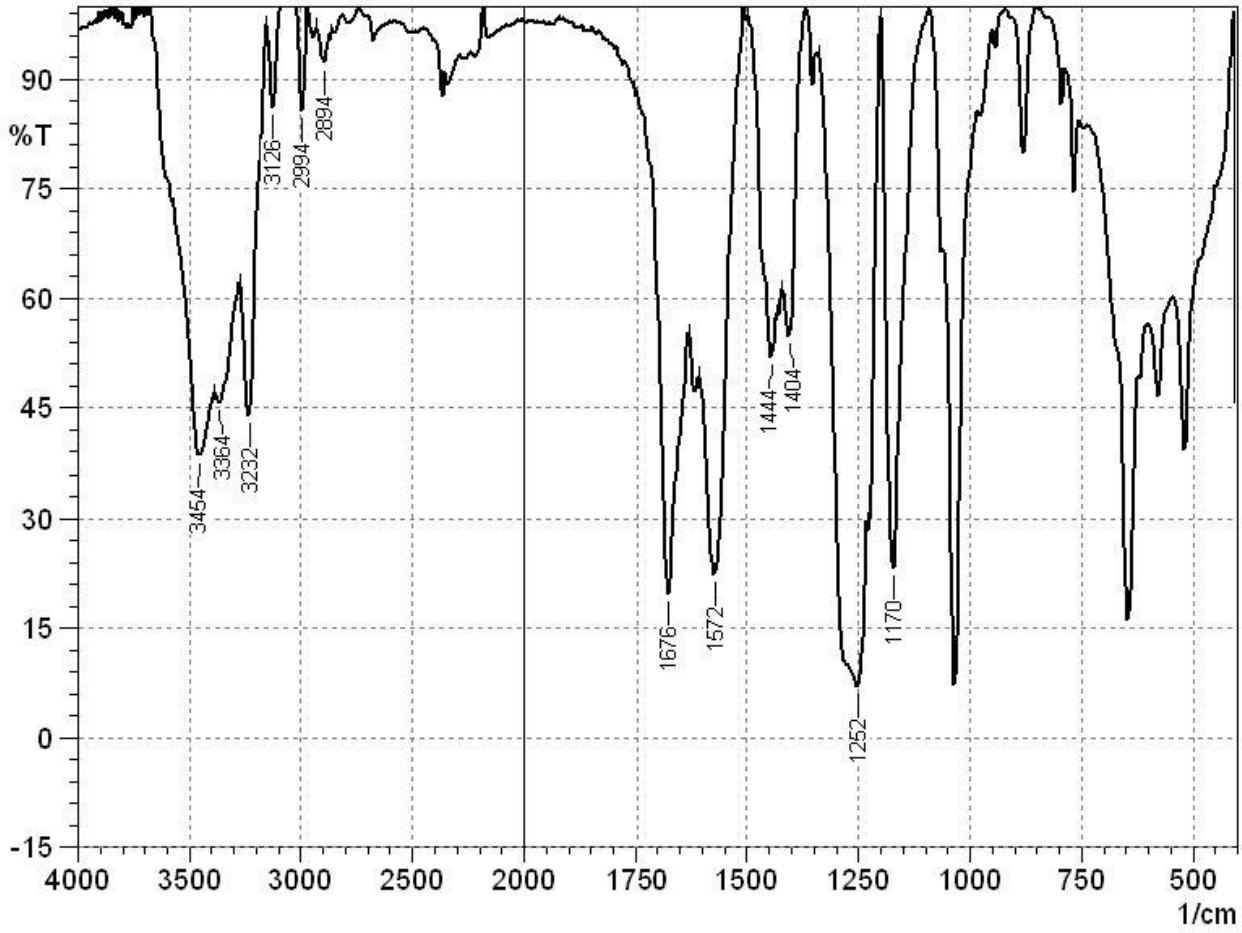

Figure 34S. IR spectrum of [**3c**](OTf)$_4$.

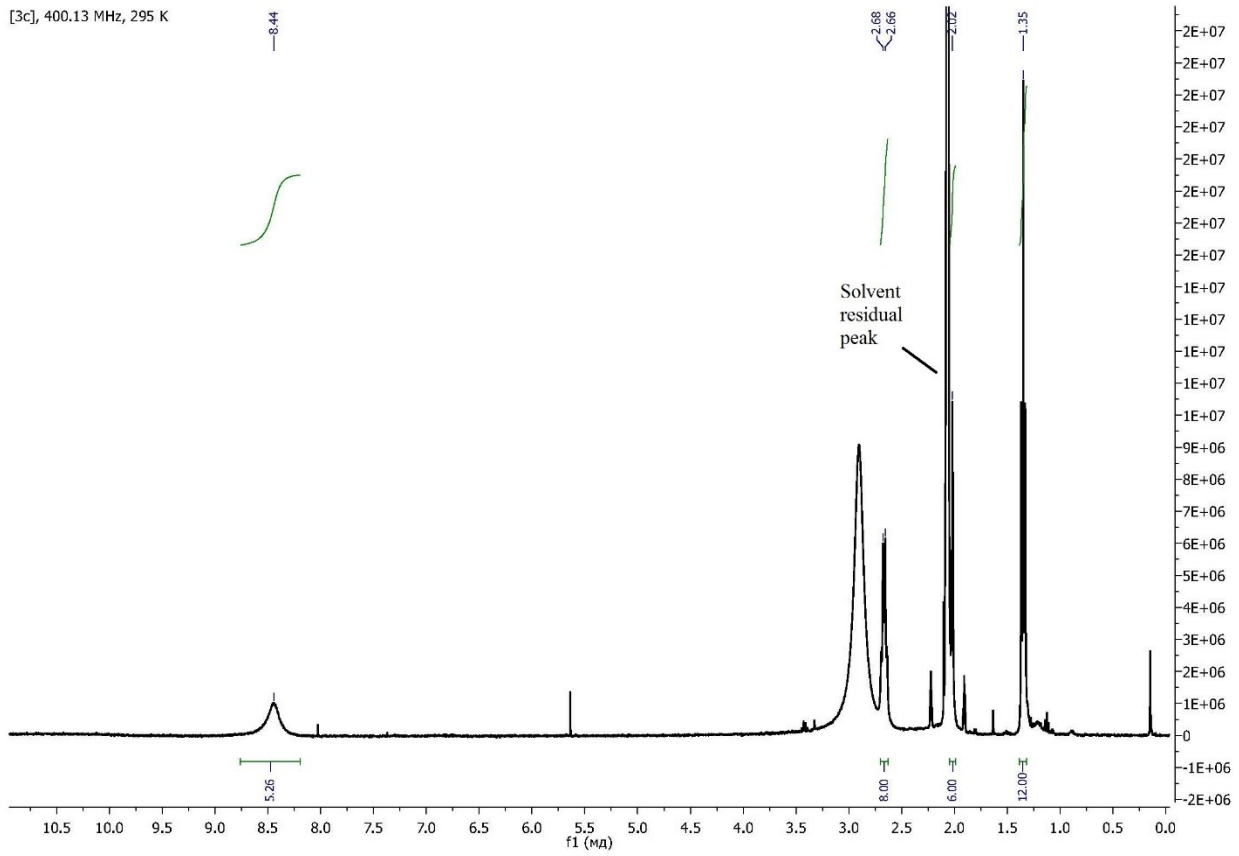

Figure 35S. ^{1}H NMR spectrum of [**3c**](OTf)$_4$.

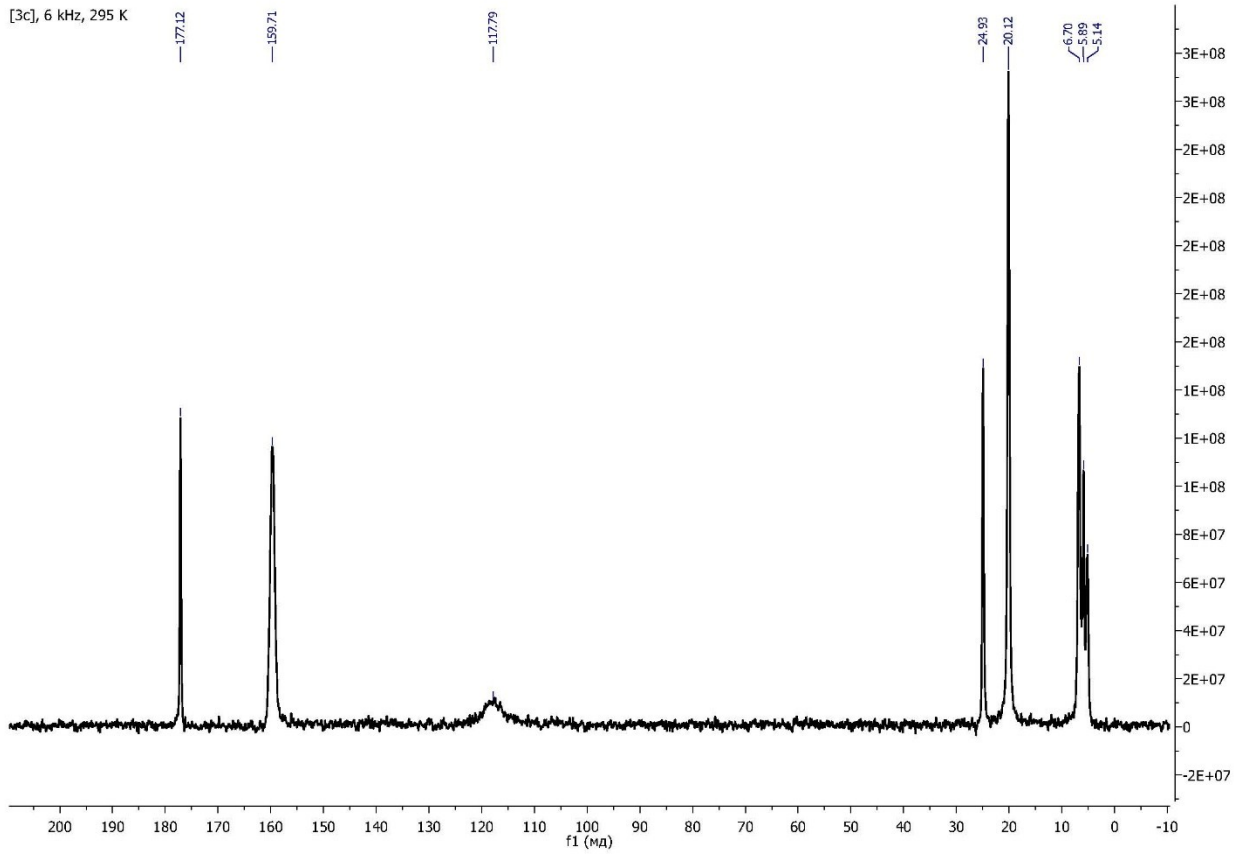

Figure 36S. 13C{1H} CP-MAS TOSS NMR spectrum of [**3c**](OTf)$_4$.

[**3d**](OTf)$_4$

Acquisition Parameter

Source Type	ESI	Ion Polarity	Positive	Set Nebulizer	0.4 Bar
Focus	Not active			Set Dry Heater	180 °C
Scan Begin	50 m/z	Set Capillary	4500 V	Set Dry Gas	4.0 l/min
Scan End	3000 m/z	Set End Plate Offset	-500 V	Set Divert Valve	Source

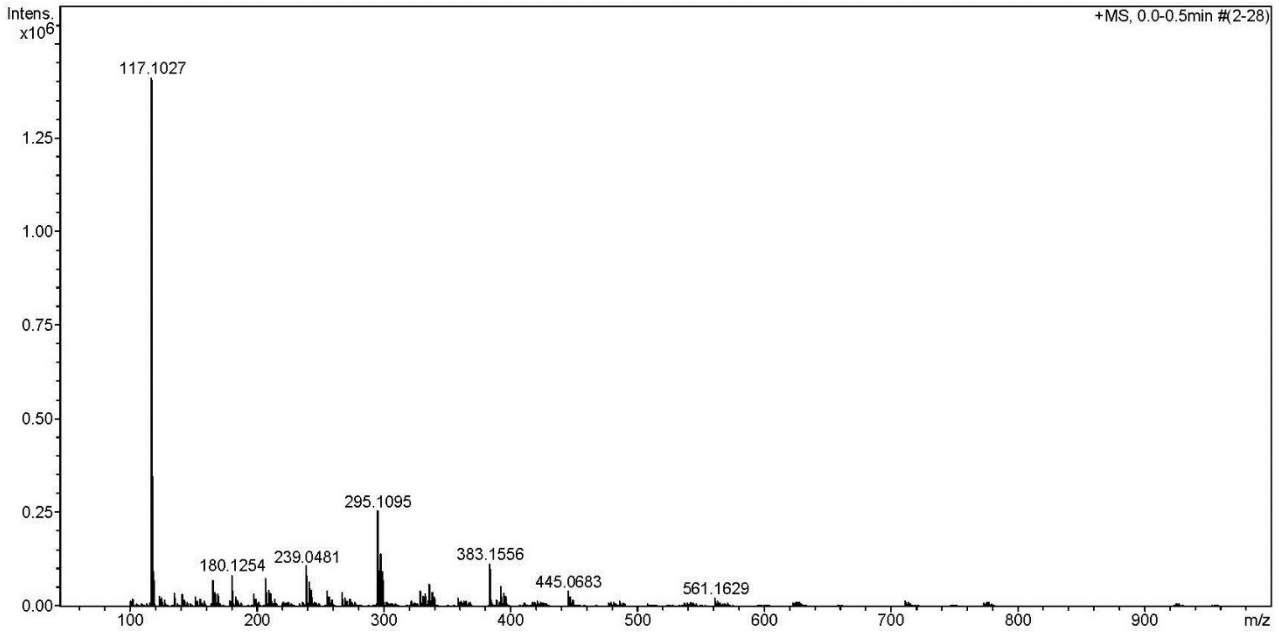

Figure 37S. Positive mass-spectrum of [**3d**](OTf)$_4$.

Acquisition Parameter

Source Type	ESI	Ion Polarity	Negative	Set Nebulizer	0.4 Bar
Focus	Not active			Set Dry Heater	180 °C
Scan Begin	50 m/z	Set Capillary	3500 V	Set Dry Gas	4.0 l/min
Scan End	3000 m/z	Set End Plate Offset	-500 V	Set Divert Valve	Source

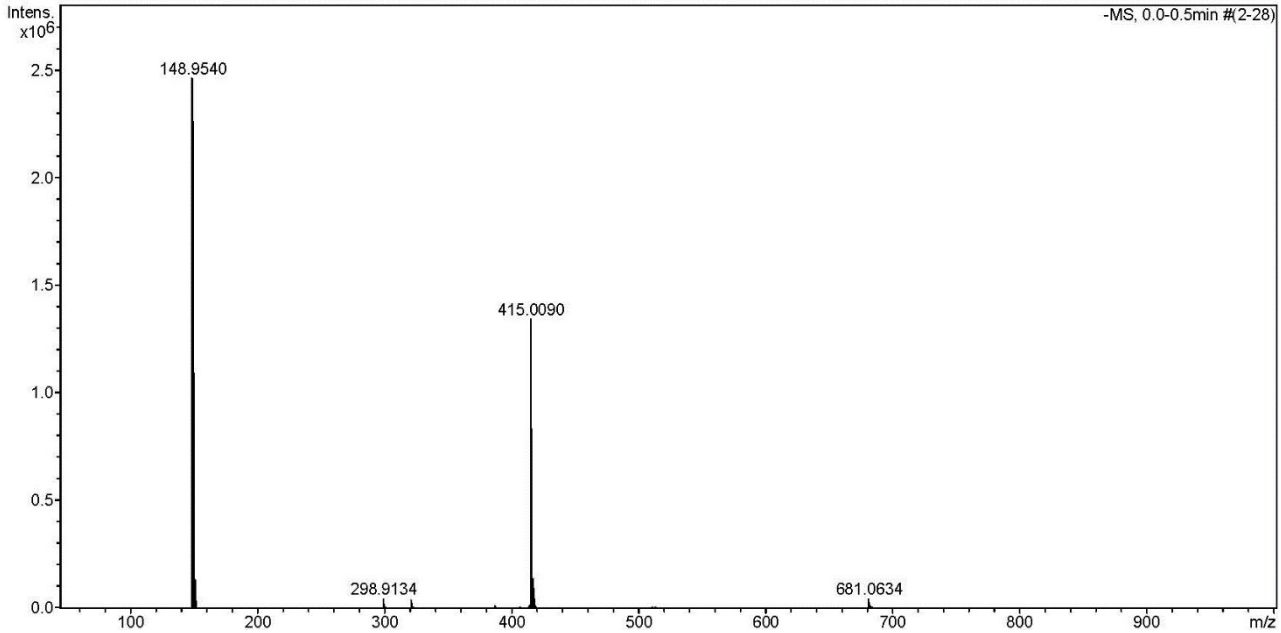

Figure 38S. Negative mass-spectrum of [**3d**](OTf)$_4$.

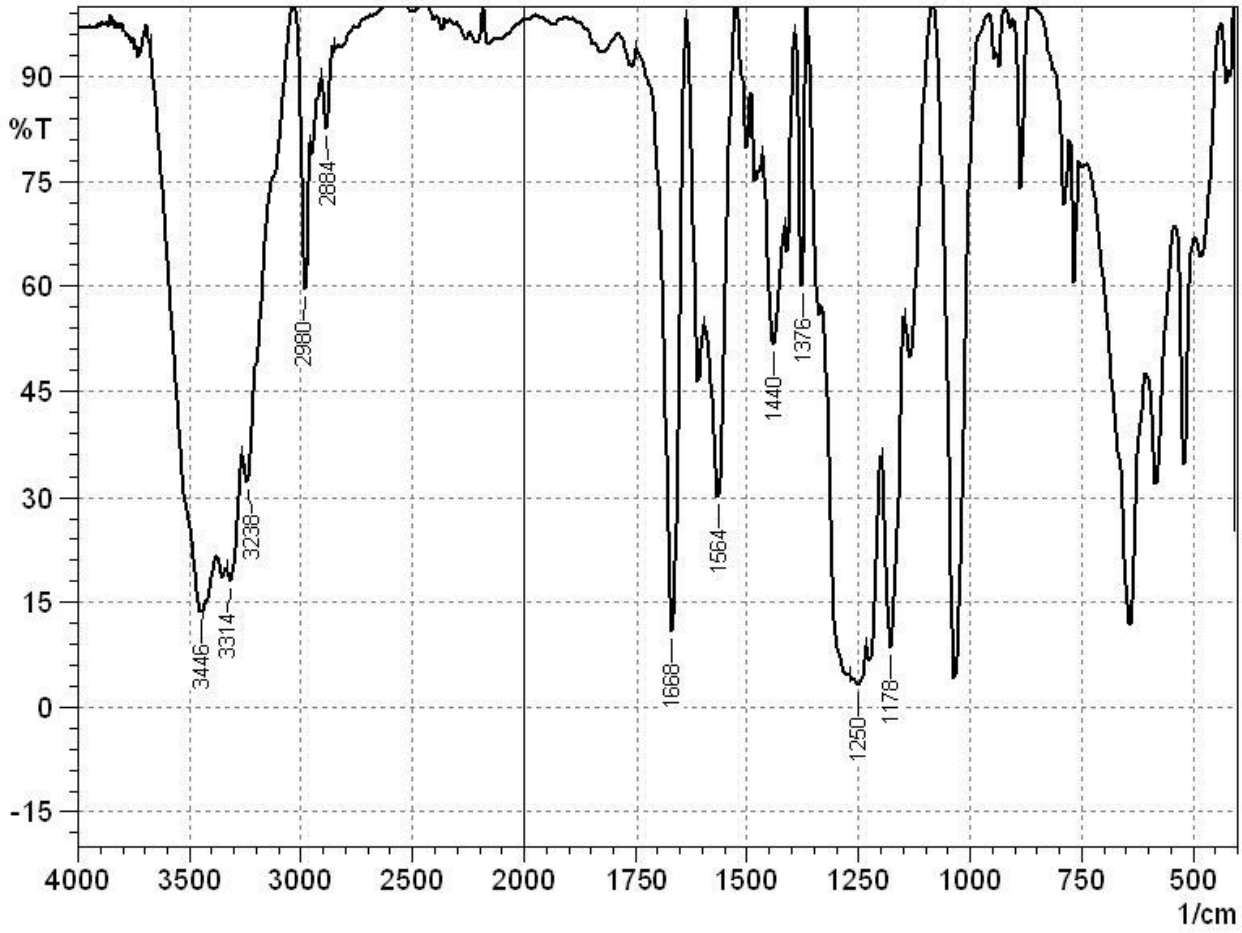

Figure 39S. IR spectrum of [**3d**](OTf)$_4$.

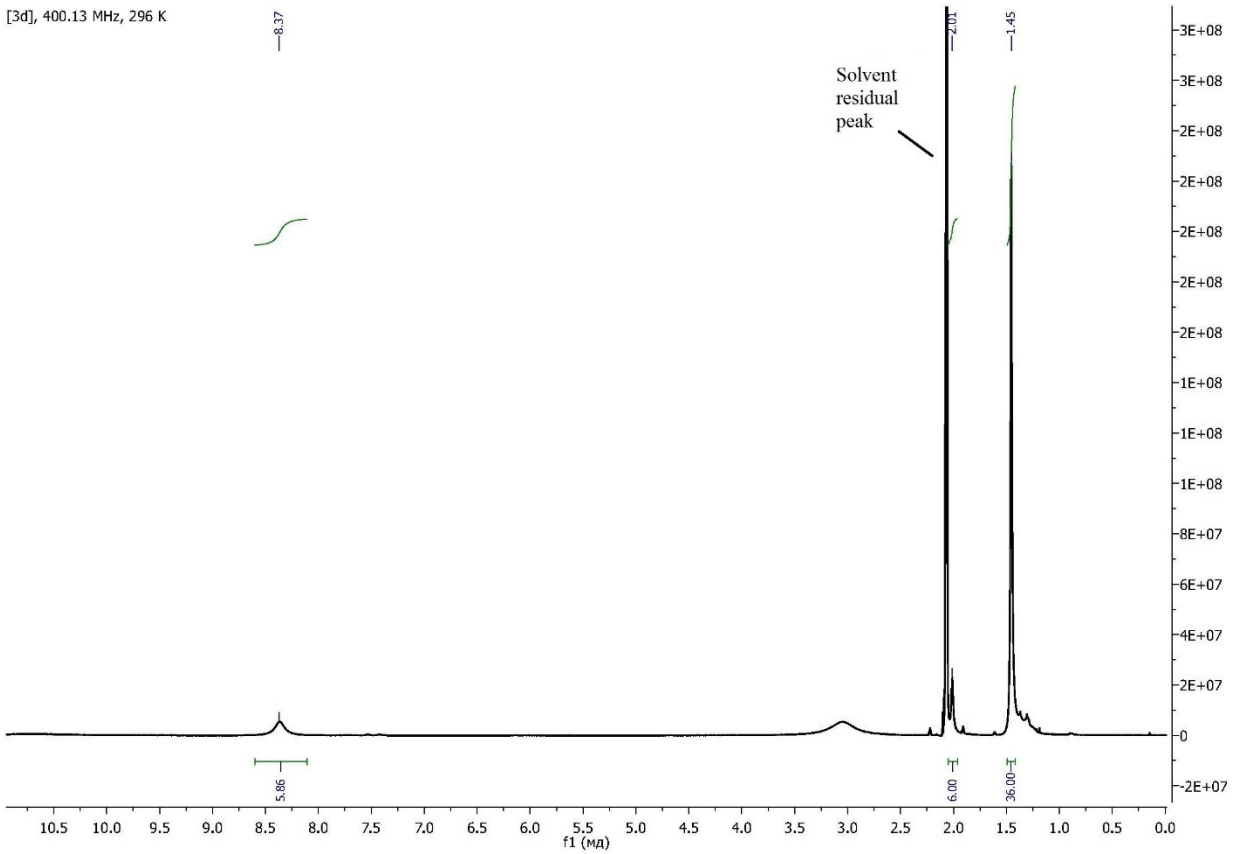

Figure 40S. ^{1}H NMR spectrum of [**3d**](OTf)$_4$.

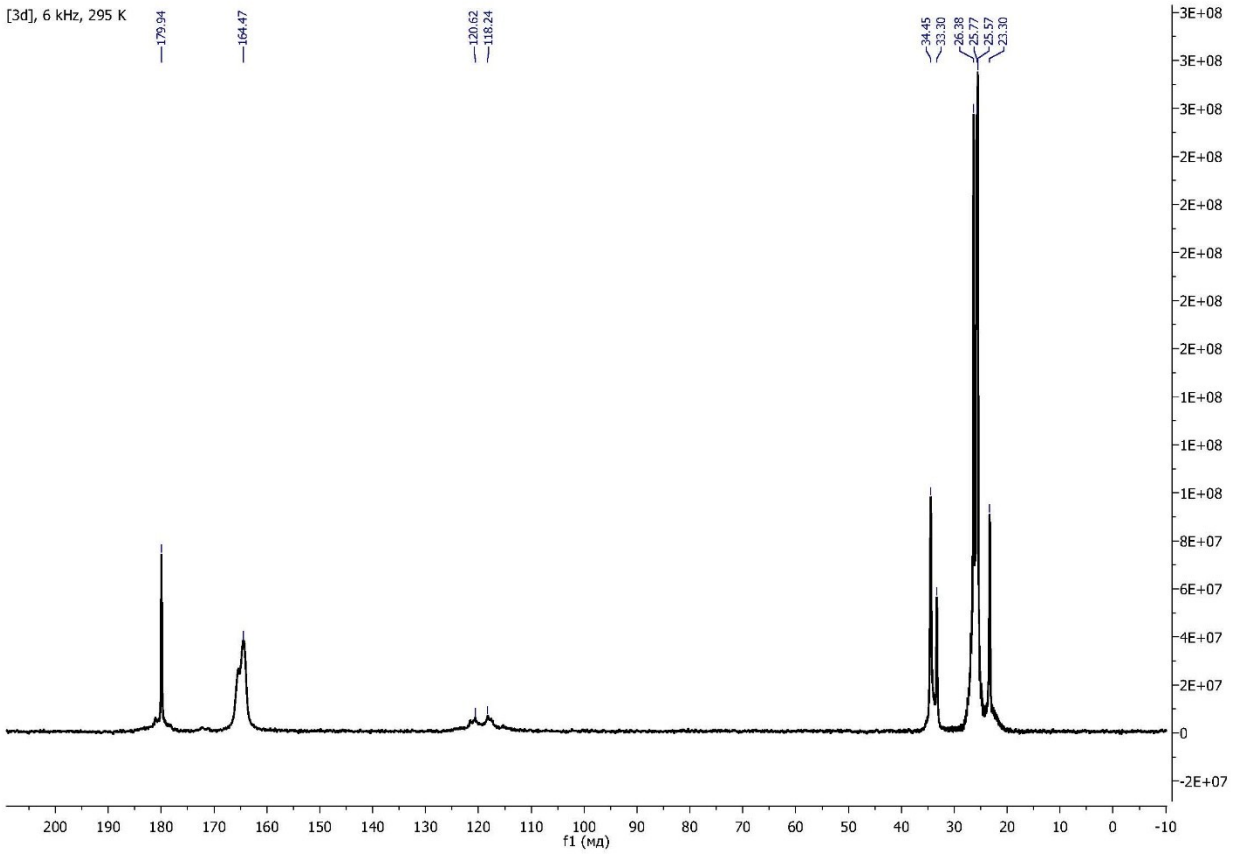

Figure 41S. 13C{1H} CP-MAS TOSS NMR spectrum of [**3d**](OTf)$_4$.

Spectra of [**4a–c**$(OTf)_2$]

[**4a**$(OTf)_2$]

Acquisition Parameter

Source Type	ESI	Ion Polarity	Positive	Set Nebulizer	1.0 Bar
Focus	Not active			Set Dry Heater	180 °C
Scan Begin	50 m/z	Set Capillary	4500 V	Set Dry Gas	6.0 l/min
Scan End	3000 m/z	Set End Plate Offset	-500 V	Set Divert Valve	Source

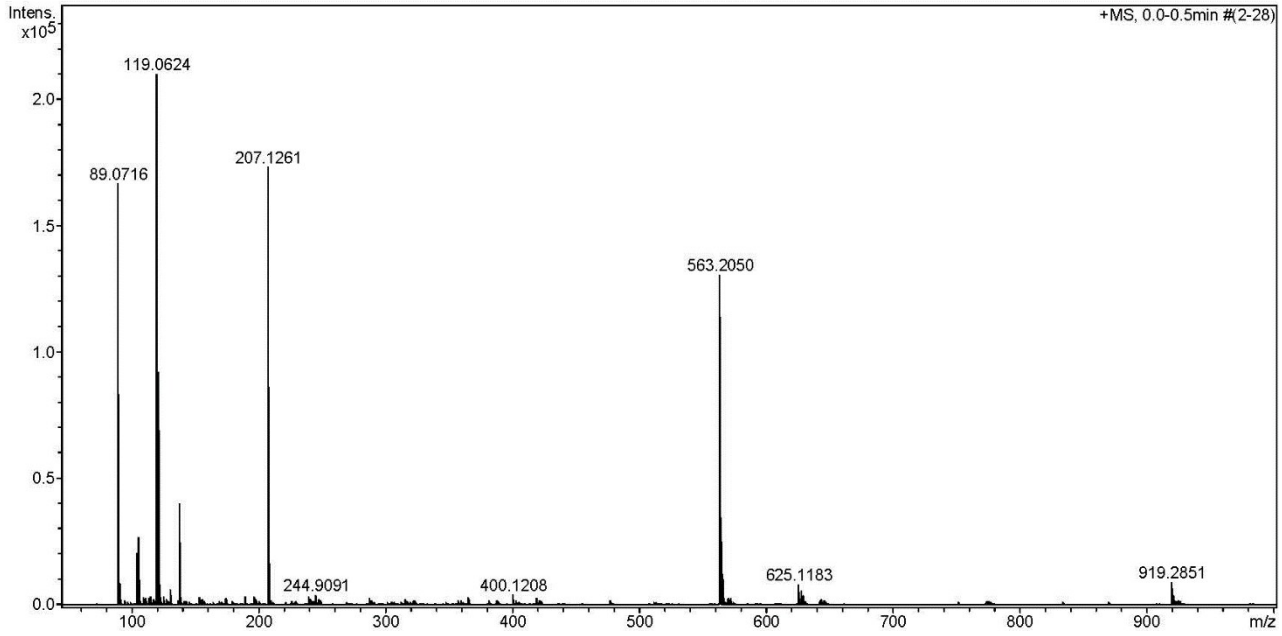

Figure 42S. Positive mass-spectrum of [**4a**$(OTf)_2$].

Acquisition Parameter

Source Type	ESI	Ion Polarity	Negative	Set Nebulizer	1.0 Bar
Focus	Not active			Set Dry Heater	180 °C
Scan Begin	50 m/z	Set Capillary	3500 V	Set Dry Gas	6.0 l/min
Scan End	3000 m/z	Set End Plate Offset	-500 V	Set Divert Valve	Source

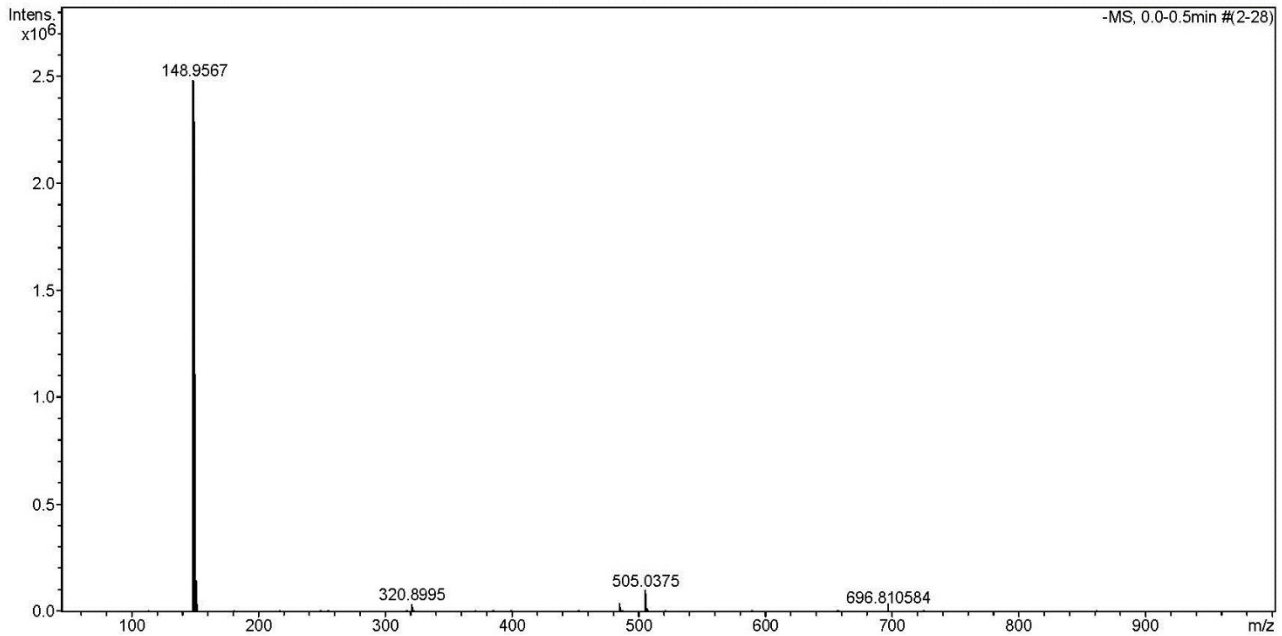

Figure 43S. Negative mass-spectrum of [**4a**$(OTf)_2$].

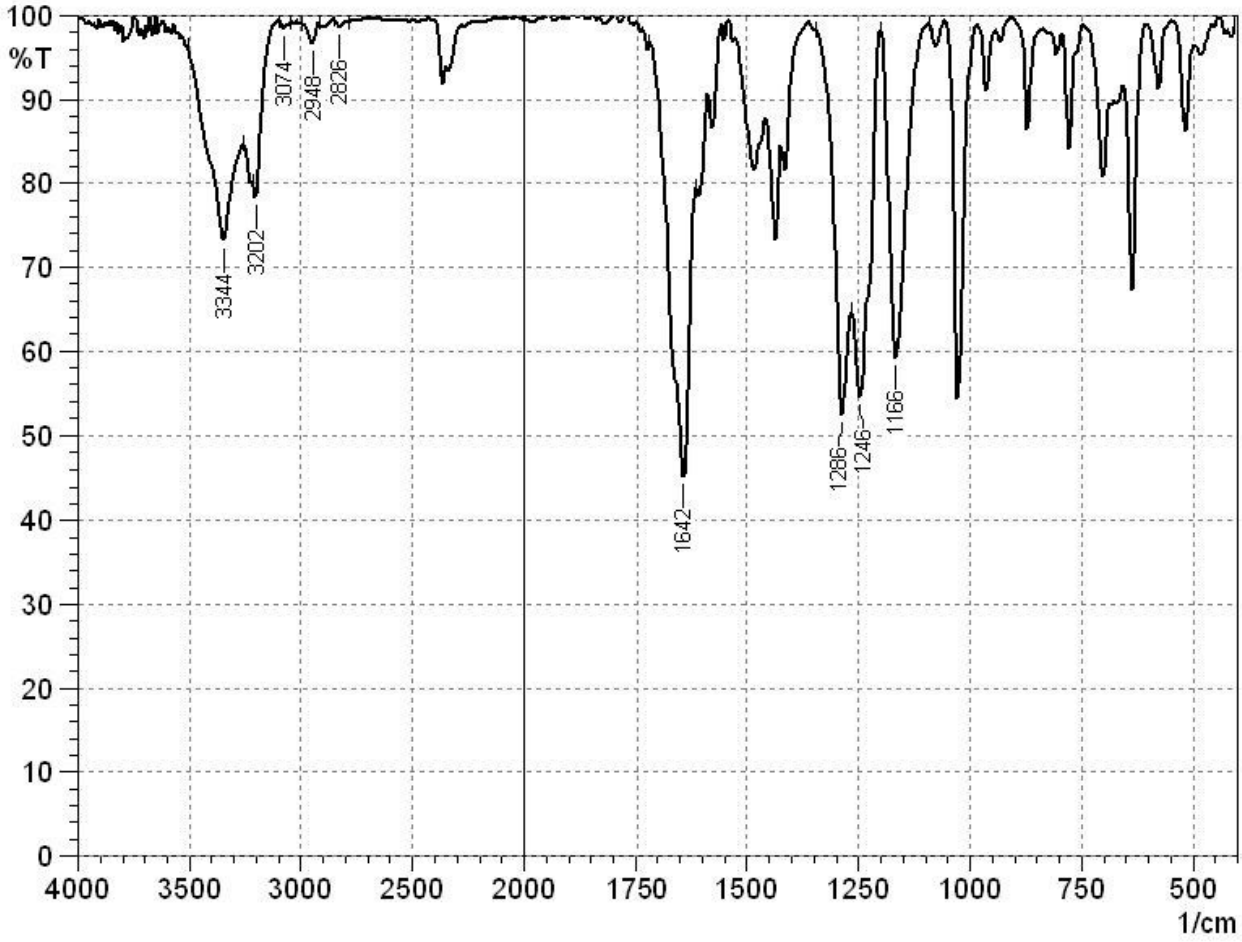

Figure 44S. IR spectrum of [**4a**$(OTf)_2$].

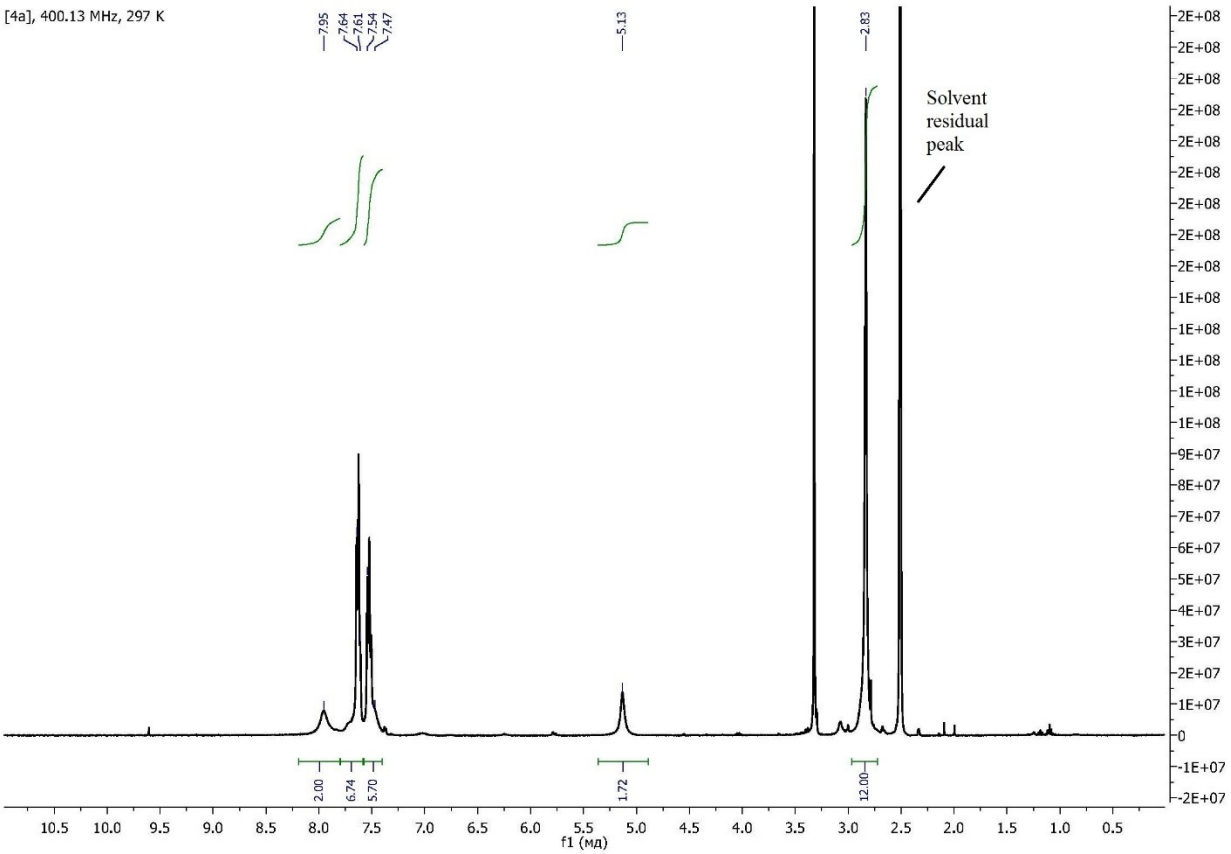

Figure 45S. ^{1}H NMR spectrum of [**4a**$(OTf)_2$].

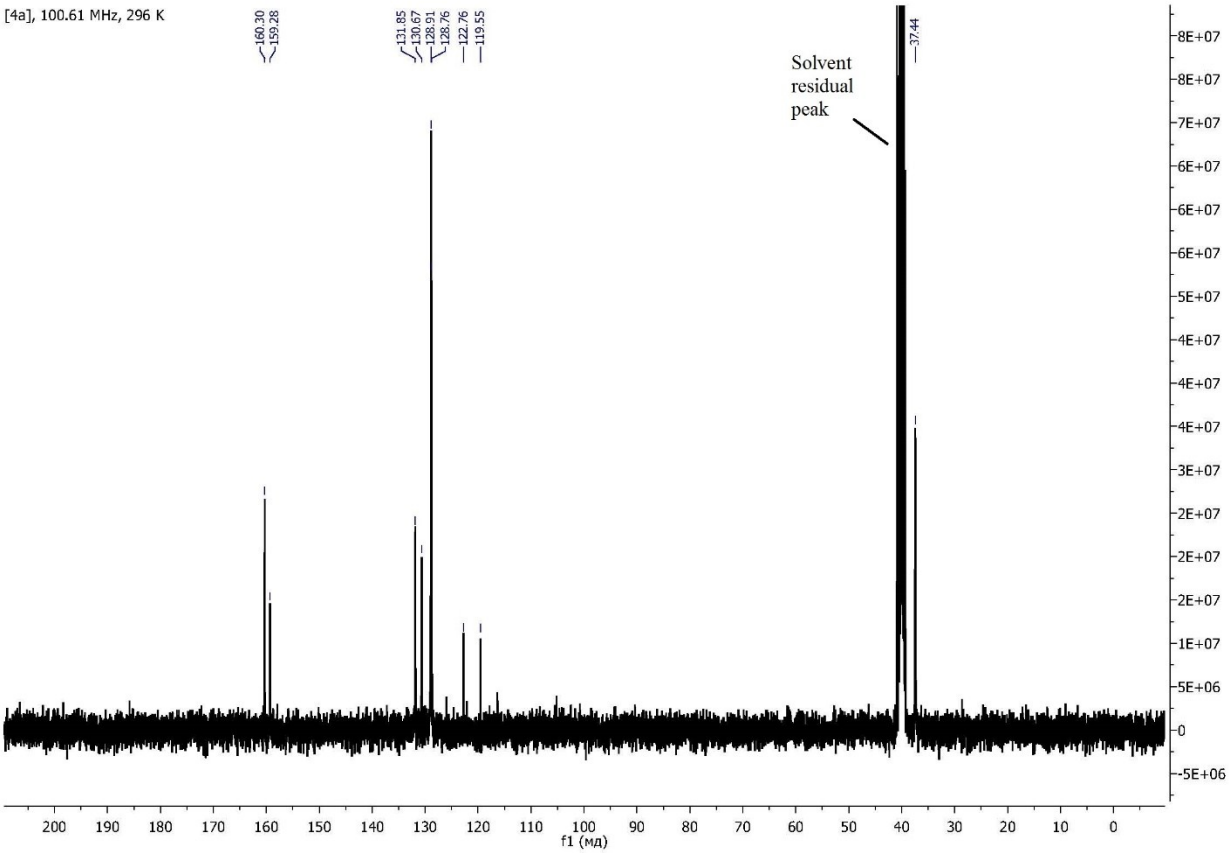

Figure 46S. ^{13}C NMR spectrum of [**4a**$(OTf)_2$].

[**4b**$(OTf)_2$]

Acquisition Parameter

Source Type	ESI	Ion Polarity	Positive	Set Nebulizer	1.0 Bar
Focus	Not active			Set Dry Heater	180 °C
Scan Begin	50 m/z	Set Capillary	4500 V	Set Dry Gas	6.0 l/min
Scan End	3000 m/z	Set End Plate Offset	-500 V	Set Divert Valve	Source

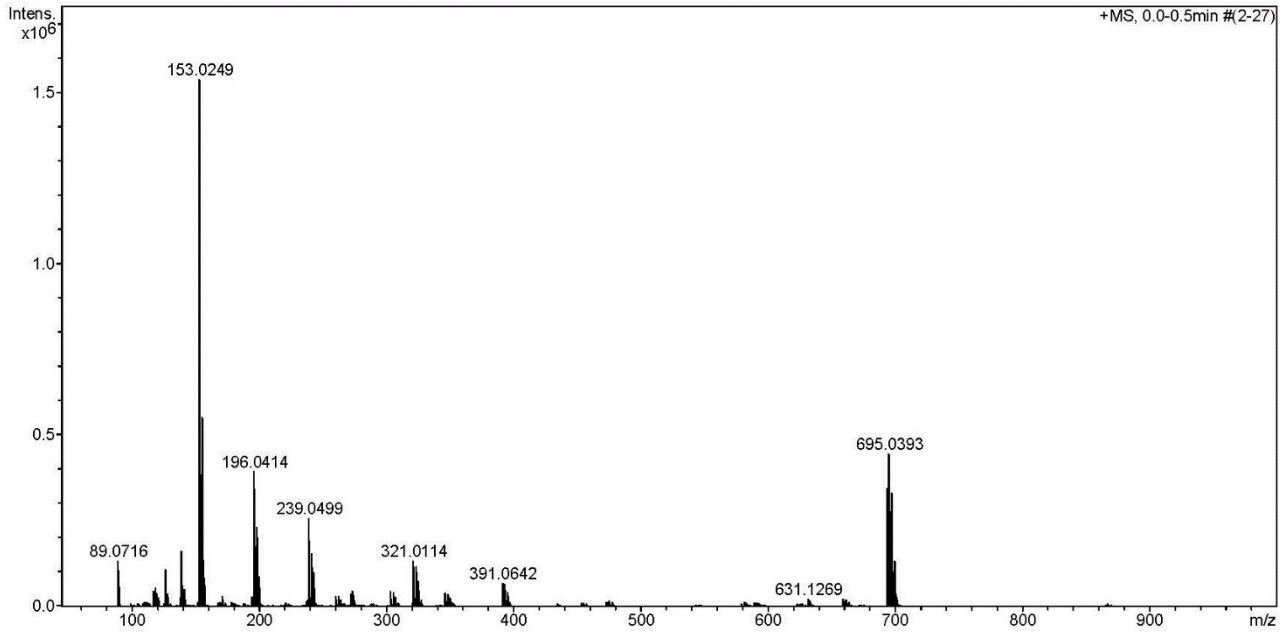

Figure 47S. Positive mass-spectrum of [**4b**$(OTf)_2$].

Acquisition Parameter

Source Type	ESI	Ion Polarity	Negative	Set Nebulizer	1.0 Bar
Focus	Not active			Set Dry Heater	180 °C
Scan Begin	50 m/z	Set Capillary	3500 V	Set Dry Gas	6.0 l/min
Scan End	3000 m/z	Set End Plate Offset	-500 V	Set Divert Valve	Source

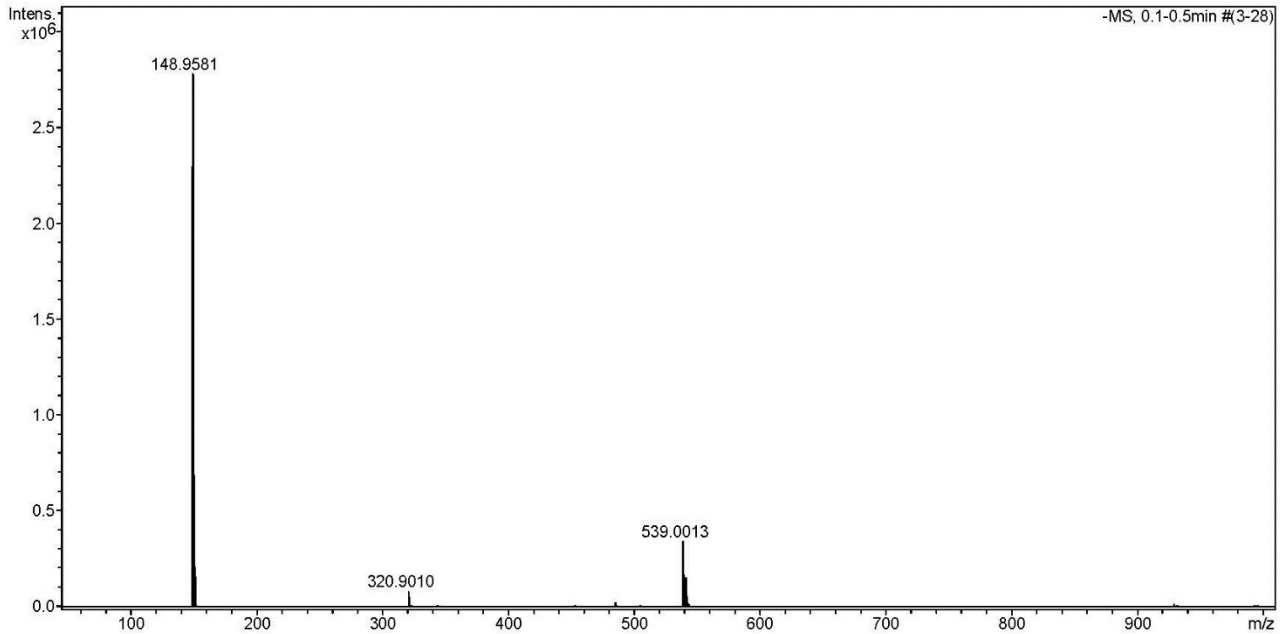

Figure 48S. Negative mass-spectrum of [**4b**$(OTf)_2$].

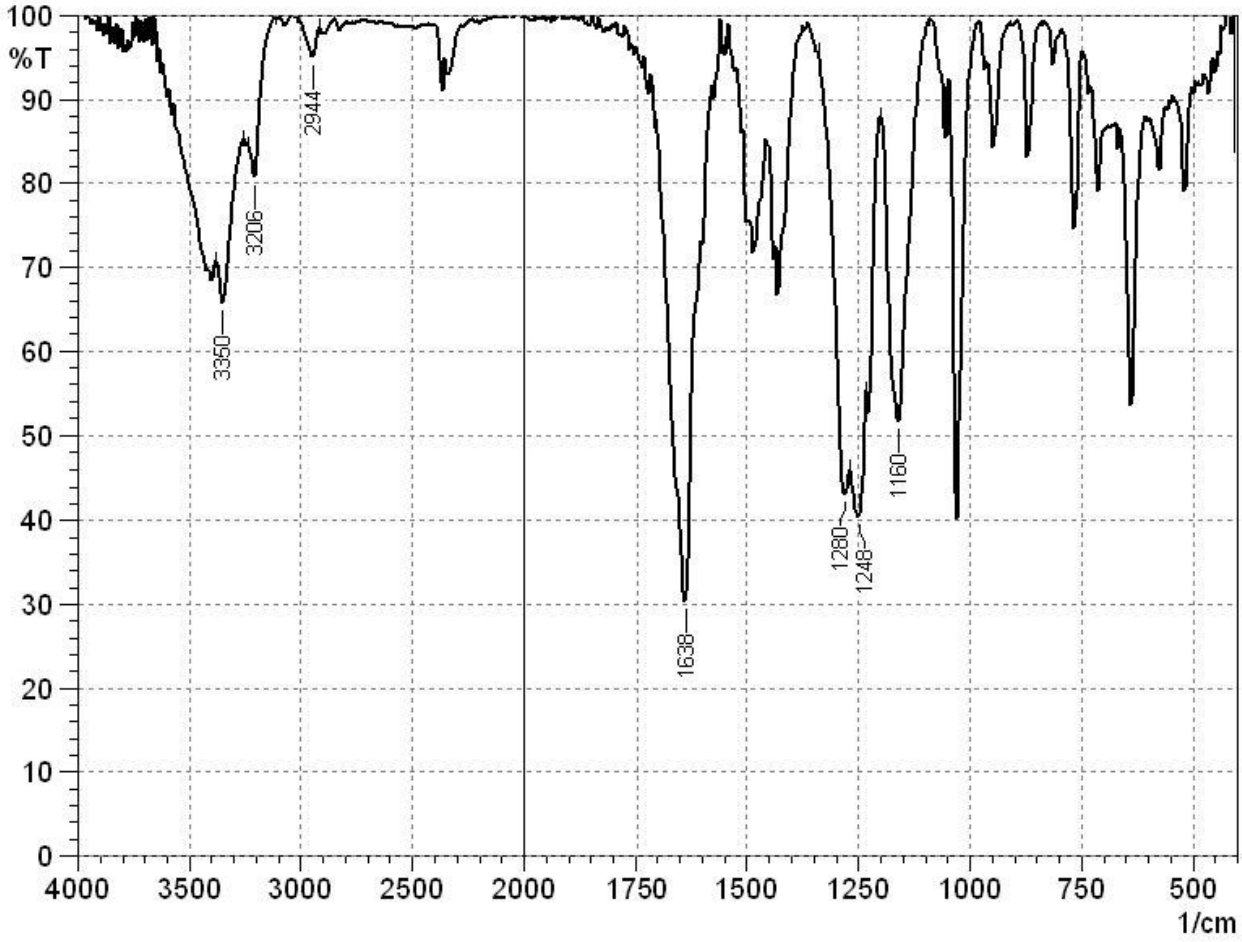

Figure 49S. IR spectrum of [**4b**$(OTf)_2$].

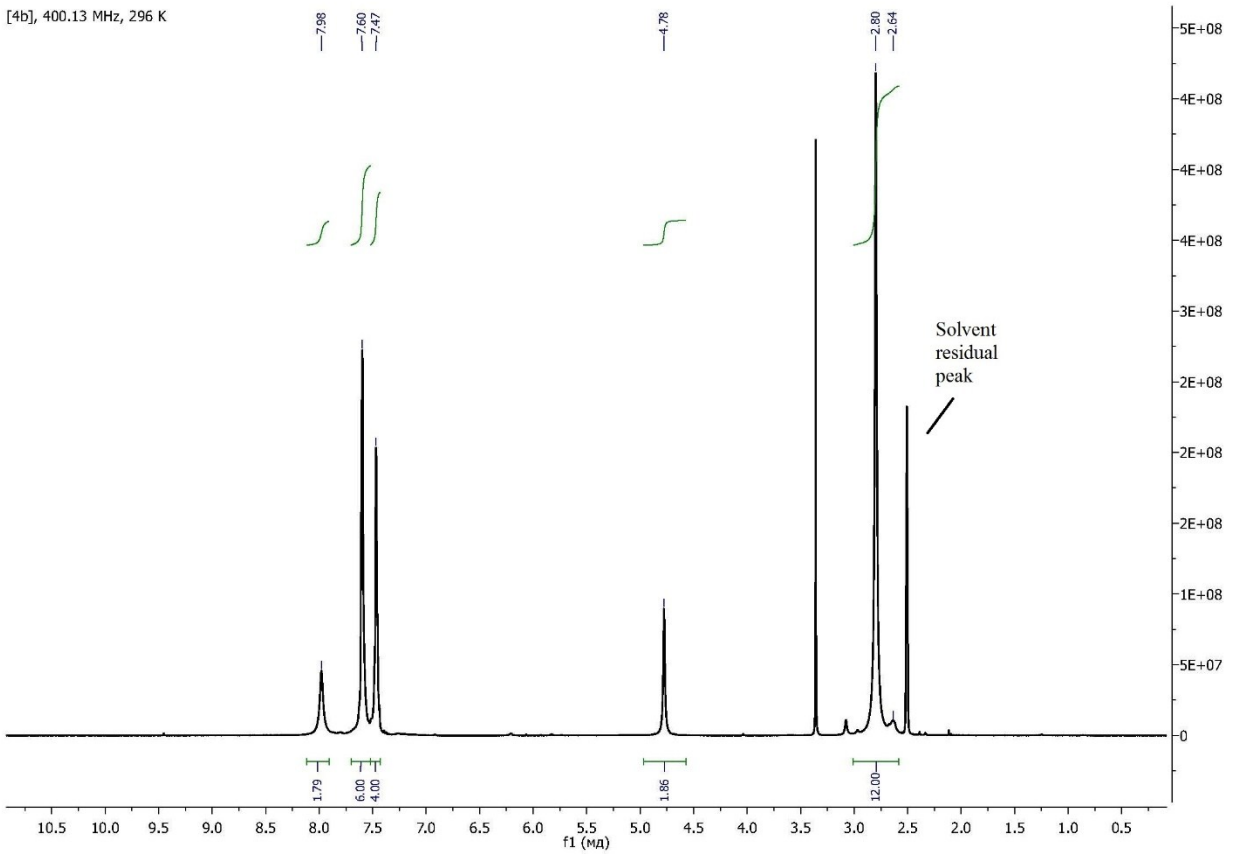

Figure 50S. ^{1}H NMR spectrum of [**4b**(OTf)$_2$].

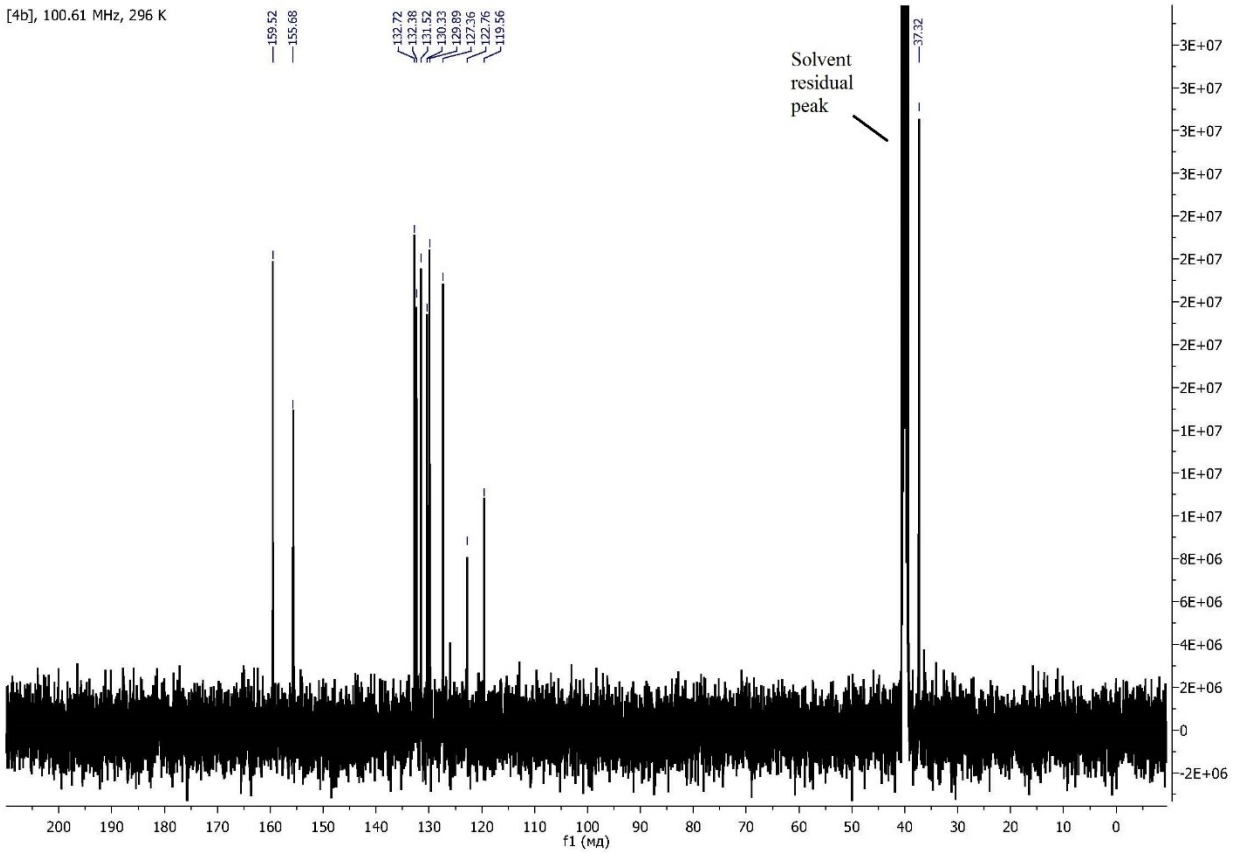

Figure 51S. ^{13}C NMR spectrum of [**4b**(OTf)$_2$].

[**4c**$(OTf)_2$]

Acquisition Parameter

Source Type	ESI	Ion Polarity	Positive	Set Nebulizer	1.0 Bar
Focus	Not active			Set Dry Heater	180 °C
Scan Begin	50 m/z	Set Capillary	4500 V	Set Dry Gas	6.0 l/min
Scan End	3000 m/z	Set End Plate Offset	-500 V	Set Divert Valve	Source

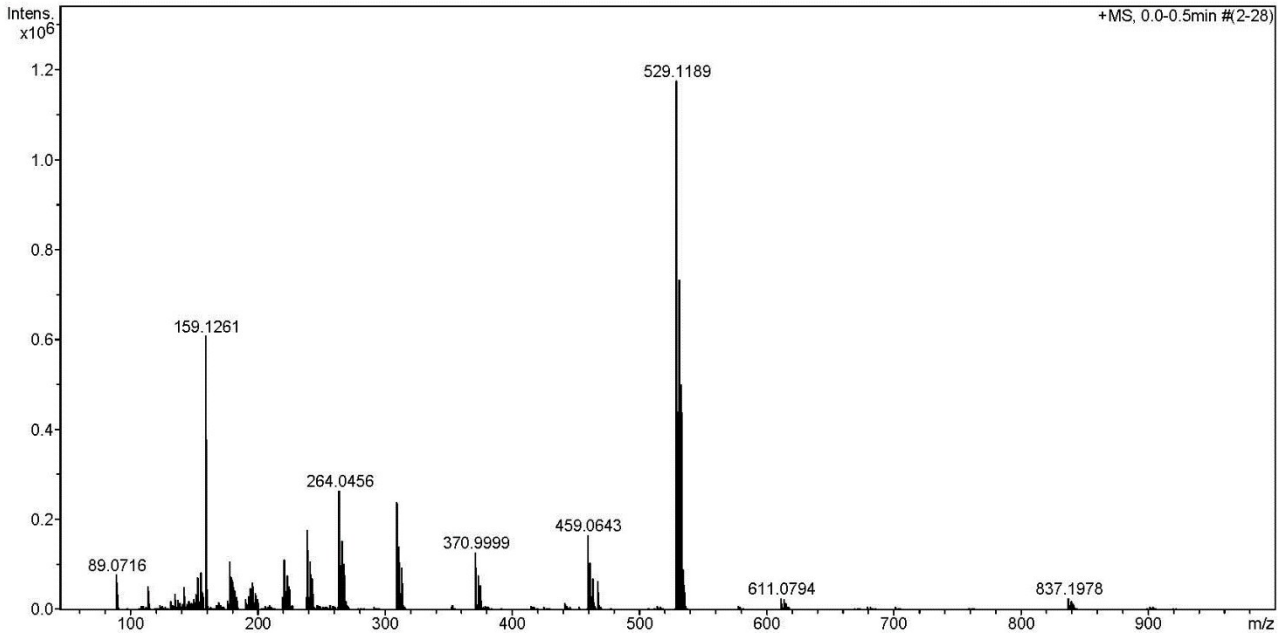

Figure 52S. Positive mass-spectrum of [**4c**$(OTf)_2$].

Acquisition Parameter

Source Type	ESI	Ion Polarity	Negative	Set Nebulizer	1.0 Bar
Focus	Not active			Set Dry Heater	180 °C
Scan Begin	50 m/z	Set Capillary	3500 V	Set Dry Gas	6.0 l/min
Scan End	3000 m/z	Set End Plate Offset	-500 V	Set Divert Valve	Source

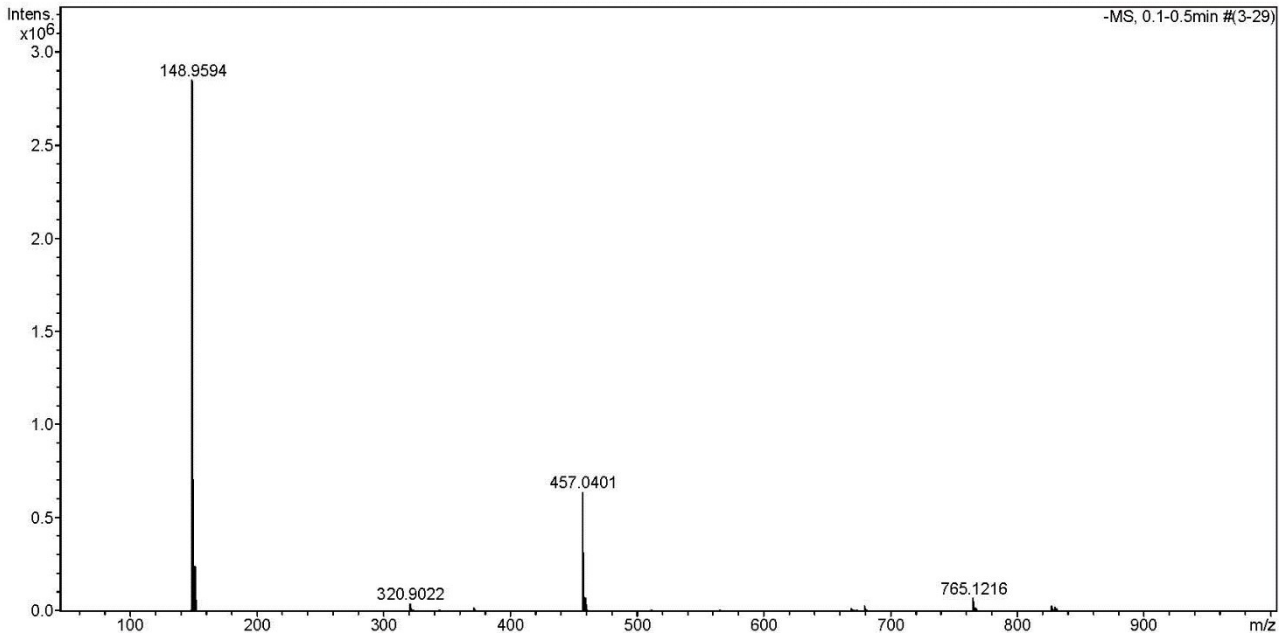

Figure 53S. Negative mass-spectrum of [**4c**$(OTf)_2$].

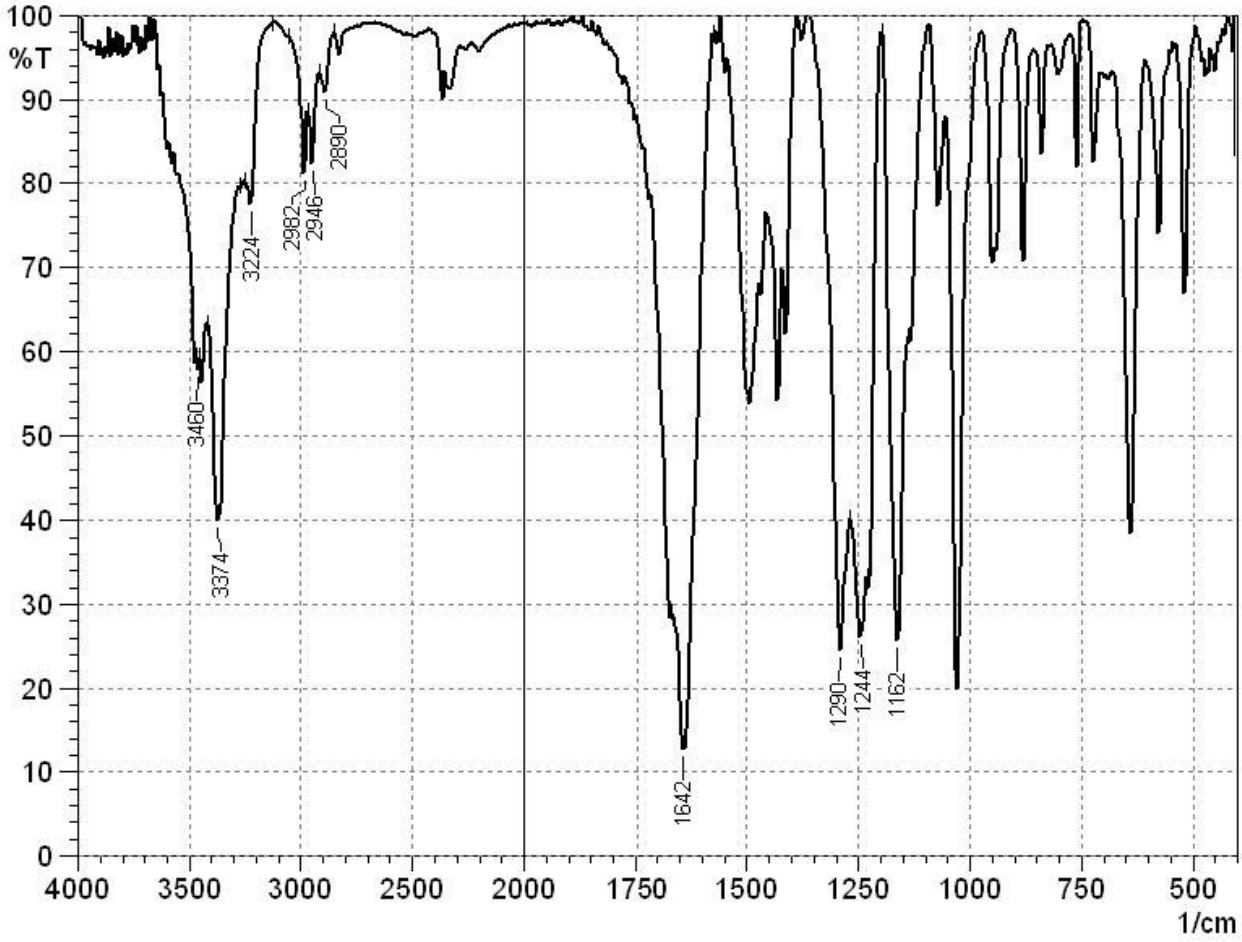

Figure 54S. IR spectrum of [**4c**$(OTf)_2$].

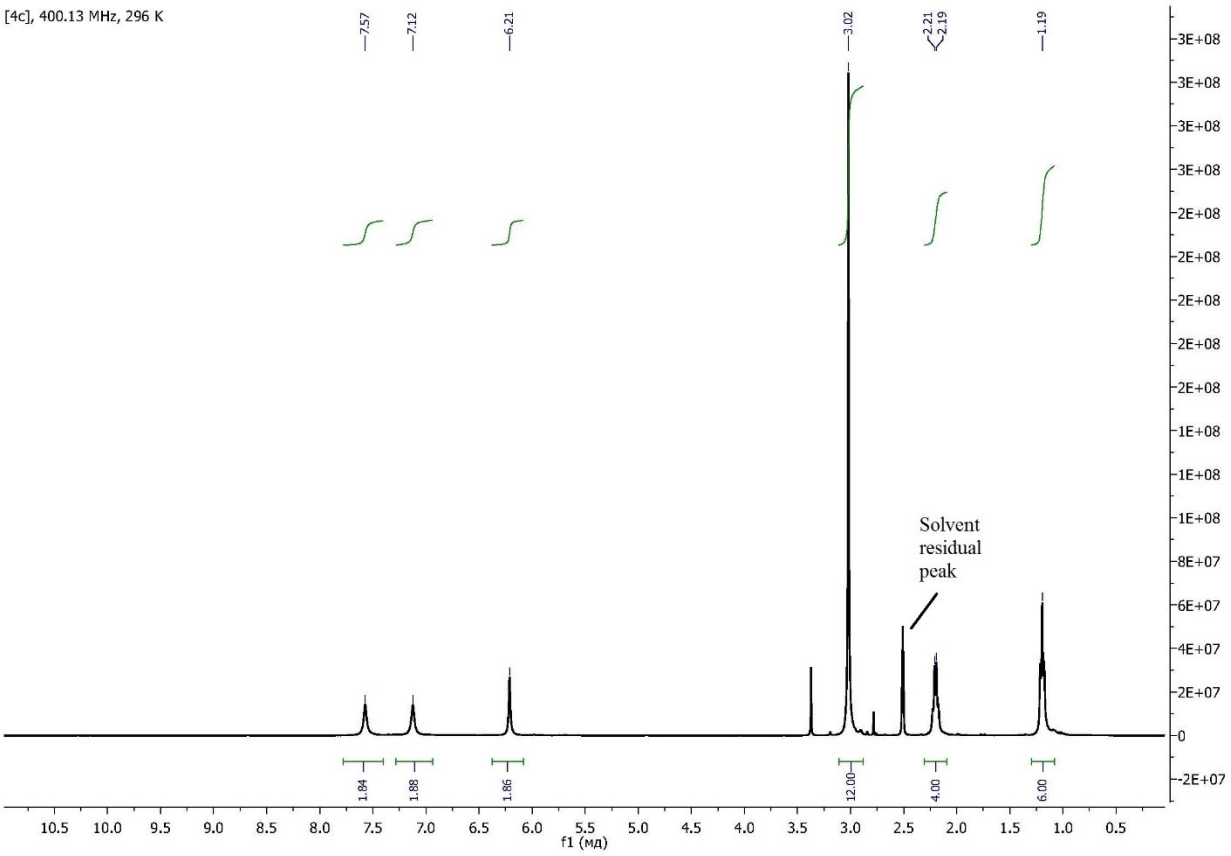

Figure 55S. ^{1}H NMR spectrum of [**4c**$(OTf)_2$].

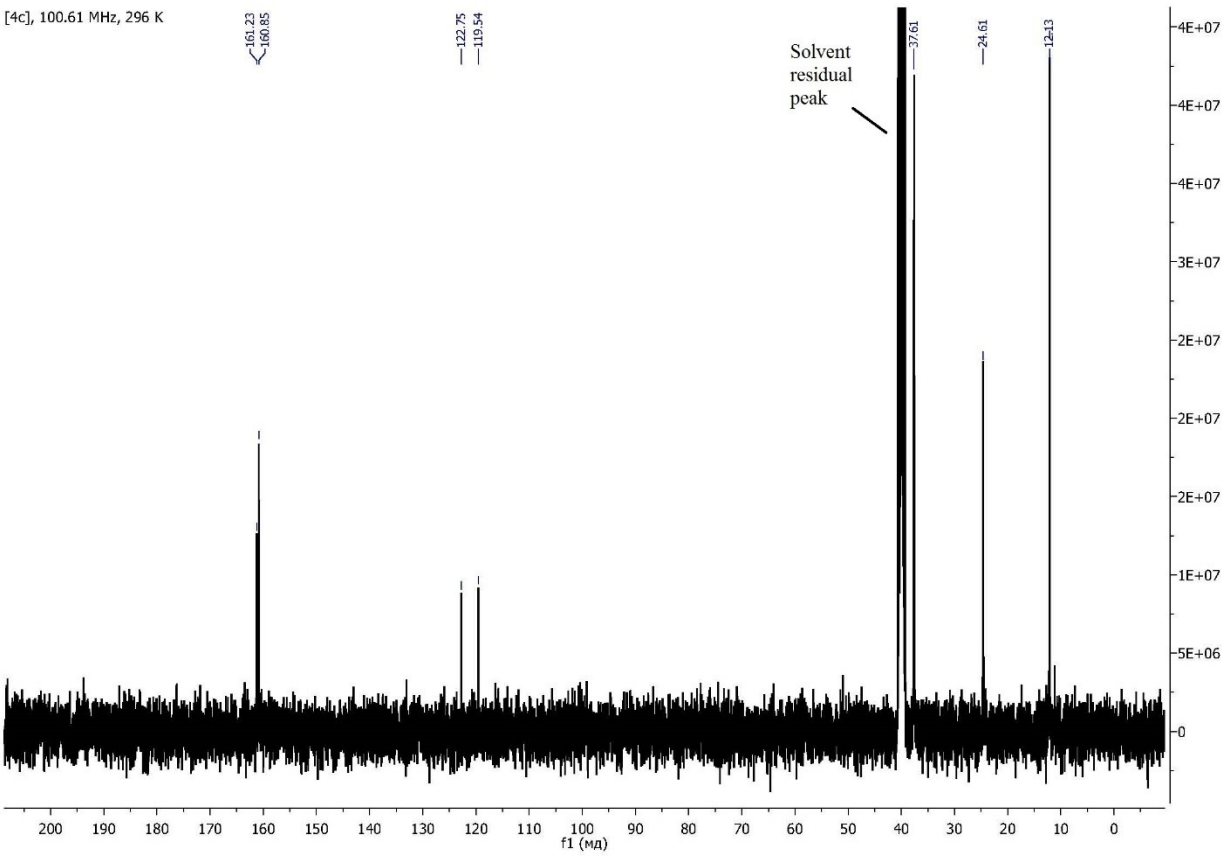

Figure 56S. ^{13}C NMR spectrum of [**4c**$(OTf)_2$].

Spectra of [5a–d](OTf)

[**5a**](OTf)

Acquisition Parameter

Source Type	ESI	Ion Polarity	Positive	Set Nebulizer	1.0 Bar
Focus	Not active			Set Dry Heater	180 °C
Scan Begin	50 m/z	Set Capillary	4500 V	Set Dry Gas	6.0 l/min
Scan End	3000 m/z	Set End Plate Offset	-500 V	Set Divert Valve	Source

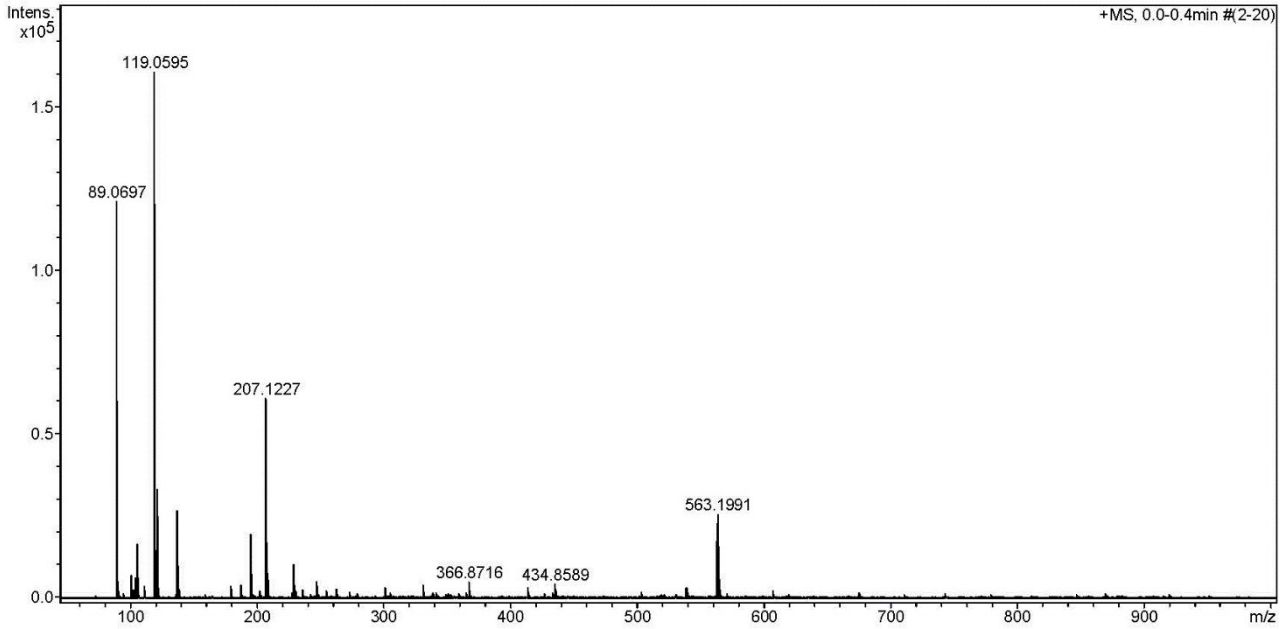

Figure 57S. Positive mass-spectrum of [**5a**](OTf).

Acquisition Parameter

Source Type	ESI	Ion Polarity	Negative	Set Nebulizer	1.0 Bar
Focus	Not active			Set Dry Heater	180 °C
Scan Begin	50 m/z	Set Capillary	3500 V	Set Dry Gas	6.0 l/min
Scan End	3000 m/z	Set End Plate Offset	-500 V	Set Divert Valve	Source

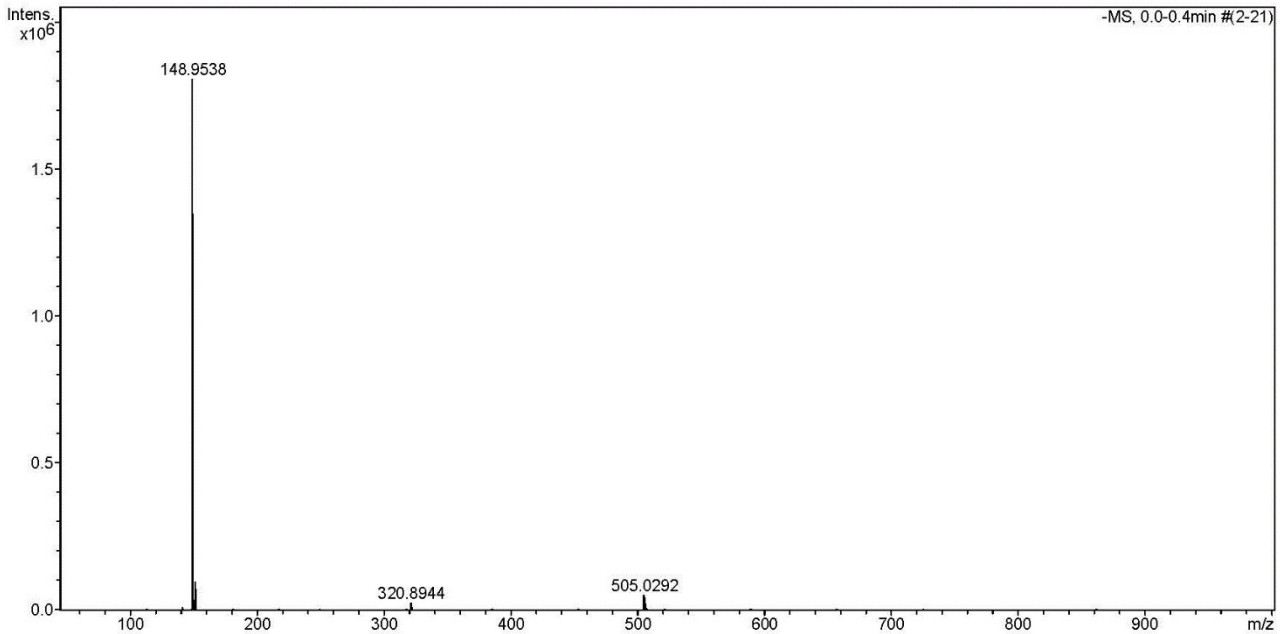

Figure 58S. Negative mass-spectrum of [**5a**](OTf).

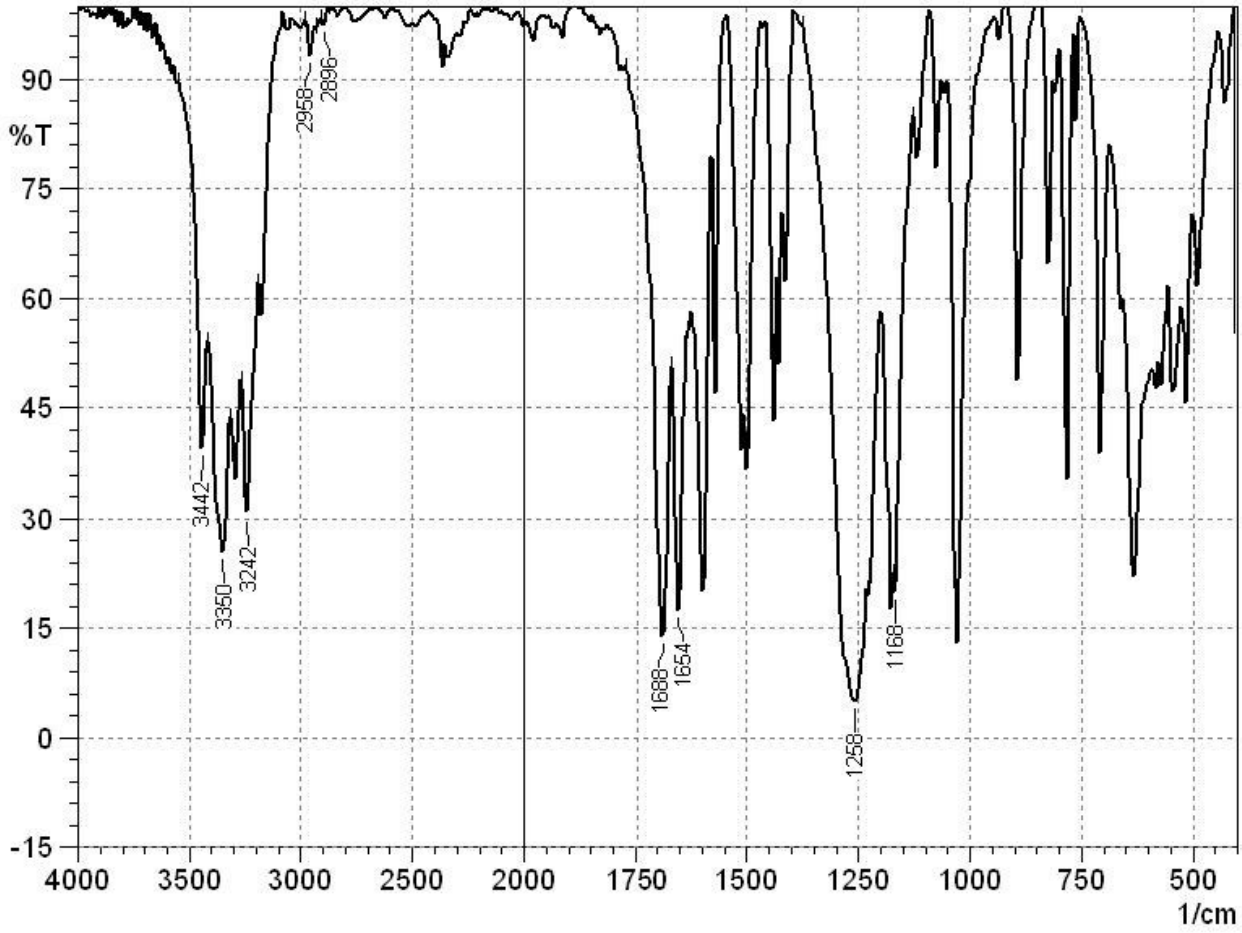

Figure 59S. IR spectrum of [**5a**](OTf).

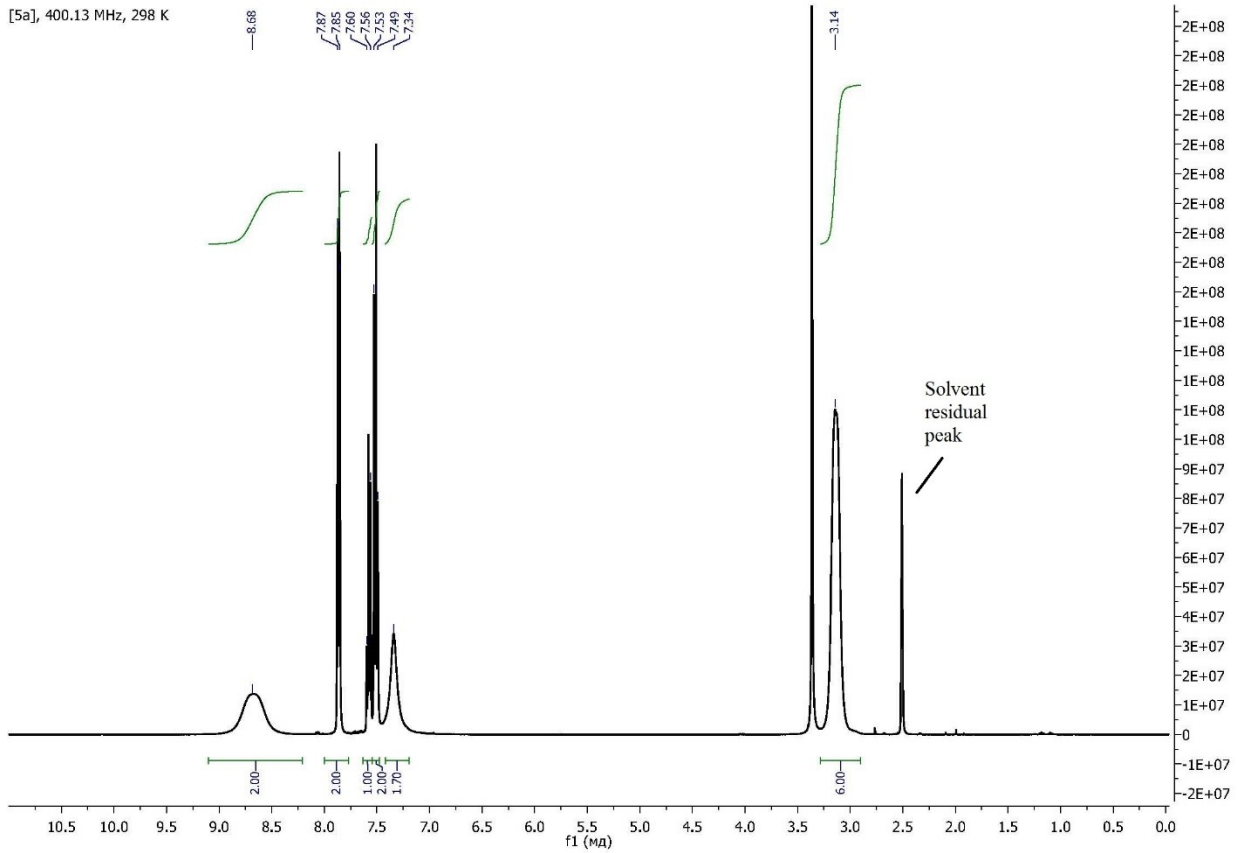

Figure 60S. ^{1}H NMR spectrum of [**5a**](OTf).

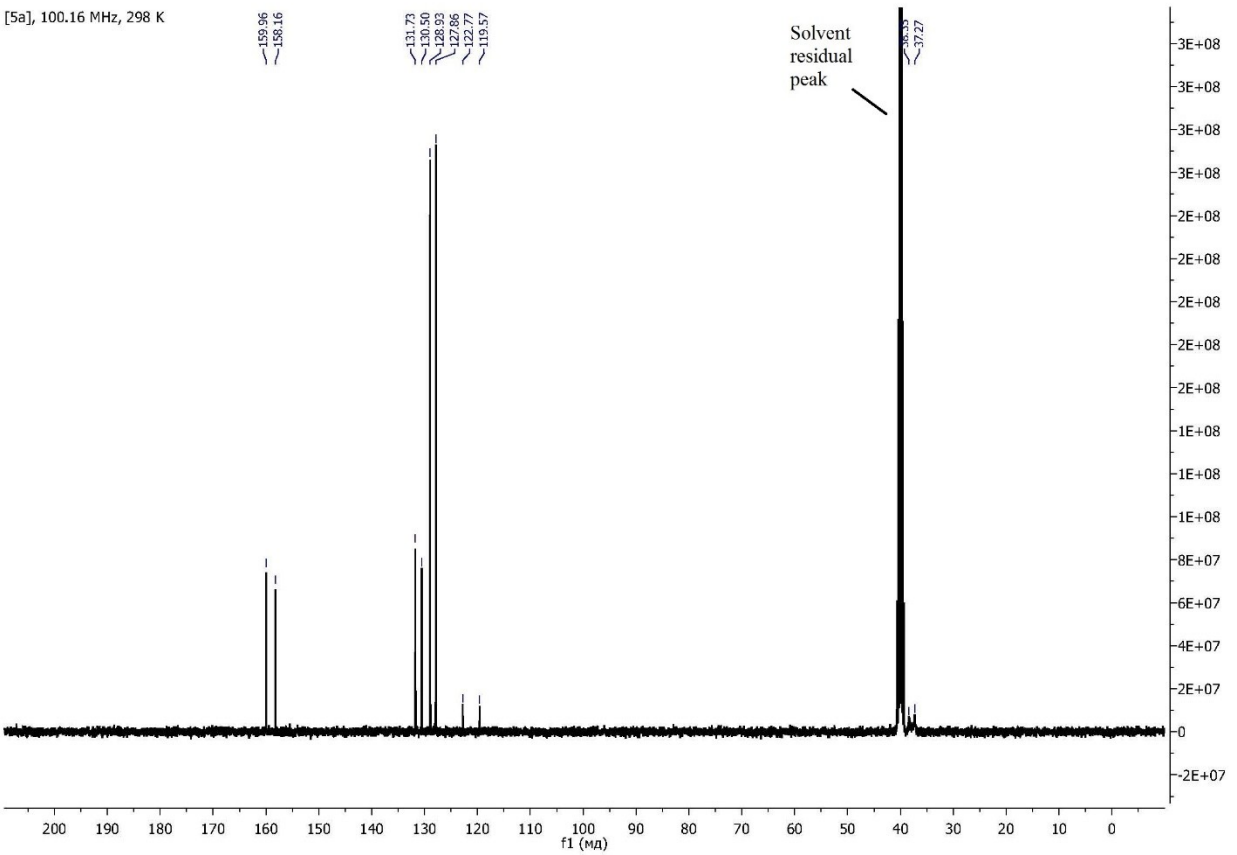

Figure 61S. ^{13}C NMR spectrum of [**5a**](OTf).

[**5b**](OTf)

Acquisition Parameter

Source Type	ESI	Ion Polarity	Positive	Set Nebulizer	1.0 Bar
Focus	Not active			Set Dry Heater	180 °C
Scan Begin	50 m/z	Set Capillary	4500 V	Set Dry Gas	6.0 l/min
Scan End	3000 m/z	Set End Plate Offset	-500 V	Set Divert Valve	Source

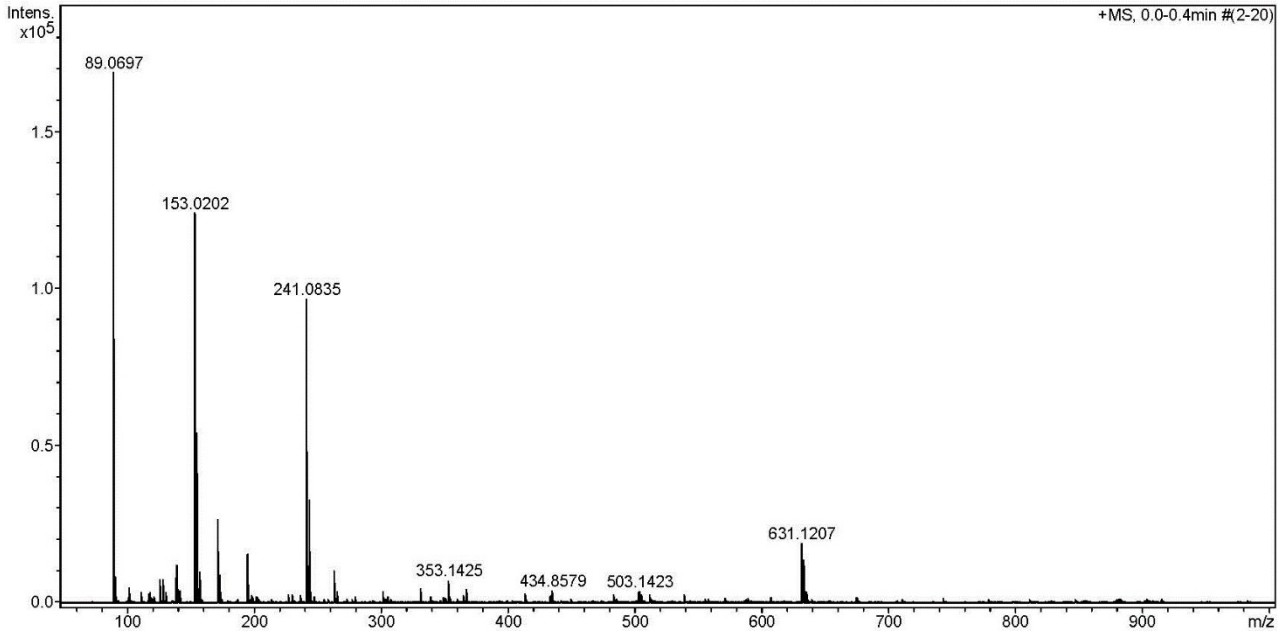

Figure 62S. Positive mass-spectrum of [**5b**](OTf).

Acquisition Parameter

Source Type	ESI	Ion Polarity	Negative	Set Nebulizer	1.0 Bar
Focus	Not active			Set Dry Heater	180 °C
Scan Begin	50 m/z	Set Capillary	3500 V	Set Dry Gas	6.0 l/min
Scan End	3000 m/z	Set End Plate Offset	-500 V	Set Divert Valve	Source

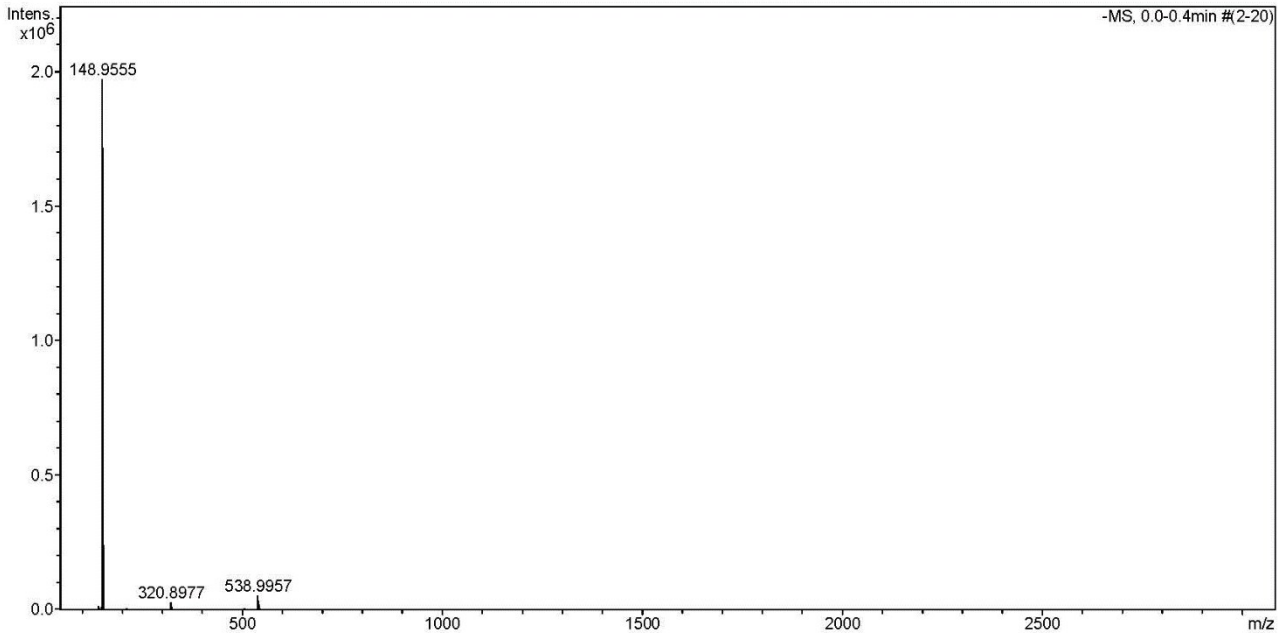

Figure 63S. Negative mass-spectrum of [**5b**](OTf).

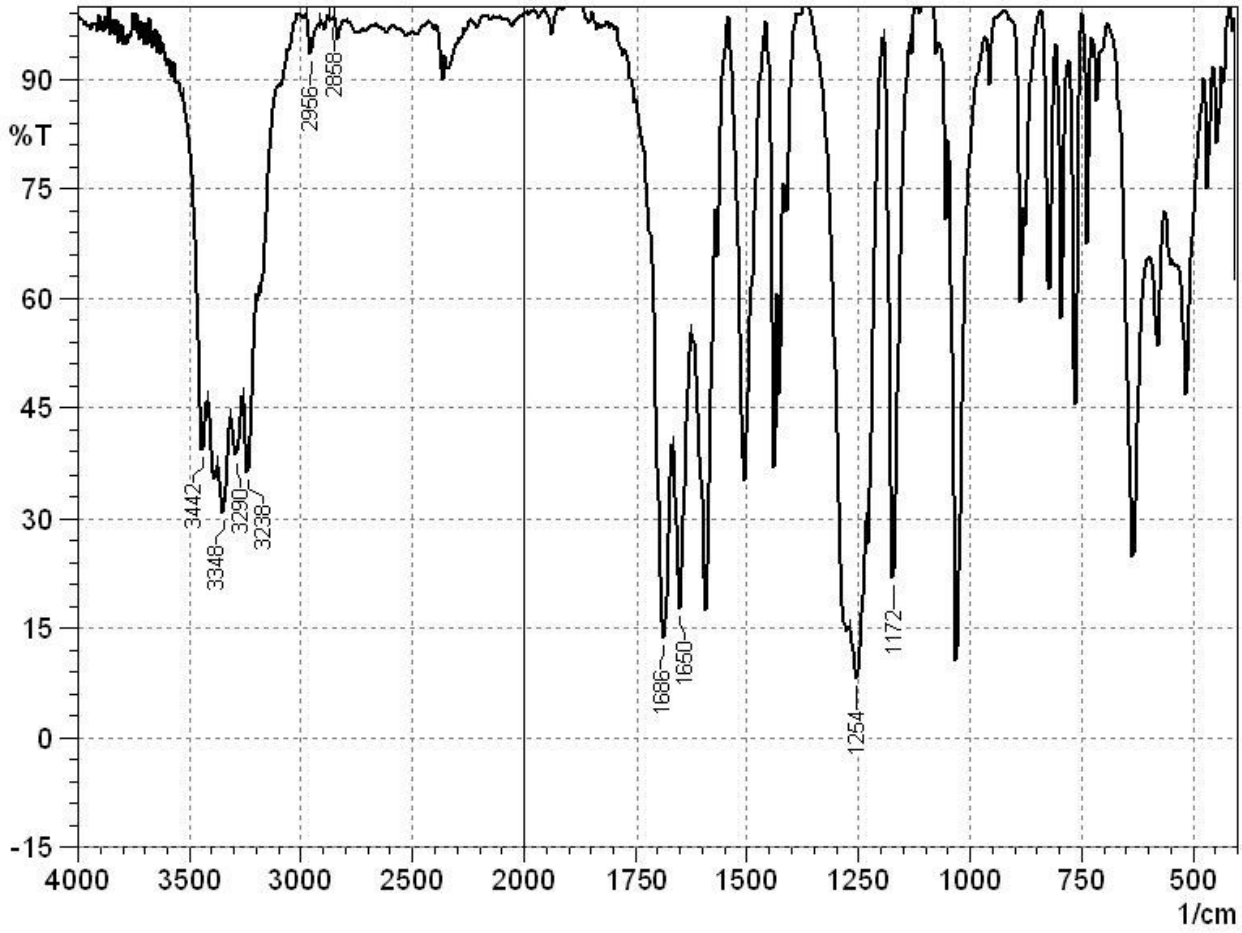

Figure 64S. IR spectrum of [**5b**](OTf).

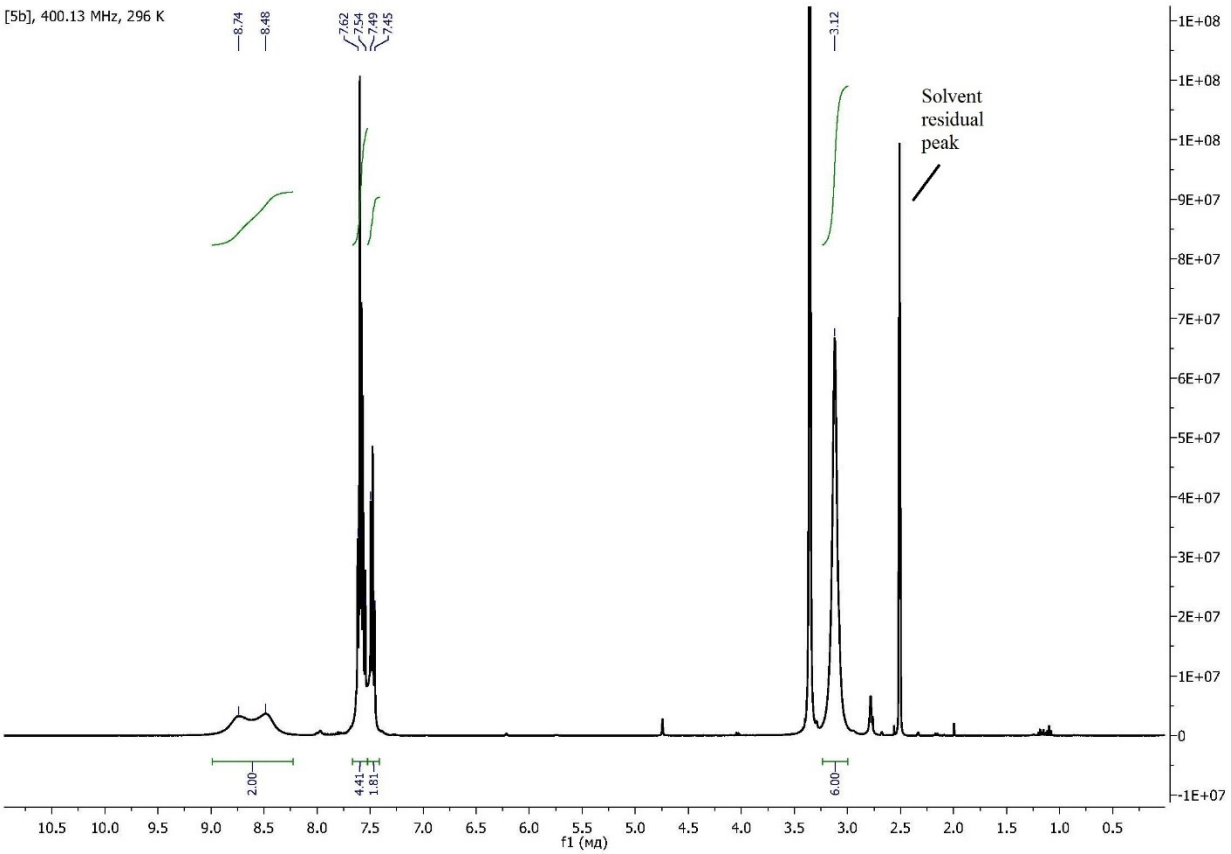

Figure 65S. ^{1}H NMR spectrum of [**5b**](OTf).

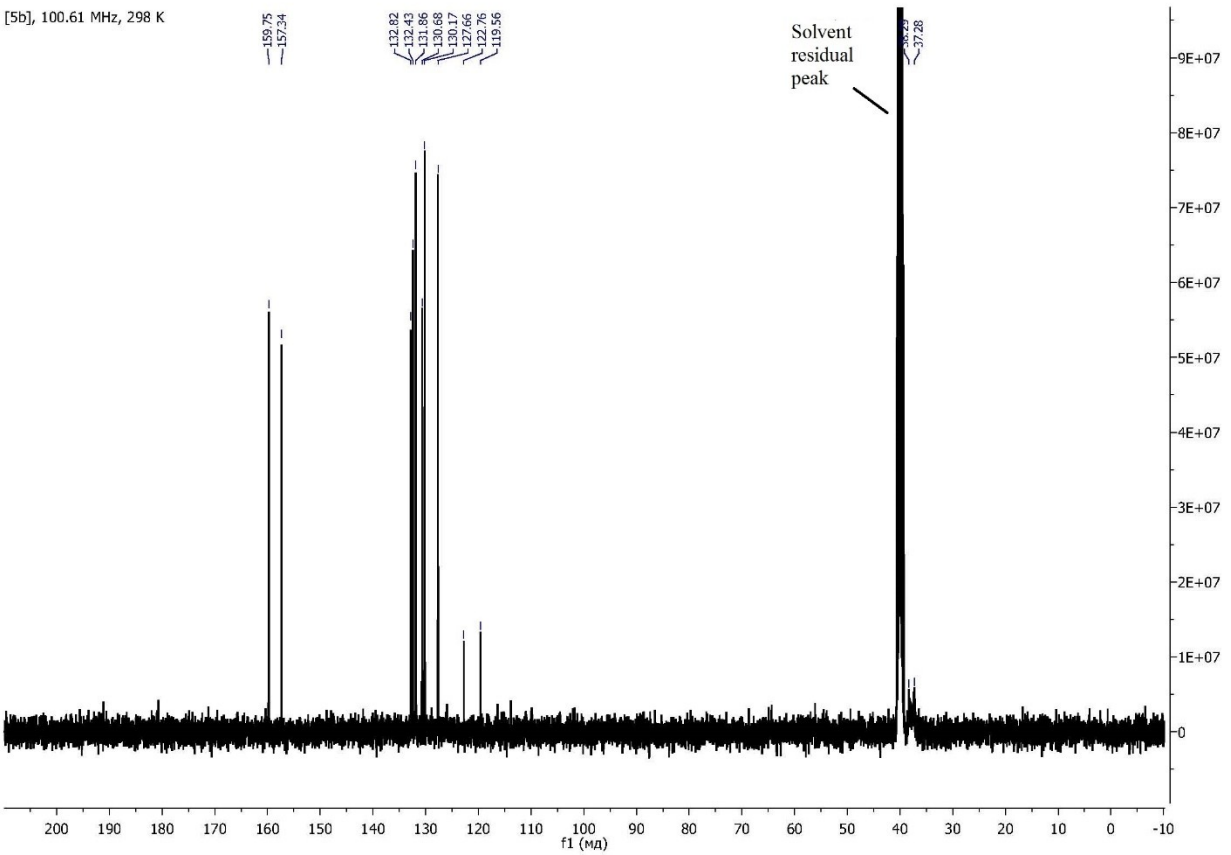

Figure 66S. ^{13}C NMR spectrum of [**5b**](OTf).

[**5c**](OTf)

Acquisition Parameter

Source Type	ESI	Ion Polarity	Positive	Set Nebulizer	1.0 Bar
Focus	Not active			Set Dry Heater	180 °C
Scan Begin	50 m/z	Set Capillary	4500 V	Set Dry Gas	6.0 l/min
Scan End	3000 m/z	Set End Plate Offset	-500 V	Set Divert Valve	Source

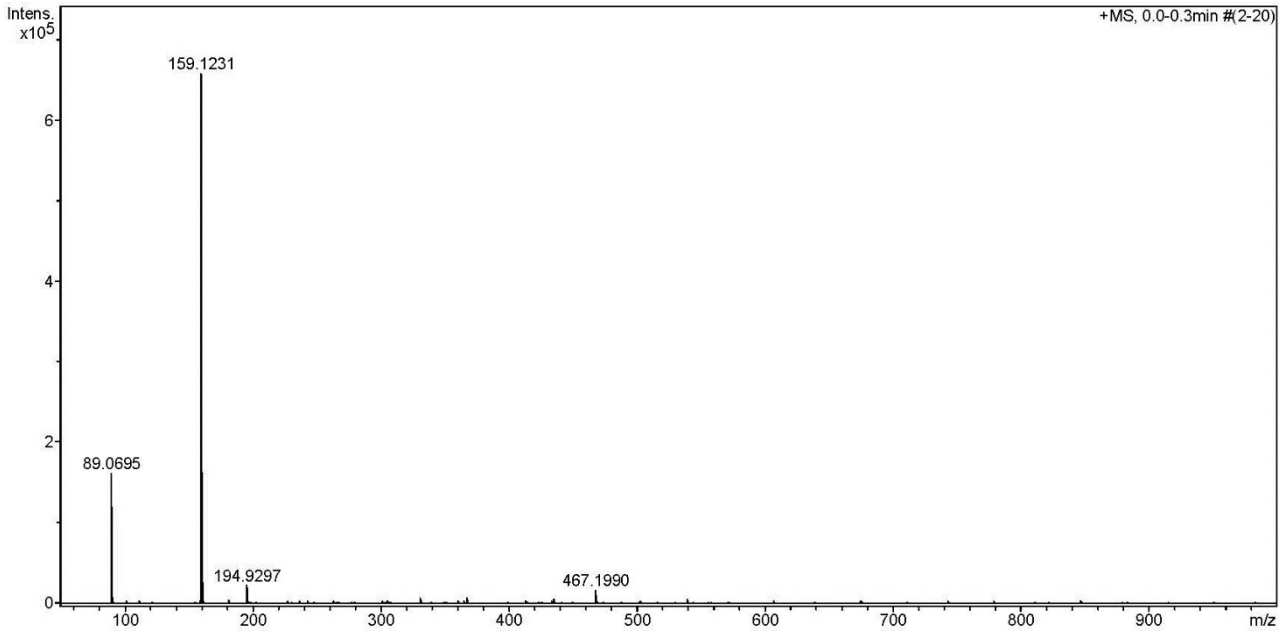

Figure 67S. Positive mass-spectrum of [**5c**](OTf).

Acquisition Parameter

Source Type	ESI	Ion Polarity	Negative	Set Nebulizer	1.0 Bar
Focus	Not active			Set Dry Heater	180 °C
Scan Begin	50 m/z	Set Capillary	3500 V	Set Dry Gas	6.0 l/min
Scan End	3000 m/z	Set End Plate Offset	-500 V	Set Divert Valve	Source

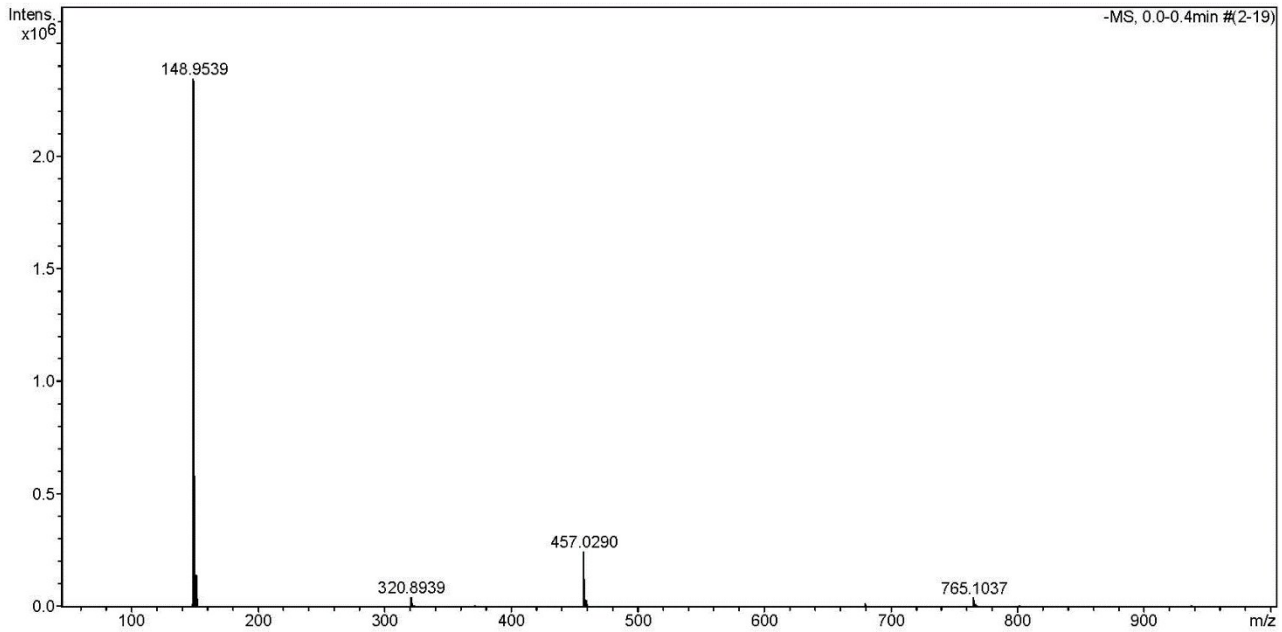

Figure 68S. Negative mass-spectrum of [**5c**](OTf).

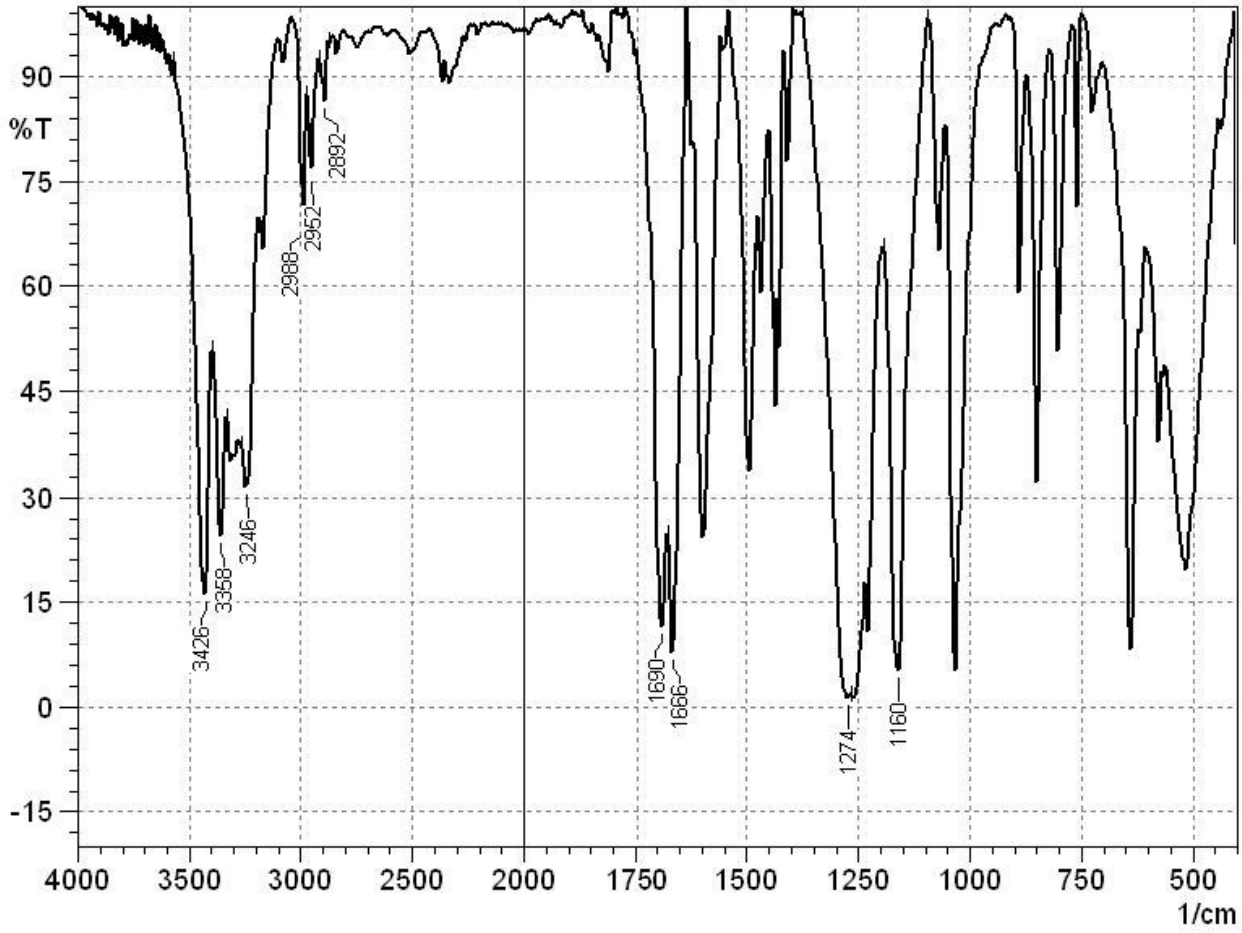

Figure 69S. IR spectrum of [**5c**](OTf).

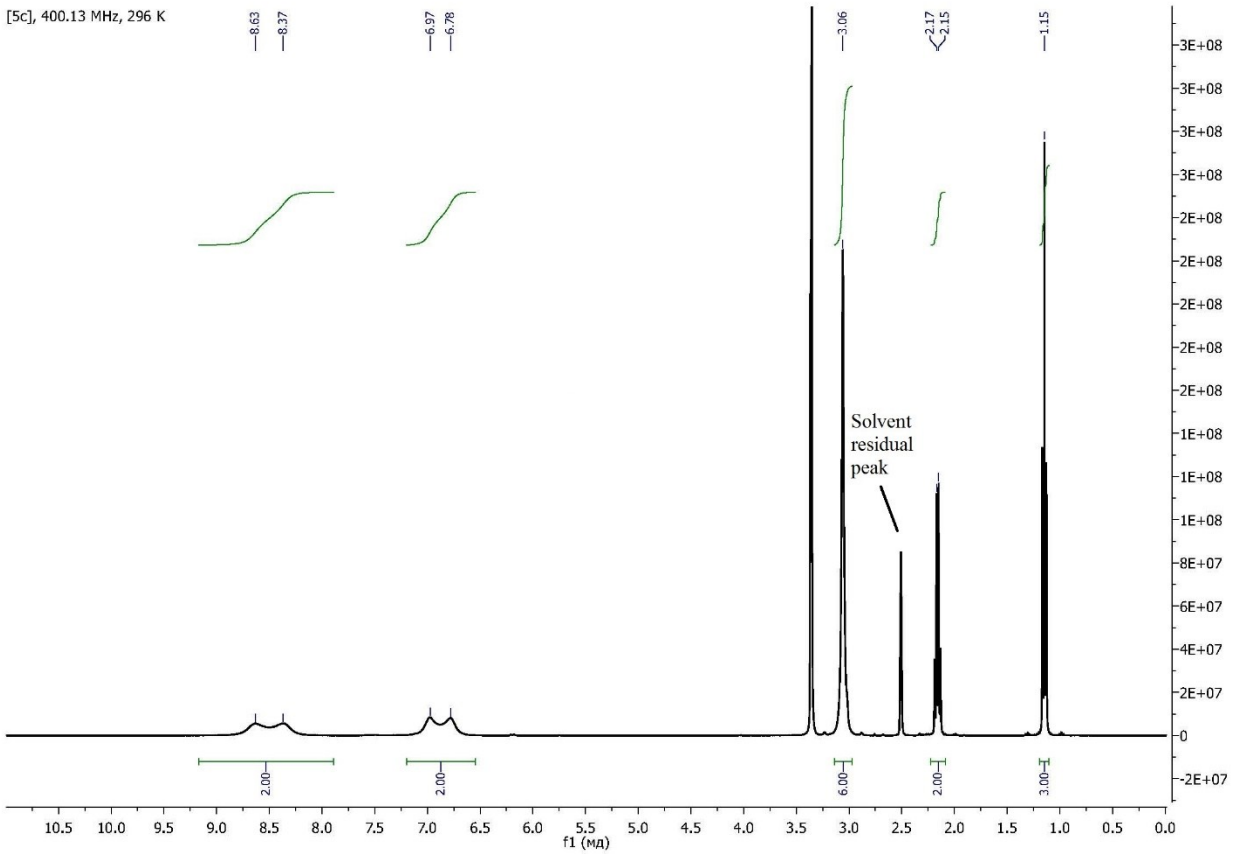

Figure 70S. ^{1}H NMR spectrum of [**5c**](OTf).

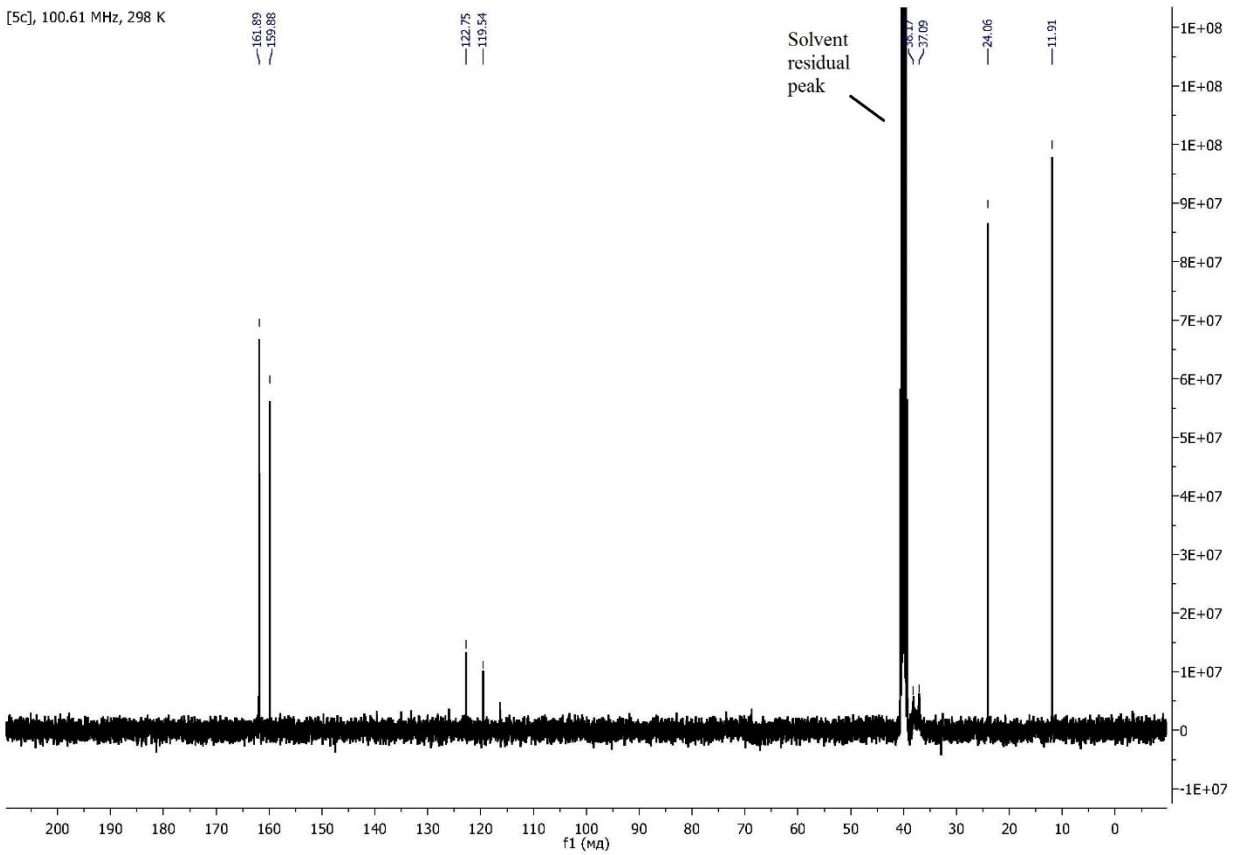

Figure 71S. ^{13}C NMR spectrum of [**5c**](OTf).

[**5d**](OTf)

Acquisition Parameter

Source Type	ESI	Ion Polarity	Positive	Set Nebulizer	1.0 Bar
Focus	Not active			Set Dry Heater	180 °C
Scan Begin	50 m/z	Set Capillary	4500 V	Set Dry Gas	6.0 l/min
Scan End	3000 m/z	Set End Plate Offset	-500 V	Set Divert Valve	Source

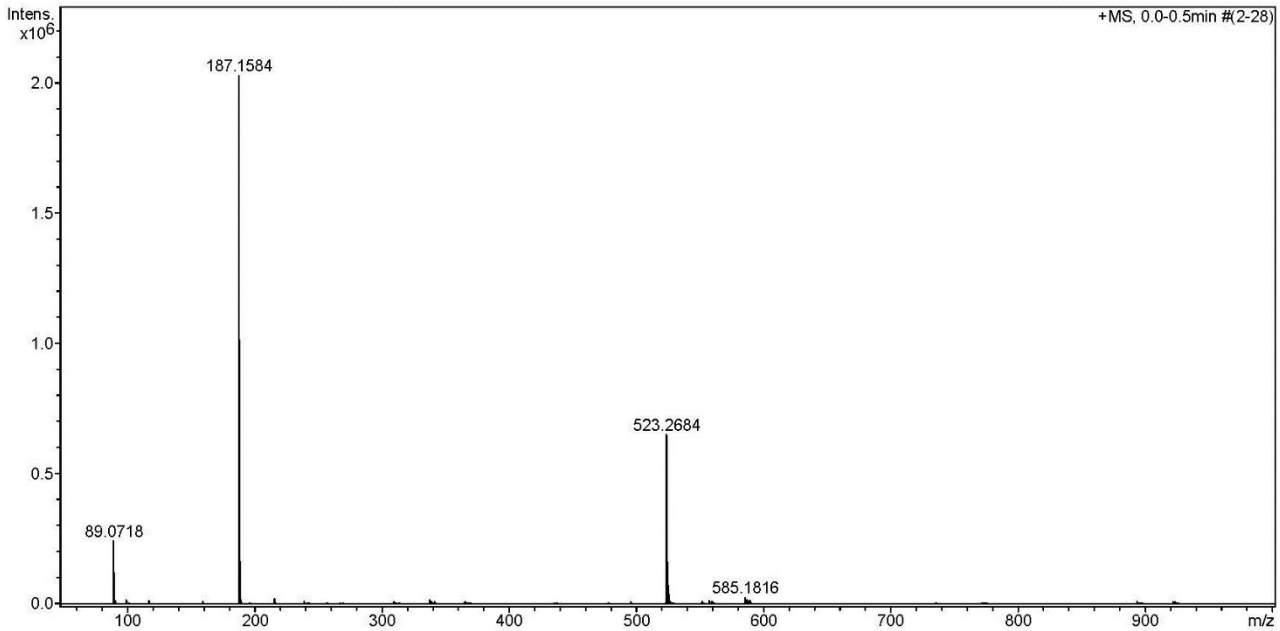

Figure 72S. Positive mass-spectrum of [**5d**](OTf).

Acquisition Parameter

Source Type	ESI	Ion Polarity	Negative	Set Nebulizer	1.0 Bar
Focus	Not active			Set Dry Heater	180 °C
Scan Begin	50 m/z	Set Capillary	3500 V	Set Dry Gas	6.0 l/min
Scan End	3000 m/z	Set End Plate Offset	-500 V	Set Divert Valve	Source

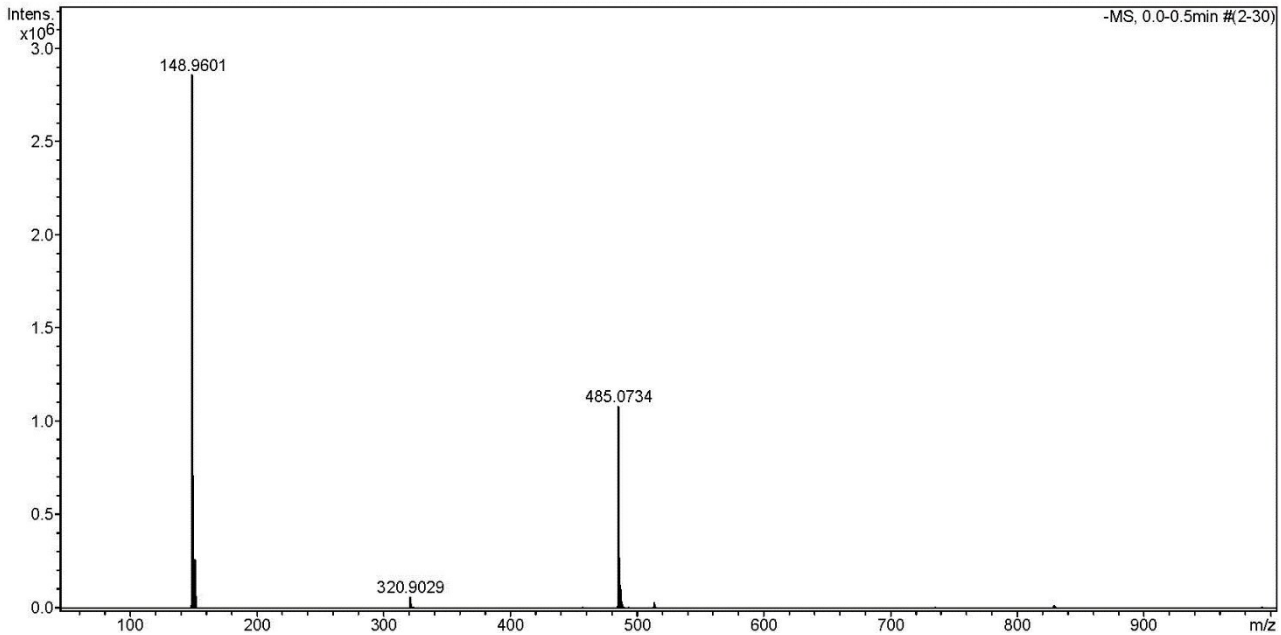

Figure 73S. Negative mass-spectrum of [**5d**](OTf).

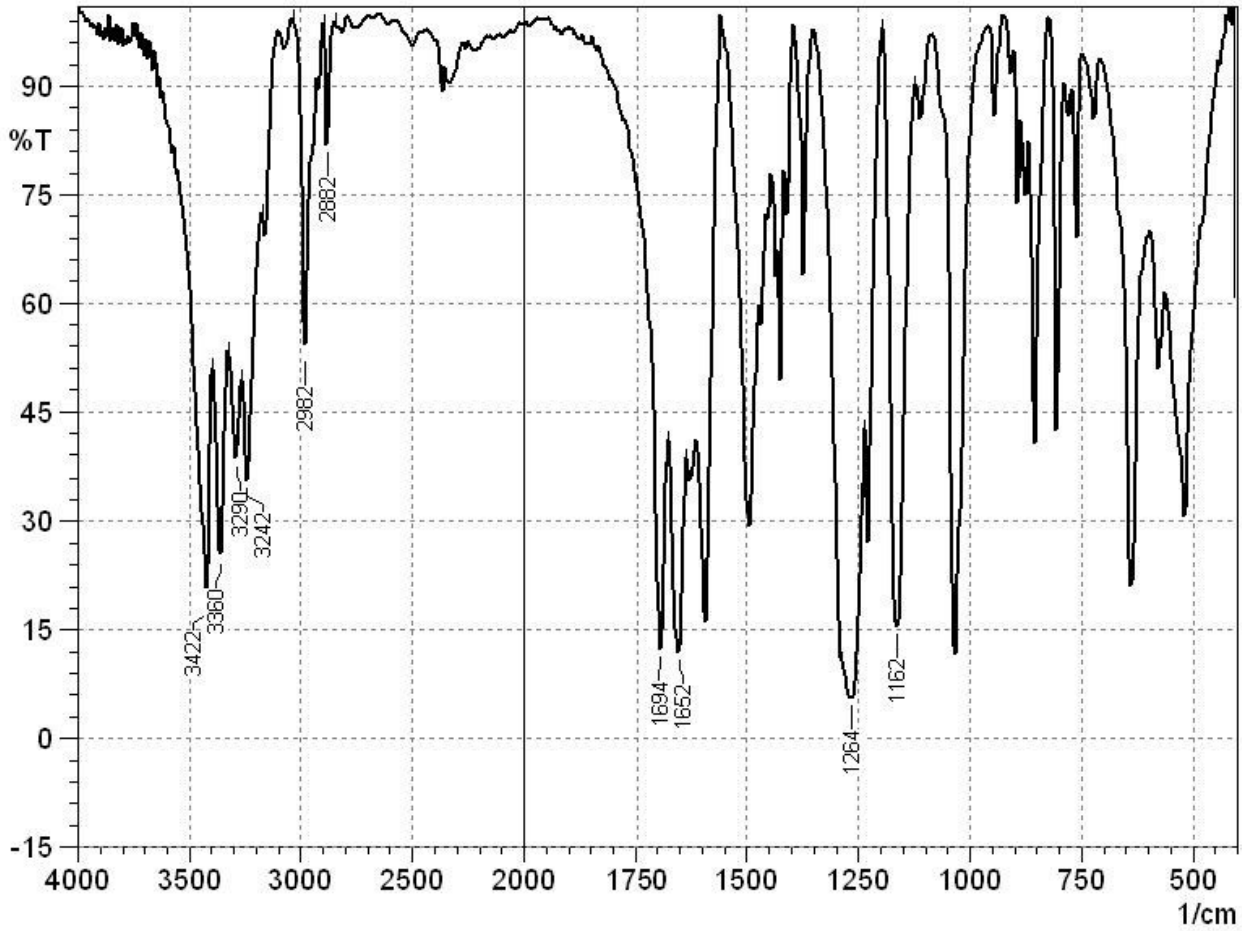

Figure 74S. IR spectrum of [**5d**](OTf).

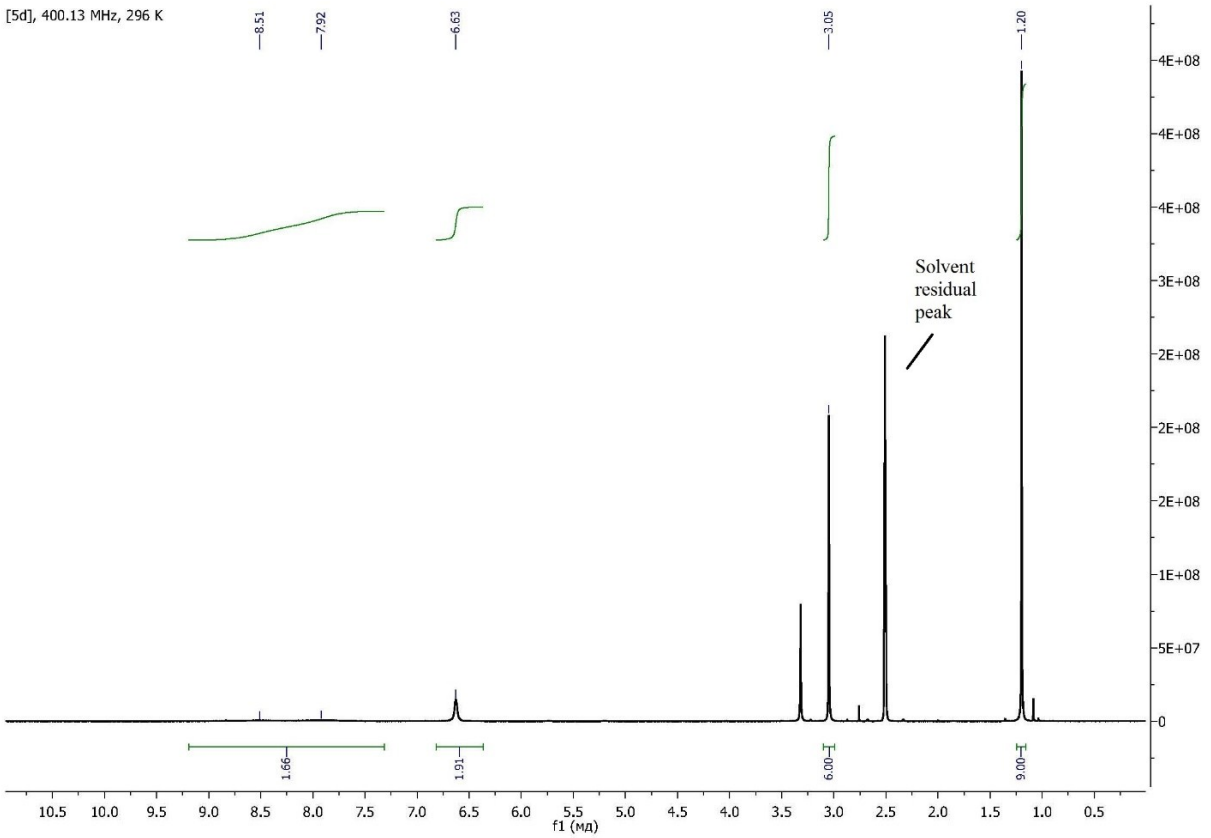

F

igure 75S. ^{1}H NMR spectrum of [**5d**](OTf).

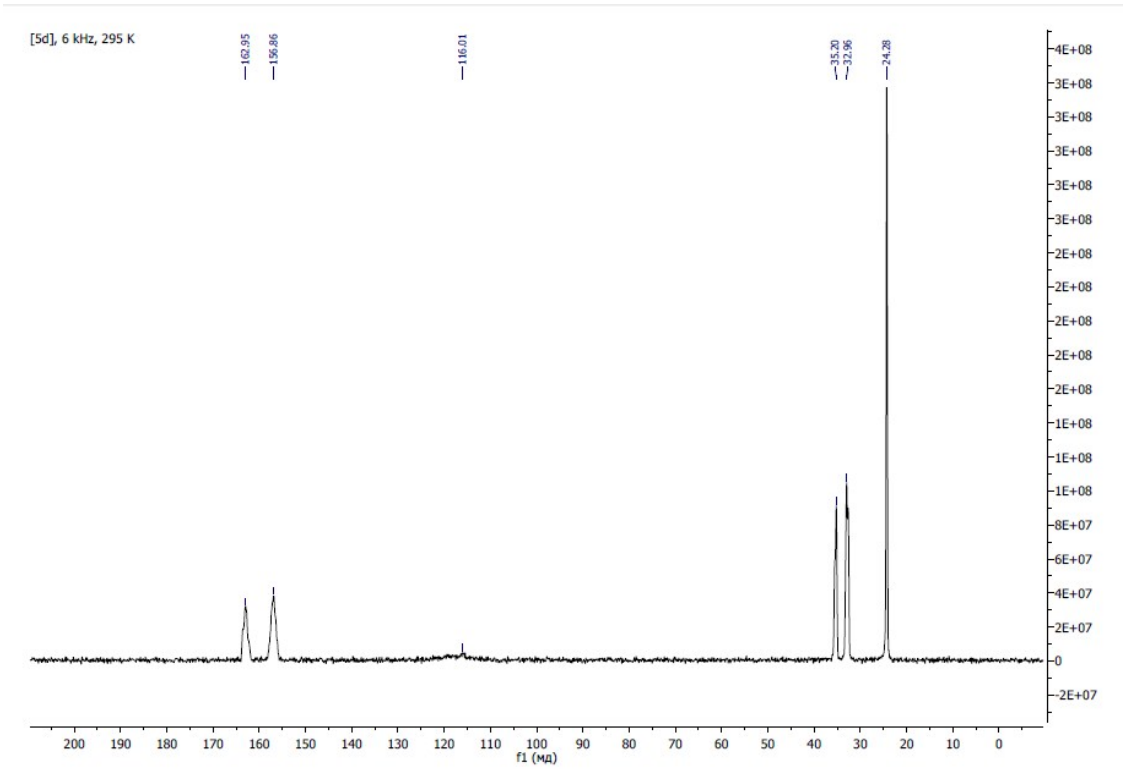

Figure 76S. 13C{1H} CP-MAS TOSS NMR spectrum of [**5d**](OTf).

Table 1S. Crystal data for **2a–c** and [**3a**](OTf)$_4$.

Identification code	**2a**	**2b**	**2c**	[**3a**](OTf)$_4$
Empirical formula	$C_{18}H_{22}N_4O_6Zn$	$C_{18}H_{20}Cl_2N_4O_6Zn$	$C_{10}H_{22}N_4O_6Zn$	$C_{36}H_{50}F_{12}N_8O_{26}S_4Zn_3$
Formula weight	455.76	524.65	359.68	1563.19
Temperature/K	100(2)	100(2)	100(2)	100(2)
Crystal system	monoclinic	monoclinic	monoclinic	triclinic
Space group	$P2_1/c$	C2/c	$P2_1/c$	P-1
a/Å	11.955(2)	32.7550(17)	14.998(5)	9.9101(6)
b/Å	17.5685(11)	10.5714(5)	8.7997(4)	17.0394(9)
c/Å	15.782(3)	13.5063(6)	23.691(8)	18.2463(6)
α/°	90	90	90	74.733(4)
β/°	139.46(4)	110.305(4)	148.87(8)	89.846(4)
γ/°	90	90	90	82.485(5)
Volume/Å^3	2154.3(14)	4386.2(4)	1616(2)	2945.2(3)
Z	4	8	4	2
ρ_{calc}g/cm^3	1.405	1.589	1.478	1.763
μ/mm^{-1}	1.180	1.406	1.550	3.890
F(000)	944.0	2144.0	752.0	1584.0
Crystal size/mm^3	0.15 × 0.1 × 0.1	0.3 × 0.25 × 0.25	0.25 × 0.25 × 0.2	0.1 × 0.1 × 0.1
Radiation	MoKα (λ = 0.71073)	MoKα (λ = 0.71073)	MoKα (λ = 0.71073)	CuKα (λ = 1.54184)
2Θ range for data collection/°	5.222 to 55	5.47 to 54.996	5.494 to 54.978	6.342 to 144.998
Index ranges	-15 ≤ h ≤ 15, -22 ≤ k ≤ 22, -20 ≤ l ≤ 20	-31 ≤ h ≤ 42, -13 ≤ k ≤ 13, -17 ≤ l ≤ 17	-18 ≤ h ≤ 19, -11 ≤ k ≤ 11, -30 ≤ l ≤ 30	-11 ≤ h ≤ 12, -21 ≤ k ≤ 21, -18 ≤ l ≤ 22
Reflections collected	37536	18244	13150	32356
Independent reflections	4962 [R_{int} = 0.0467, R_{sigma} = 0.0257]	5042 [R_{int} = 0.0343, R_{sigma} = 0.0341]	3720 [R_{int} = 0.0224, R_{sigma} = 0.0190]	11567 [R_{int} = 0.0918, R_{sigma} = 0.0936]
Data/restraints/parameters	4962/0/266	5042/0/284	3720/0/196	11567/0/813
Goodness-of-fit on F^2	1.059	1.080	1.053	1.020
Final R indexes [I>=2σ (I)]	R_1 = 0.0299, wR_2 = 0.0706	R_1 = 0.0402, wR_2 = 0.1001	R_1 = 0.0226, wR_2 = 0.0600	R_1 = 0.0793, wR_2 = 0.2065
Final R indexes [all data]	R_1 = 0.0380, wR_2 = 0.0748	R_1 = 0.0471, wR_2 = 0.1039	R_1 = 0.0266, wR_2 = 0.0629	R_1 = 0.1152, wR_2 = 0.2496
Largest diff. peak/hole / e Å^{-3}	0.42/-0.34	1.53/-0.73	0.32/-0.37	1.66/-1.03
CCDC number	**1504005**	**1504000**	**1503999**	**1504006**

Table 2S. Crystal data for [**4b**(OTf)(EtOH)](OTf), [**4c**$(OTf)_2$], [**5a**](OTf), and [**5d**](OTf).

Identification code	[**4b**(OTf)(EtOH)](OTf)	[**4c**$(OTf)_2$]	[**5a**](OTf)	[**5d**](OTf)
Empirical formula	$C_{24}H_{32}Cl_2F_6N_8O_9S_2Zn$	$C_{14}H_{28}F_6N_8O_8S_2Zn$	$C_{11}H_{15}F_3N_4O_4S$	$C_9H_{19}F_3N_4O_4S$
Formula weight	890.96	679.93	356.33	336.34
Temperature/K	100(2)	100(2)	100(2)	100(2)
Crystal system	triclinic	orthorhombic	monoclinic	monoclinic
Space group	P-1	$Pna2_1$	C2/c	$P2_1/c$
a/Å	8.7052(5)	16.8415(3)	16.7859(5)	11.8893(13)
b/Å	12.9506(6)	20.4363(4)	8.3599(2)	18.4419(14)
c/Å	17.0474(7)	16.1946(3)	21.9907(5)	7.2746(7)
α/°	108.023(4)	90	90	90
β/°	90.814(4)	90	90.745(2)	103.177(11)
γ/°	95.484(4)	90	90	90
Volume/$Å^3$	1817.27(16)	5573.83(17)	3085.67(15)	1553.0(3)
Z	2	8	8	4
$\rho_{calc}g/cm^3$	1.628	1.621	1.534	1.438
μ/mm^{-1}	1.027	1.124	2.429	0.260
F(000)	908.0	2784.0	1472.0	704.0
Crystal size/mm^3	0.15 × 0.1 × 0.1	0.2 × 0.2 × 0.2	0.1 × 0.1 × 0.1	0.2 × 0.2 × 0.2
Radiation	MoKα (λ = 0.71073)	MoKα (λ = 0.71073)	CuKα (λ = 1.54184)	MoKα (λ = 0.71073)
2Θ range for data collection/°	5.232 to 55	5.298 to 55	8.042 to 153.006	5.648 to 54.998
Index ranges	$-11 \le h \le 11$, $-16 \le k \le 16$, $-22 \le l \le 22$	$-21 \le h \le 21$, $-26 \le k \le 26$, $-21 \le l \le 21$	$-20 \le h \le 21$, $-10 \le k \le 10$, $-27 \le l \le 24$	$-14 \le h \le 15$, $-23 \le k \le 23$, $-9 \le l \le 8$
Reflections collected	16514	53585	21892	7523
Independent reflections	8351 [R_{int} = 0.0246, R_{sigma} = 0.0384]	12565 [R_{int} = 0.0373, R_{sigma} = 0.0327]	3225 [R_{int} = 0.1226, R_{sigma} = 0.0425]	3561 [R_{int} = 0.0336, R_{sigma} = 0.0539]
Data/restraints/parameters	8351/2/477	12565/14/721	3225/0/210	3561/0/195
Goodness-of-fit on F^2	1.045	1.046	1.033	1.055
Final R indexes [I>=2σ (I)]	R_1 = 0.0509, wR_2 = 0.1203	R_1 = 0.0420, wR_2 = 0.0983	R_1 = 0.0569, wR_2 = 0.1174	R_1 = 0.0494, wR_2 = 0.1108
Final R indexes [all data]	R_1 = 0.0688, wR_2 = 0.1342	R_1 = 0.0489, wR_2 = 0.1023	R_1 = 0.0630, wR_2 = 0.1223	R_1 = 0.0740, wR_2 = 0.1229
Largest diff. peak/hole / e $Å^{-3}$	2.59/-0.58	1.27/-1.11	0.37/-0.55	0.46/-0.28
CCDC number	**1504001**	**1504002**	**1504004**	**1504003**

Theoretical study of bonding situation in solid state structures of 2 and [4(OTf)$_2$]

Inspection of the crystallographic data suggests the presence of different types of non-covalent interactions in solid-state structures of **2a**–**c**, [**4b**(OTf)(EtOH)](OTf), and [**4c**(OTf)$_2$], viz. intra- and intermolecular hydrogen (HB's) and halogen (XB's) bonds. Besides, in [**4c**(OTf)$_2$], the coordination polyhedron of zinc metal center is supplemented by two triflate anionic ligands to distorted octahedron. In order to (*i*) confirm or deny the hypothesis on the existence of these weak contacts in **2a**–**c**, [**4b**(OTf)(EtOH)](OTf), and [**4c**(OTf)$_2$], and to quantify their energies from theoretical point of view; (*ii*) to understand more deeply the nature of Zn–O contacts and to compare them with other ordinary Zn–N coordination bonds in [**4c**(OTf)$_2$], we carried out DFT calculations and performed topological analysis of the electron density distribution within the formalism of Bader's theory (QTAIM method)[4] for **2a**–**c**, [**4b**(OTf)(EtOH)](OTf), and [**4c**(OTf)$_2$]. Results are summarized in **Table 3S**, the contour line diagrams of the Laplacian distribution $\nabla^2\rho(\mathbf{r})$, bond paths, and selected zero-flux surfaces for **2a**–**b**, [**4b**(OTf)(EtOH)](OTf), and [**4c**(OTf)$_2$] are shown in **Figures 76S** and **77S**. The Poincare-Hopf relationship in all cases is satisfied, thus all critical points have been found.

Table 3S. Values of the density of all electrons – $\rho(\mathbf{r})$, Laplacian of electron density – $\nabla^2\rho(\mathbf{r})$, energy density – H_b, potential energy density – $V(\mathbf{r})$, and Lagrangian kinetic energy – $G(\mathbf{r})$ (Hartree) at the bond critical points (3, –1), corresponding to non-covalent interactions and coordination bonds in solid state structures of **2a**–**c**, [**4b**(OTf)(EtOH)](OTf), and [**4c**$(OTf)_2$], bond lengths – *l* (Å) and Wiberg bond indices – WI, as well as energies for these contacts E_{int} (kcal/mol), defined by two approaches.

Contact	$\rho(\mathbf{r})$	$\nabla^2\rho(\mathbf{r})$	H_b	$V(\mathbf{r})$	$G(\mathbf{r})$	E_{int}[a]	E_{int}[b]	*l*	WI
2a									
O–H···O	0.038	0.155	0.000	-0.038	0.038	11.9	10.2	1.76	0.04
	0.036	0.149	0.001	-0.036	0.037	11.3	10.0	1.78	0.03
N–H···O	BCP not found							2.19	0.00
	BCP not found							2.22	0.00
2b									
O–H···O	0.035	0.153	0.001	-0.035	0.037	11.0	10.0	1.79	0.03
	0.032	0.139	0.002	-0.031	0.033	9.7	8.9	1.83	0.01
N–H···O	BCP not found							2.26	0.00
	BCP not found							2.24	0.00
Cl···Cl	0.009	0.035	0.002	-0.005	0.007	1.6	1.9	3.33	0.01
2c									
O–H···O	0.033	0.143	0.002	-0.033	0.034	10.4	9.2	1.81	0.03
	0.028	0.117	0.002	-0.025	0.027	7.8	7.3	1.90	0.02
N–H···O	BCP not found							2.23	0.00
	BCP not found							2.25	0.00
[**4b**(OTf)(EtOH)](OTf)									
Cl···F	0.007	0.033	0.001	-0.005	0.007	1.6	1.9	3.09	0.00
[**4c**$(OTf)_2$]									
Zn–O	0.023	0.087	-0.002	-0.025	0.023	7.8	6.2	2.51	0.14
	0.019	0.074	0.000	-0.019	0.019	6.0	5.1	2.60	0.12
Zn–N	0.095	0.422	-0.023	-0.152	0.129	47.7	34.7	1.95	0.31
	0.091	0.402	-0.021	-0.143	0.122	44.9	32.8	1.97	0.29
	0.067	0.288	-0.013	-0.097	0.085	30.4	22.9	2.09	0.25
	0.064	0.272	-0.012	-0.093	0.080	29.2	21.5	2.11	0.24

[a] $E_{int} = -V(\mathbf{r})/2$ [5]

[b] $E_{int} = 0.429G(\mathbf{r})$ [6]

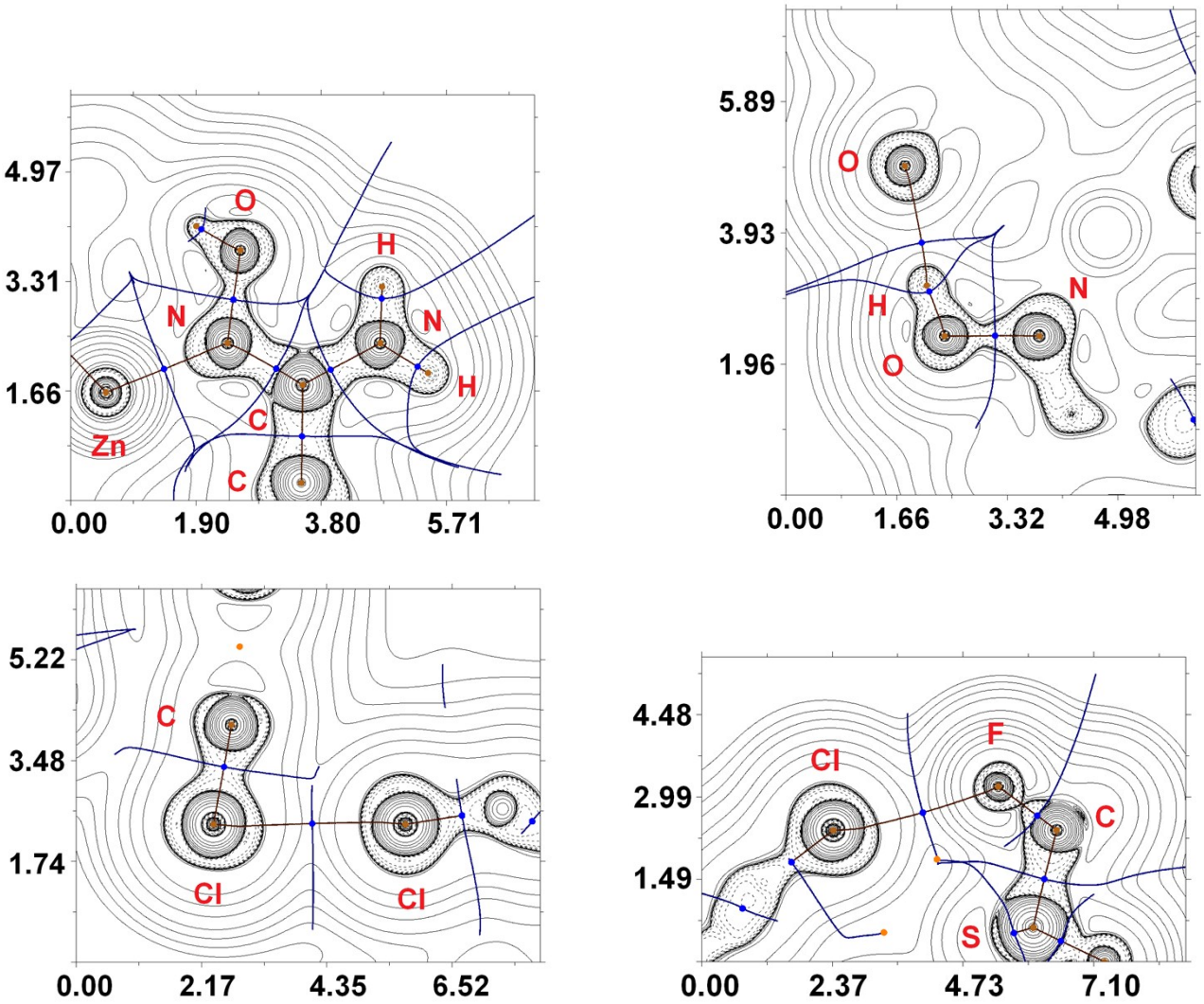

Figure 77S. Contour line diagrams of the Laplacian distribution $\nabla^2\rho(\mathbf{r})$, bond paths and selected zero-flux surfaces for HB's in **2a** (top) and XB's in **2b** (down left) and [**4b**(OTf)(EtOH)](OTf) (down right). Bond critical points (3, –1) are shown in blue, nuclear critical points (3, –3) – in pale brown, ring critical points (3, +1) – in orange, length unit – Å.

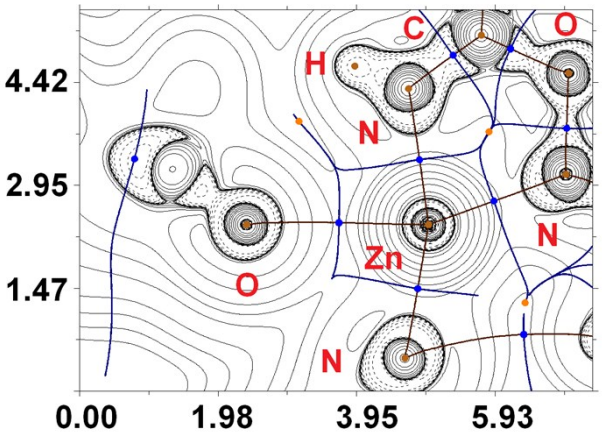

Figure 77S. Contour line diagram of the Laplacian distribution $\nabla^2\rho(\mathbf{r})$, bond paths and selected zero-flux surfaces for contacts Zn–O and Zn–N in [**4c**$(OTf)_2$]. Bond critical points (3, –1) are shown in blue, nuclear critical points (3, –3) – in pale brown, ring critical points (3, +1) – in orange, length unit – Å.

The QTAIM analysis demonstrates the presence of appropriate bond critical points (BCPs) (3, –1) for intramolecular O–H···O HB's in **2a**–**c**, but does not reveals any BCPs for intramolecular N–H···O HB's, despite the fact that lengths of corresponding contacts are less than the sum of Bondi's (the shortest)[7] van der Waals radii of these atoms (vdw r(H + O) = 2.72 Å) (**Table 3S**, **Figure 77S**). In **2b** and [**4b**(OTf)(EtOH)](OTf), the BCPs for intermolecular Cl···Cl and intramolecular Cl···F XB's were successfully found (vdw r(Cl + Cl) = 3.50 Å; vdw r(Cl + F) = 3.22 Å) (**Table 3S**, **Figure 77S**). The low magnitude of the electron density, positive values of the Laplacian, and zero or close to zero positive energy density in these BCPs are typical for hydrogen and halogen bonding. We have defined energies for these contacts according to the procedures proposed by Espinosa et al.[5] and Vener et al.[6] (**Table 3S**), and one can state that strength of O–H···O contacts (7.3–11.9 kcal/mol) is corresponds to moderate HB's following the classification of Jeffrey ("weak" HB's: <4 kcal/mol, "moderate" HB's: 15–4 kcal/mol, "strong" HB's: 40–15 kcal/mol),[8] and both Cl···Cl and Cl···F XB's are weak (1.6–1.9 kcal/mol). The balance between the Lagrangian kinetic energy G(**r**) and potential energy density V(**r**) at the BCPs (3, –1) reveals the nature of these interactions, if the ratio –G(**r**)/V(**r**) > 1 is satisfied, than the nature of appropriate interaction is purely non-covalent, in case the –G(**r**)/V(**r**) < 1 some covalent component takes place.[9] Based on this criterion one can state that the covalent contribution in all discussed above HB's and XB's is absent. The negligible values of the Wiberg bond indices for these contacts (0.00–0.04) computed by using the natural bond orbital (NBO) partitioning scheme[10] additionally confirm the electrostatic nature of these non-covalent interactions.

In [**4c**$(OTf)_2$], the QTAIM analysis reveals the presence of two BCPs for Zn–O and four BCPs for Zn–N contacts. The properties of electron density in BCPs for Zn–N contacts are typical for ordinary coordination bonds (the $\rho(\mathbf{r})$ and $\nabla^2\rho(\mathbf{r})$ values are positive and relatively high; the H_b values are significantly negative; the –G(**r**)/V(**r**) << 1; Wiberg bond indices for these contacts are noticeable), whereas Zn–O contacts can be classified as non-covalent close shell interactions with some contribution of covalent component.

Table 4S. Calculated Wiberg bond indices for selected bonds in **2a**–**c**.

Bond	**2a**	**2b**	**2c**
Zn–O	0.29	0.29	0.31
O–C	1.31	1.29	1.30
C=O	1.53	1.55	1.54
O•••H	0.03	0.03	0.03
H–O	0.72	0.73	0.73
O–N	1.01	1.00	1.00
Zn–N	0.30	0.29	0.31

Table 5S. Cartesian atomic coordinates of model structures.

Atom	X	Y	Z
2a			
Zn	-2.190015	4.359975	6.321676
O	-3.532308	2.985942	5.872890
O	-3.549543	5.739980	6.704811
O	-1.747598	2.976104	8.907298
H	-2.205242	2.427967	8.463847
O	-3.242129	7.192544	5.037789
O	-1.836431	5.491913	3.662709
H	-2.298640	6.075187	4.051896
O	-2.966952	1.343815	7.270743
N	-1.262692	3.996131	8.045835
N	-1.192107	4.674275	4.630138
C	0.348072	5.753684	7.837290
C	0.691615	3.208887	4.955520
N	0.267296	4.278105	9.766300
H	-0.079080	3.610327	10.222062
H	0.954325	4.722413	10.090760
N	0.361408	4.485062	2.923007
H	-0.083223	5.056214	2.420880
H	1.105532	4.123327	2.625013
C	-0.443350	6.830106	7.455899
H	-1.370165	6.837660	7.663725
C	-0.247685	4.616650	8.578941
C	-3.637786	1.794974	6.327113
C	-3.806857	6.835728	6.080101
C	2.078090	3.382815	5.068255
H	2.501555	4.104002	4.618136
C	1.712974	5.734534	7.551298
H	2.257544	5.008779	7.831956
C	-0.098427	4.167248	4.143500
C	-4.653775	0.911629	5.641881
H	-5.555074	1.164792	5.931155
H	-4.486101	-0.024596	5.878840
H	-4.579588	1.020730	4.670451
C	0.085364	2.135978	5.594694
H	-0.850373	1.992268	5.504424
C	-4.868129	7.714328	6.691270
H	-5.638999	7.166191	6.948745
H	-5.150201	8.387202	6.037838
H	-4.505291	8.160568	7.485237
C	2.831725	2.508430	5.833705
H	3.772321	2.628248	5.903459
C	0.127580	7.896689	6.767179
H	-0.404648	8.640188	6.510730
C	1.477261	7.864012	6.459440
H	1.866424	8.583969	5.975264
C	2.260059	6.803929	6.845140

H	3.186194	6.799010	6.627671
C	0.855933	1.271257	6.371222
H	0.440605	0.542867	6.819495
C	2.219544	1.463983	6.492266
H	2.733971	0.876668	7.031835
2b			
Zn	2.883620	9.253886	2.543660
Cl	3.458599	7.176923	6.056853
Cl	4.597284	6.448660	-0.820062
O	2.308390	9.029033	0.690098
O	5.694311	8.502577	3.345735
H	5.697802	9.321861	3.377022
O	3.364905	11.162870	2.510599
O	0.120170	8.666434	0.920764
O	0.196826	8.372549	3.544607
H	0.095681	8.429634	2.733539
O	5.403670	11.085064	3.441624
N	0.418175	9.063918	5.996938
H	-0.314141	8.726691	5.700150
H	0.487678	9.280632	6.826246
N	4.508867	8.058578	2.715552
N	1.441485	8.957147	3.907643
N	5.804218	6.169469	2.274993
H	6.501207	6.508811	2.648670
H	5.842795	5.381900	1.931718
C	1.133184	8.865176	0.230539
C	2.414150	5.812156	2.462465
H	2.407810	6.076441	3.354222
C	3.693344	8.905347	6.235964
C	4.427804	11.704654	2.978012
C	2.369857	5.053129	-0.209006
H	2.354815	4.811044	-1.105829
C	3.398719	5.834356	0.287541
C	4.659554	6.868239	2.226859
C	1.367690	5.045729	1.970985
H	0.665741	4.802587	2.529600
C	1.448913	9.251032	5.169403
C	4.063536	11.636997	6.523505
H	4.195672	12.553538	6.613441
C	4.839762	9.376832	6.868048
H	5.471827	8.782719	7.201190
C	1.013277	8.911690	-1.283167
H	1.252672	9.787002	-1.597309
H	0.107616	8.717176	-1.539041
H	1.601324	8.261549	-1.672044
C	2.909709	11.151770	5.916756
H	2.261387	11.745883	5.617815
C	2.719640	9.781716	5.755885
C	1.368865	4.639787	0.643484
H	0.691401	4.086903	0.326809

C	3.467952	6.188498	1.641643
C	4.468007	13.216364	2.964078
H	3.966700	13.543021	2.212925
H	5.379435	13.512363	2.891876
H	4.086015	13.554649	3.776033
C	5.021851	10.737371	6.994718
H	5.794577	11.060856	7.400062
Zn	0.540159	1.317514	8.877161
Cl	1.115138	3.394477	12.390353
Cl	2.253823	4.122740	5.513439
O	-0.035071	1.542367	7.023598
O	3.350850	2.068823	9.679235
H	3.354341	1.249539	9.710522
O	1.021444	-0.591470	8.844100
O	-2.223291	1.904966	7.254264
O	-2.146635	2.198851	9.878107
H	-2.247780	2.141766	9.067039
O	3.060209	-0.513664	9.775124
N	-1.925286	1.507482	12.330438
H	-2.657602	1.844709	12.033650
H	-1.855784	1.290768	13.159747
N	2.165406	2.512822	9.049052
N	-0.901977	1.614253	10.241143
N	3.460757	4.401931	8.608493
H	4.157745	4.062589	8.982170
H	3.499334	5.189500	8.265218
C	-1.210277	1.706224	6.564040
C	0.070689	4.759244	8.795965
H	0.064349	4.494959	9.687722
C	1.349883	1.666053	12.569464
C	2.084342	-1.133254	9.311512
C	0.026395	5.518271	6.124495
H	0.011354	5.760356	5.227671
C	1.055258	4.737044	6.621041
C	2.316092	3.703161	8.560359
C	-0.975771	5.525671	8.304485
H	-1.677720	5.768813	8.863100
C	-0.894549	1.320368	11.502903
C	1.720075	-1.065597	12.857005
H	1.852211	-1.982137	12.946941
C	2.496301	1.194568	13.201548
H	3.128365	1.788681	13.534690
C	-1.330184	1.659710	5.050333
H	-1.090789	0.784398	4.736191
H	-2.235846	1.854224	4.794460
H	-0.742137	2.309851	4.661456
C	0.566248	-0.580370	12.250256
H	-0.082074	-1.174483	11.951315
C	0.376179	0.789684	12.089385
C	-0.974597	5.931613	6.976984

H	-1.652060	6.484497	6.660309
C	1.124491	4.382902	7.975143
C	2.124546	-2.644964	9.297578
H	1.623239	-2.971621	8.546425
H	3.035974	-2.940963	9.225376
H	1.742554	-2.983249	10.109533
C	2.678389	-0.165971	13.328218
H	3.451116	-0.489456	13.733562
2c			
Zn	-17.635972	2.247619	11.418879
O	-17.025260	1.255805	8.684065
H	-17.552626	1.891056	8.529376
O	-18.339308	1.247445	14.111805
H	-17.799322	1.870816	14.269925
O	-18.409430	3.567310	8.768943
O	-16.487325	3.704762	12.044007
N	-18.254229	0.881114	12.738213
N	-19.070117	-1.134633	13.543385
H	-19.041582	-0.847411	14.375256
H	-19.352851	-1.949134	13.368486
O	-16.545848	3.172028	14.200847
O	-19.271025	3.111398	10.772930
N	-14.727987	0.186202	9.127804
H	-15.098355	0.153995	8.329736
H	-13.943034	-0.188314	9.264244
C	-16.155831	3.882604	13.262297
C	-19.294682	3.695962	9.633761
C	-15.355986	0.803325	10.129920
C	-18.684621	-0.335005	12.547148
N	-16.509867	1.377065	10.007686
C	-18.744826	-0.866858	11.141099
H	-18.601520	-0.121436	10.506172
H	-19.645629	-1.238998	10.972814
C	-14.677344	0.847587	11.472157
H	-14.364289	-0.060718	11.708907
H	-15.330514	1.131641	12.158402
C	-15.216785	5.026917	13.554408
H	-14.340345	4.672641	13.816756
H	-15.580928	5.570210	14.283397
H	-15.117225	5.580770	12.752421
C	-13.487861	1.810098	11.481221
H	-12.794730	1.478350	10.872382
H	-13.123112	1.870816	12.388661
H	-13.782348	2.697108	11.187151
C	-17.697061	-1.954501	10.884752
H	-17.760409	-2.255363	9.953796
H	-17.859660	-2.712068	11.484772
H	-16.802814	-1.591866	11.051200
C	-20.477282	4.593795	9.373617
H	-20.421497	5.383656	9.951346

H	-21.305521	4.106820	9.566765
H	-20.474064	4.874154	8.435067
[**4b**(OTf)(EtOH)](OTf)			
Zn	3.259403	8.460107	2.552270
Cl	0.328229	11.239742	1.837162
S	2.376821	9.117224	-0.912670
Cl	2.510289	8.447731	7.506858
O	2.922323	10.449315	-0.850001
N	2.498329	6.677781	2.875008
H	2.857197	5.979470	2.477618
O	2.031644	8.527875	0.367918
F	0.134660	8.153425	-1.870035
O	0.861155	7.585595	4.214541
N	0.005984	9.691526	5.433270
H	-0.334468	8.901763	5.624031
H	-0.284301	10.408489	5.852360
F	-0.076744	10.100480	-1.006917
N	3.938055	10.211261	1.984685
H	3.647465	10.571655	1.237190
N	5.505065	11.934202	2.394545
N	1.483173	8.834580	3.816179
C	1.458259	4.098458	3.478381
H	1.533906	4.163591	2.503528
H	0.862387	3.355340	3.711569
H	2.344366	3.939035	3.865408
N	0.911755	5.344735	4.008883
N	4.567812	9.065569	4.192032
O	5.139540	10.365435	3.946376
C	1.486732	6.509244	3.654567
F	0.870220	9.896771	-2.922617
C	6.281712	12.670194	3.399033
H	6.937924	13.243558	2.948851
H	6.749235	12.034386	3.980382
H	5.678572	13.224444	3.936660
C	4.811466	10.837355	2.707729
C	2.656546	13.699069	3.939898
H	3.041425	14.560611	3.824924
C	2.897248	12.975558	5.105836
H	3.446423	13.343973	5.789205
C	1.305870	11.902336	3.111273
C	2.337715	11.723670	5.271011
H	2.499954	11.240549	6.074212
O	3.024035	8.212377	-1.825826
C	1.535880	11.154650	4.276239
C	3.339411	7.137803	6.751104
C	4.753466	8.769962	5.452379
O	4.841762	7.438047	1.361880
H	4.837824	6.587090	1.425035
C	2.963936	5.814955	7.073356
H	2.283918	5.650083	7.716241

C	0.963127	9.799674	4.507969
C	0.745659	9.336590	-1.708423
C	1.854494	13.160072	2.943993
H	1.683061	13.653423	2.148888
N	5.291140	9.561126	6.371364
H	5.560519	10.370622	6.151941
H	5.378982	9.278595	7.199666
C	-0.095506	5.244063	5.060494
H	-0.845800	4.698650	4.743100
H	-0.418576	6.141029	5.288824
H	0.300207	4.827302	5.853979
C	4.326856	7.393231	5.824831
C	4.953482	6.284216	5.178707
H	5.627668	6.432945	4.526106
C	5.305651	12.538479	1.073634
H	4.458135	13.028964	1.063918
H	5.283932	11.833825	0.393504
H	6.042240	13.155605	0.882550
C	4.576705	4.990711	5.505817
H	4.996515	4.250958	5.081546
C	3.592273	4.777659	6.448284
H	3.344756	3.885924	6.666897
C	6.067425	7.868966	0.772434
H	5.915877	8.733982	0.317394
H	6.340208	7.210804	0.084207
C	7.203015	8.032519	1.773197
H	8.023989	8.280512	1.297106
H	7.343839	7.188189	2.247669
H	6.973331	8.735232	2.416082
[**4c**$(OTf)_2$]			
Zn	12.972334	19.228923	11.253628
S	11.218292	20.852792	14.061771
O	12.321241	20.087452	13.519252
O	15.634807	18.793630	12.448789
O	11.952413	19.488056	8.519979
N	13.663509	17.642658	12.194534
H	13.180158	16.937605	12.290082
O	10.256474	21.293807	13.075520
N	14.906412	19.837925	11.757280
N	11.696422	20.524176	10.547543
H	11.442115	21.208792	11.002611
N	15.499232	16.755722	13.371881
O	10.642144	20.317769	15.269888
N	13.058899	18.842269	9.185577
F	12.878695	22.197909	15.566250
N	10.136899	20.763281	8.770995
F	11.100233	23.272858	15.039925
N	16.929076	20.959469	12.073074
H	17.287800	20.280984	12.464984
H	17.382112	21.680871	11.964570

N	13.298048	17.924679	7.052748
H	12.636177	18.374277	6.740193
H	13.735927	17.389248	6.542618
C	14.860940	17.691705	12.665797
C	15.671016	20.887942	11.637440
C	13.648352	18.061602	8.328883
C	11.258543	20.293246	9.355620
F	12.631125	22.984707	13.577553
C	15.071458	22.087553	10.970222
H	15.153982	22.853914	11.556467
H	14.124966	21.928150	10.819612
C	11.997885	22.420665	14.591335
C	14.835677	15.480497	13.652048
H	14.273171	15.574504	14.422911
H	15.497548	14.804056	13.820472
H	14.301802	15.223000	12.895760
C	14.769996	17.219626	8.856827
H	15.079879	17.589523	9.698946
H	15.511022	17.242106	8.231715
C	9.348717	21.797358	9.413921
H	9.437977	21.721743	10.366163
H	8.427487	21.697220	9.167763
H	9.663653	22.659769	9.130515
C	16.804449	16.962129	14.000232
H	17.169909	17.802061	13.711968
H	17.397270	16.250946	13.747596
H	16.701716	16.968260	14.955713
C	15.748487	22.396141	9.634168
H	15.578388	21.682914	9.015534
H	16.694979	22.484017	9.768583
H	15.398183	23.217680	9.281125
C	9.840488	20.536438	7.360446
H	10.155425	21.282363	6.843838
H	8.892312	20.442431	7.242225
H	10.280052	19.735335	7.065704
C	14.337169	15.776824	9.070595
H	14.071073	15.394665	8.231715
H	13.597827	15.752300	9.682751
H	15.069774	15.274091	9.433355
S	10.222622	16.671116	11.766672
F	9.249352	14.345261	11.013947
O	11.051392	16.018381	12.751628
O	10.877925	17.712141	11.017186
O	8.888944	16.976434	12.205870
F	9.309981	15.805434	9.462505
F	11.117074	14.867408	10.084377
C	9.968484	15.349705	10.516773

References

1. D. S. Bolotin, N. A. Bokach and V. Y. Kukushkin, *Coordination Chemistry Reviews*, 2016, **313**, 62-93.
2. F. H. Allen, O. Kennard, D. G. Watson, L. Brammer and G. Orpen, *J. Chem. Soc. Perkin Trans. II,*, 1987, S1–S19.
3. a) D. S. Bolotin, K. I. Kulish, N. A. Bokach, G. L. Starova, V. V. Gurzhiy and V. Y. Kukushkin, *Inorganic Chemistry*, 2014, **53**, 10312-10324; b) K. I. Kulish, A. S. Novikov, P. M. Tolstoy, D. S. Bolotin, N. A. Bokach, A. A. Zolotarev and V. Y. Kukushkin, *Journal of Molecular Structure*, 2016, **1111**, 142-150.
4. R. F. W. Bader, *Chemical Reviews*, 1991, **91**, 893-928.
5. E. Espinosa, E. Molins and C. Lecomte, *Chemical Physics Letters*, 1998, **285**, 170-173.
6. M. V. Vener, A. N. Egorova, A. V. Churakov and V. G. Tsirelson, *Journal of Computational Chemistry*, 2012, **33**, 2303-2309.
7. A. Bondi, *J. Phys. Chem.* , 1964, **68**, 441–451.
8. T. Steiner, *Angew. Chem. Int. Ed.*, 2002, **41**, 48–76.
9. E. Espinosa, I. Alkorta, J. Elguero and E. Molins, *Journal of Chemical Physics* 2002, **117**, 5529-5542.
10. E. D. Glendening, C. R. Landis and F. Weinhold, *Wiley Interdiscip. Rev. Comput. Mol. Sci.* , 2012, **2**, 1–42.